Pressure Losses Associated with Slurry Flow in Horizontal Pipelines

Tahir Hussein Hasan Alzuhd

A thesis submitted in partial fulfilment of the requirements of the University of Hertfordshire for the degree of Doctor of Philosophy

The programme of research was carried out in the Department of Aerospace, Automotive and Mechanical Engineering, University of Hertfordshire

in collaboration with

The Arab Potash Company Limited- Jordan

June 2003

To the soul of my late sister Fatima who encouraged me to keep it up throughout the long days of this work until her last days with us but left shortly before the completion of this work

Acknowledgement

I express my deepest thanks to my principal supervisor, Professor F. S. Bhinder for his advice, support, guidance and encouragement throughout this research exercise Also, I express my gratitude to my second supervisor, Professor P. Bullen for his fruitful comments, guidance and help during the various stages of this work.

I am indebted to the management of The Arab Potash Co. Ltd. for their continued support of this project. Special thanks are due to Eng. N. Sadoun for his valuable support without which the idea of this work would not have been endorsed. I thank all the employees of The Arab Potash Co. for their help during the building of the test rig and creative suggestions during the execution of the experimental part. In particular, my thanks go to Eng. M. Shananir, Eng. I. Shalakhti, Eng. M. Abdelkareem and F. Nsour for their indispensable help.

I was gifted to share the same interests, determination to keep up and support of G. Khdeiry, M. Ebeid, S. Jamil, O. Quraan. T. Elahasan and Q. Hamdan who all obtained their Ph.D. on the same lines of constructive thought.

I would like to extend my gratitude to the staff of the administrative office at the STRC of the University of Hertfordshire for their continued help. I would like to thank the University of Hertfordshire, Aerospace, Automotive and Mechanical Engineering Department for their encouragements and resource support in several forms.

Most importantly, I wish to thank my wife and children who managed to endure the demanding hard times and patience during my research work.

Abstract

The flow of solid liquid mixtures (slurries) has attracted much attention in research work because of its importance to industry. Prediction of pressure losses associated with slurry flow helps pipe designers select the correct pipe sizes for optimum energy consumption, equipment sizing and reliable operation of the pipeline networks.

Many workers developed empirical correlations, but due to the randomness of the problem they seem of limited use in design applications because they do not contain an assessment except by trial and error, which is costly.

The existence of more than one particle size poses more complexities to the slurry flow problem but it is in need in practical applications. The aims of this work are justified under the light of the observations on the state of the art in slurry transport.

An experimental program is designed to highlight the effects of this problem through a predetermined set of test runs. The variables are grouped to optimise the number of experiments and to remove the effect of dimensions on the prediction method.

The test rig is built to serve the aims of this exercise and test runs conducted, results grouped and discussed for polyfractional slurries. A mathematical model is developed in the form of an empirical correlation. Statistical tests are employed to verify the goodness of fit.

Finally, conclusions and recommendations for further work are listed.

Table of Contents

List of Symbols

A	Area [L^2],
A, *a*	Constant [-]
Ar	Archimedes number [-]
B, *b*	Constant [-]
C	Percent Volumetric Concentration of Solid Particles [-]
C, *c*	Constant [-]
C_D	Coefficient of Drag [-]
D	Pipeline diameter [L]
d	Particle Size Diameter [L]
	Durbin Watson Statistic for Goodness of Fit
f	Fanning Friction Factor [-]
F	Normal Force [ML/T^2]
	Significance Statistic for Goodness of Fit
Fr	Froude Number [-]
g	Gravitational Constant [L/T^2]
i	Pressure Gradient (meter H2O per Meter Pipe Length [L/L]
k	Von Karman Constant [-]
	Correlation Constant
MW	Power [Megawatt]
N_I	Dimensionless Parameter denoting Settling Tendency [-]
n	Number of Particle Sizes
	Number of Degrees of Freedom (Observations or Independent Variables)
P	Pressure drop [M/LT^2]
PSD	Particle Size Distribution
PUC	Annual Money Value Cost per Unit Pipe Length [$/L]
R, r	Radius [L]
R^2	Coefficient of Determination Statistic for Goodness of Fit
Re	Reynolds Number [-]
Re_p	Reynolds Number defined for Particle Diameter [-]

S	Specific Gravity of solid Particles [-]
	Perimeter [L]
U_t	Terminal Velocity of a Solid Particle [L/T]
V	Average Velocity of Flow [L/T]
V_l	Solids Suspension Velocity [L/T]
x	Direction Along Pipe Axis [L]
Y	Non Dimensional Parameter [-]

Greek Symbols

ε	Pipe Roughness [L]
τ	Shear Stress [M/LT^2]
ϕ	Pressure Loss Coefficient [-]
ψ	Flow Coefficient [-]
	Dynamic viscosity [M/LT]
M	Density [M/L^3]
ρ	Laplacian operator (compact form for denoting 3-dimensional partial
∇	derivatives)

Subscripts

$1, 2$	Layer Number
C	Critical
f	Finer Fraction of Solids
h	Hydraulic (perimeter)
L, l	Liquid Part of Slurry
m	Mixture (Slurry)
p	Solid Particle
S	Solid Part of Slurry
t	Terminal
v	Volumetric
w	Water

Chapter 1

Introduction

1.1. Introduction

1.2. Economical Considerations

1.3. Classification of Slurries

1.4. Problem Statement

1.5. The Aims

1.1. Introduction:

In the chemical process industries (CPI), solid materials are mixed with liquids and conveyed hydraulically in pipelines. The mixture of solids, in particle form, with a liquid medium is called slurry. The flow of slurries in pipelines is associated with consumption of energy that is needed to overcome their resistance to flow. This resistance is translated in pressure losses across the length of the pipeline. It is necessary to reliably estimate these losses in order to design pipelines so that the correct pipe diameter can be selected. The design procedure includes the selection of the pumping equipment and the corresponding power rating. Inadequate design may prove to be costly in terms of equipment cost, running cost and plant reliable operation.

Prediction of pressure losses due to the flow of slurries is not an easy task because it contains many variables pertaining to the properties of the liquid, the geometrical and physical properties of the solids, the flow characteristics and the pipe geometry. In a pipeline conveying liquids only, the problem is relatively easier. The existence of solids brings in the complexities of the interaction between these solids themselves, with the liquid that carries them and with the pipeline boundaries. A more complex situation arises when the solids are of different sizes, shapes and concentrations. The flow regimes in slurry flow become more complex than the laminar-transition-turbulent patterns known in the clear liquid case.

The standard procedures used in the prediction of the pressure losses in pipelines carrying liquid (for example water) use a pressure loss coefficient that relates the friction experienced at the pipe boundary to a flow regime number (Reynolds number) for a given pipe specification (relative roughness ε / D).

In the case of slurries, the added solids affect the flow characteristics so that the pressure loss coefficient as defined for liquids alone becomes inapplicable. Because of the importance of slurry flow, significant work has been done to predict its behaviour mostly by deriving empirical correlations. Most of the research work has been experimental in nature. The prediction of pressure losses, in particular,

occupied a significant part of research on slurries due to their importance in pipeline design.

In order to reduce the number of variables, non-dimensional parameters were employed in various forms. As a result, numerous correlations emerged and the pipeline designer is faced with the problem of which one to choose. Further experimental work tried to depart from the pure empirical approach by introducing mechanistic models based on physical mechanisms taking place in slurry flow. These models tried to analyse slurry flow under the effects of turbulent eddies, dispersion and granular collisions of solid particles. Due to the complexities of these flow mechanisms; drastic simplifications were needed to develop working formulas. The resulting models, although employing physical principles, in theory, are empirical in nature. They are tedious to solve and could hardly be merited over the other correlations based on empirical approach.

The state of knowledge is still far from rendering the slurry flow amenable to analytical solution. The best that can be done is to conduct further well thought experimental work to develop a justified correlation that may be applicable to a reasonably general slurry flow problem.

1.2. Economical Considerations:

The selection and implementation of a particular configuration of a pipe network, pumping equipment and associated valves and fittings incur a great impact on the expenditure of the budget allocated to build up a process plant. Furthermore, the operating cost of such a selection, thereafter, will affect the economics, profitability and reliable operation of such a process plant for its whole lifetime.

Thus, the engineering stage in which the selection of pipe size and pumping power are fixed is very important. The pipeline designer needs to know with fair accuracy the pressure losses so that his determination of pipe/ pump sizes is correct. Failure to achieve correct design the first time will result in either a costly replacement of the non-performing equipment or living with the wrong selection on the expense of

higher operating cost and/ or less reliable plant operation. This will be translated in higher running cost, more frequent plant shutdowns for maintenance and, consequently, loss of production and revenues.

To illustrate the difficulties in designing a slurry pipeline, Appendix (B) shows a relatively simple example that solves the problem for a 6" horizontal steel pipe for a mixture of water and sand of an assumed spherical diameter of 5 mm and volumetric concentration of sand content of 10%. Searching the literature, six correlations that are of wide use were tried and the friction factor (as a ratio of the friction factor for clear water) for each of them was plotted against Reynolds number, fig. (B.1). The results show clearly the confusion as to which correlation to adopt. For the normal range of velocity of flow encountered in practice (in the neighbourhood of 2 m/s), the correlation of Zandi and Govatos [1] gives an average friction factor that is approx. 23 times the clear water friction factor, Durand [2] 15 times, Fangary *et al* [3] 7 times while for the other three correlations (Chhabra and Richardson [4], Turian *et al* [5] and Swamee [6]) the range is from 6 down to 2 times.

Furthermore, the operating cost was studied in terms of annual money value per unit of pipe length (PUC). Figure (B.2) shows that this could be anywhere between 145 and 10 $/m annually. Details of the calculations are covered in appendix (B).

In case a design error takes place by using an improper correlation, a decision has to be made for plant optimisation that is costly and should have been avoided in the first place. It is not only the operational cost that is to be studied further but, also, the additional capital investment implications in replacements of equipment. These replacements may prove to be of major nature that necessitates a revision of the feasibility of the plant. The industrial practice for conducting feasibility studies centres the capital expenditure on the major part of the project [7] (i.e. main equipment purchase cost) and concludes the associated components as percentages of the main equipment. Table (1.1) below exhibits the capital cost elements incurred in a replacement of a system that has not been correct the first time. It is worth noting that it is quite common, in industrial practice, not to consider those incidental losses due to loss of production, service of capital and administration costs because they are

not good for obtaining bank loans but still they could a significant monetary burden.

Table (1.1), Capital Expenditure for Equipment Replacement

Cost Element	% of Equipment Price
A) Direct Cost	
- Pumping Equipment (Purchase Price)	100
- Piping	31
- Installation	39
- Instrumentation & Control	13
Direct Cost Total	**170**
B) Indirect Cost	
- Engineering & Supervision (*)	32
- Contractors Fees (*)	30
Total (Direct + Indirect)	**232**
C) Contingencies (10% of A+B)	23
Grand Total of Replacement Cost	**255**

(*) Sensitive to Project Scale

If, for example, the installed power that needs to be replaced is in the range of 1 MW, then the cost of pumping equipment including electrical motors and switchgear could easily be in the range of quarter a million dollars. The total replacement cost may exceed double the equipment price.

To conclude the economical considerations, although the pipeline designer work has a serious impact on the cost of a plant, he may only be left with much of guess and/ or trial and error work (or at best imitating similar application if he can find one). To the knowledge of the researcher, in a sister company, a one million plus pipeline and associated equipment project was never put into operation due to a design error of the kind described.

1.3. Classification of Slurries:

Classification of slurries is an attempt to provide a rational basis for describing the physical appearance and flow behaviour of solid- liquid mixtures [8]. Classification of slurries is important in delineating their flow patterns. Mainly, classification relies on visual observation [9][10]. The classification of slurries, in this manner, maps the observed flow pattern to the pressure drop- flow rate relation [9][10].

At high flow velocities and for smaller particle sizes, the flow pattern (regime) is said to be *homogeneous* in which all particles are evenly dispersed in the fluid medium. All the solids in this regime are in suspension. Pressure losses in homogeneous regime are excessively high so that this regime is avoided in practice.

As the velocity of flow decreases and (or) the particle size increases, the flow pattern becomes *heterogeneous*. This pattern is marked with vertical concentration gradient increasing towards the pipe bottom. In practice, some form of heterogeneous pattern prevails because slurries normally contain mixed sizes of solids and flow velocities fall within an acceptable range of pressure drop and reliable operation of a pipeline system.

Other patterns are observed at lower flow velocities or significantly coarser solids. *Moving bed* and *stationary bed* patterns are observed as the flow velocities are lowered beyond the industrially acceptable limits. Moving beds appear as the fluid partially fails to suspend part of the particles. Instead, they crawl at the pipe bottom. Stationary bed marks the total failure of fluid to suspend particles. Thus, a permanent bed of solids settles at the pipe bottom. The solids density maps the flow patterns settling tendency in a reverse relationship. Higher densities give rise to settling tendencies while lower densities assist in suspension. Moving and stationary bed patterns are avoided in industry as they produce higher-pressure drops, pose the dangers of pipe blockage and render the system operation unstable. These patterns may only be tolerated, in industry, if they do not interfere with the process continuity. Most of the applications in which these patterns may exist are those of one single mode of hydraulic transport of solids (such as a point-to-point coal

transport, loading/ unloading of minerals and dredging applications). Also, they naturally occur in rivers and gravitational flow applications. Hydraulic transport of solids in multi- modes between different unit operations cannot tolerate bed formations due to the necessity of changing the operating conditions of the separate production units to stabilize the yield and/ or the quality of the product (such as crystal growth, retention time for chemical/ physical processes, product washing and/ or purity).

It is worth mentioning that the distribution of solid particles in a real pipeline cross section could hardly follow a so clearly defined pattern as described above. A simple pictorial representation [11] (Figs. (1.1), (1.2)) reflects the complexity and randomness of these patterns. In fig. (1.1), the homogeneous pattern (a) represents small size particles at high velocity while (b) represents larger particle size and the last picture (c) represents a separated localized pattern. These patterns may well exist simultaneously in a real problem. Moreover, particles deposition is shown in fig. (1.2), it is apparent that the layer is forming in a crescent shape. The first picture shows a wider span of the sides towards the upper side of the pipeline cross section while the second picture shows a higher deposit at the bottom. Looking at longitudinal cross section of a pipeline (fig. (1.3)) [12], the picture shows distribution of solid spheres set in motion from rest until inception of turbulence (more pictures were reported by Govier and Aziz [13]). Combining the different possible shapes of the particles distribution in a three dimensional space, an irregular shape will accrue having different wavy entities of solids. The complexity of these flow patterns has been experimentally established by several workers [14]. Scarlett and Grimley [14] and Patanakar *et al* [12] reported experimental results, using optical techniques, showing spatial heterogeneity of the concentration distribution of solids in a pipe cross-section. The complexity of these flow patterns is believed to result from the complex interaction between the properties of the suspension, the dynamic flow conditions and the pipe geometry (Rastiero [14] cites numerous references on the subject, though no account is given on how to resolve these complexities).

(a) Homogeneous Pattern

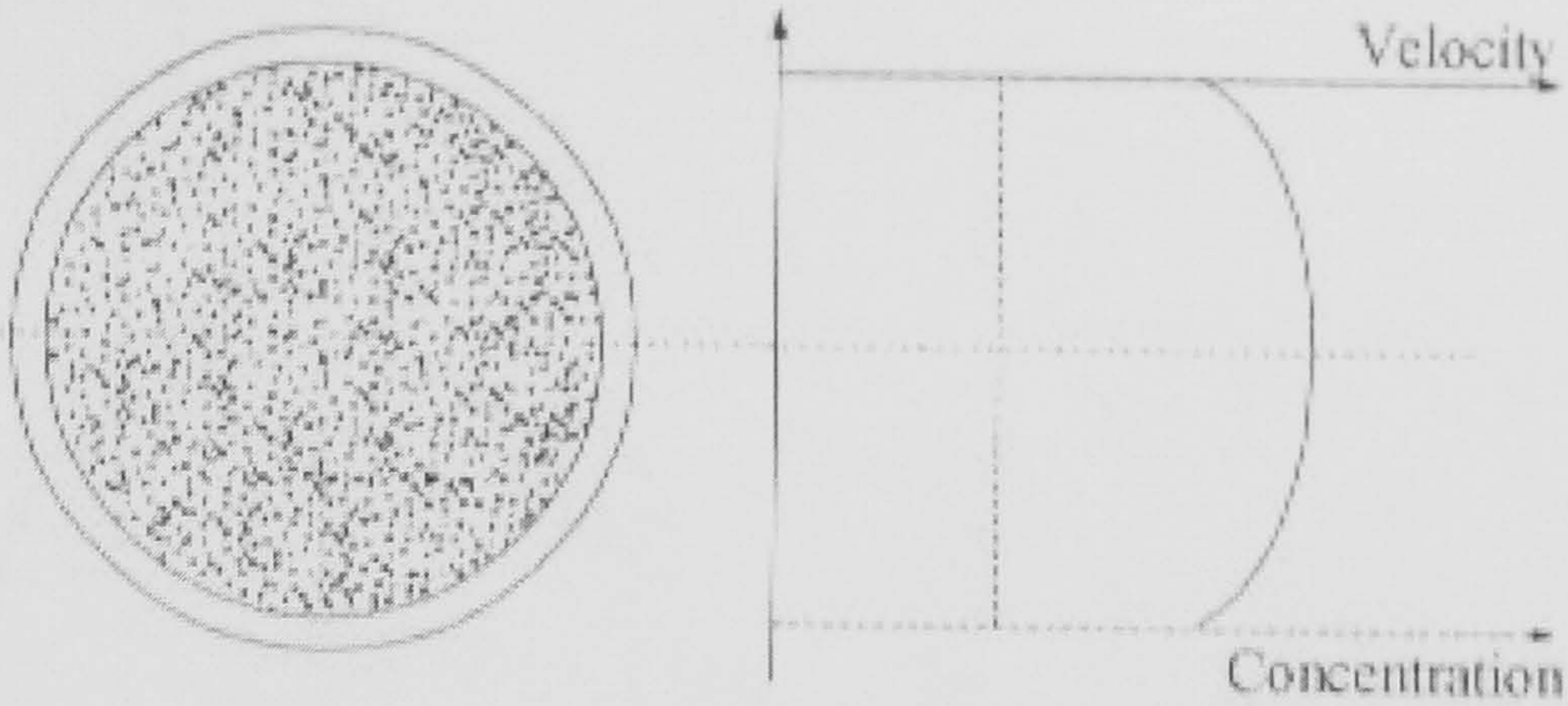

(b) Heterogeneous (Stratified) Pattern

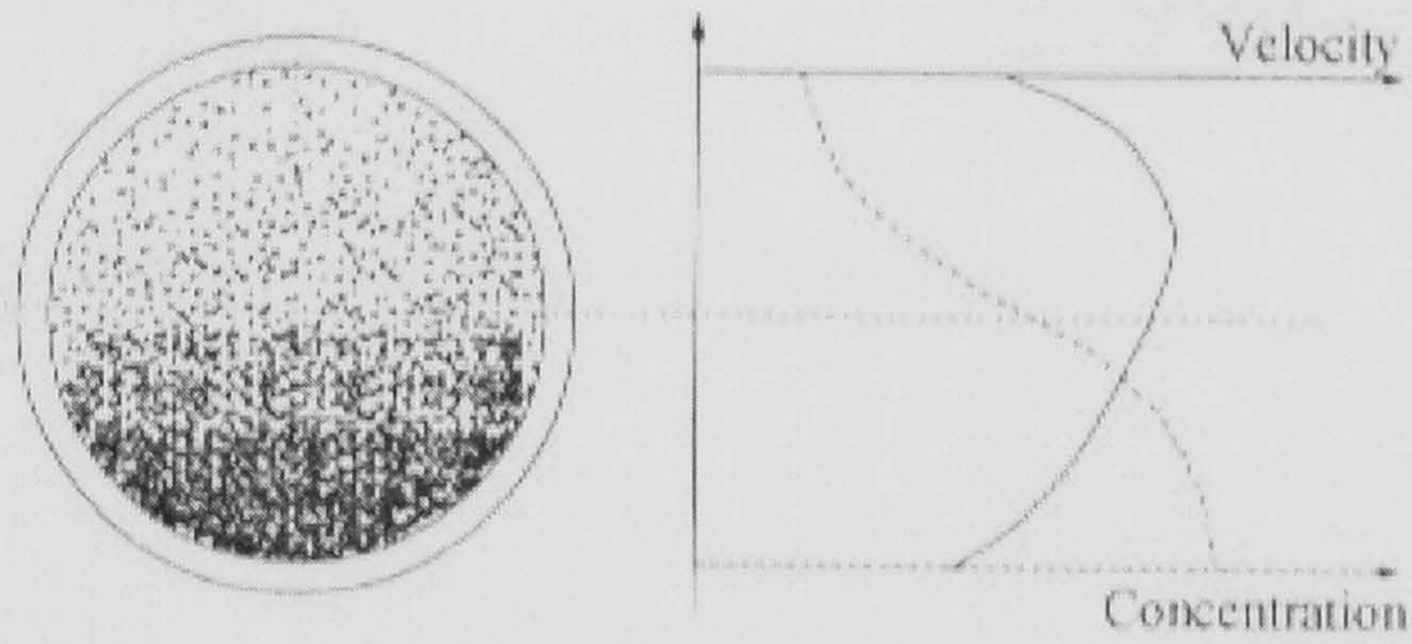

(c) Roping Pattern

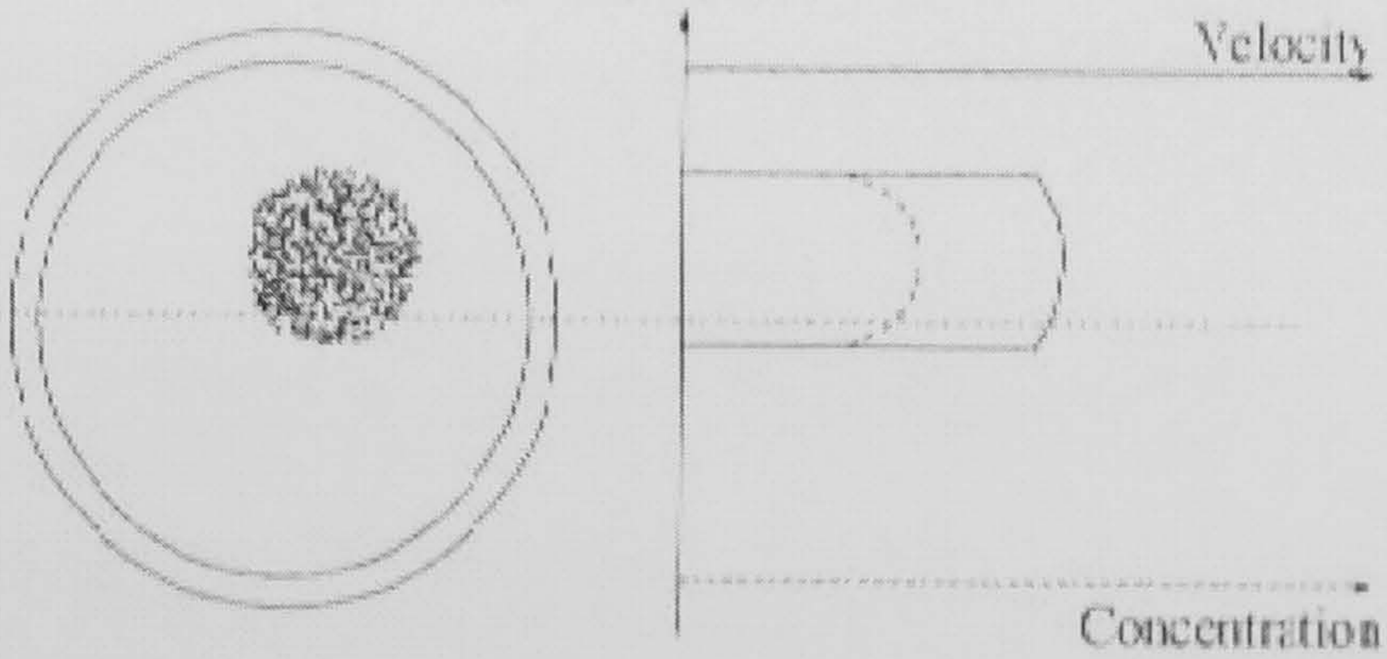

_____ Velocity ---------- Concentration

Fig. (1.1) Pictorial Examples of Solids and Velocity Distributions in a Pipe Cross- Section [11]

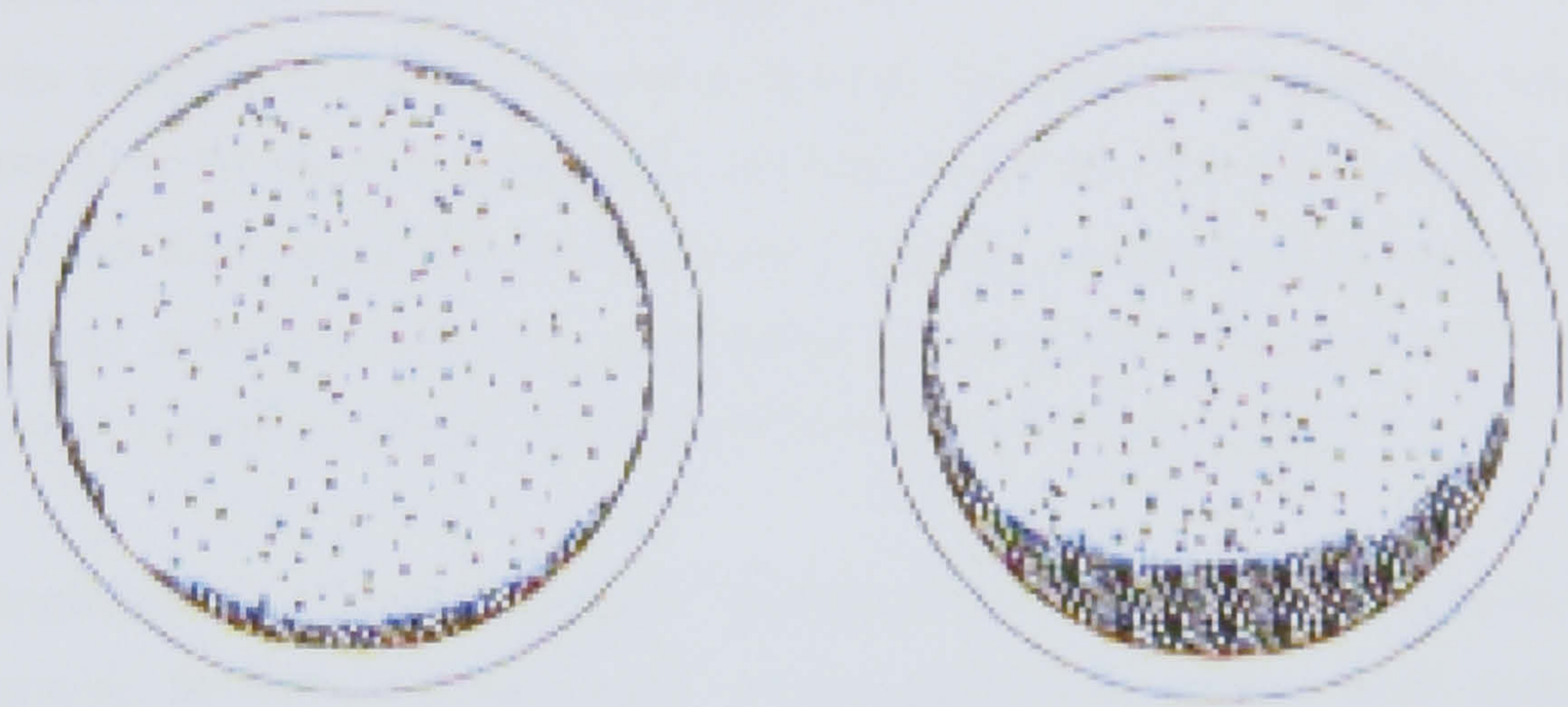

Fig. (1.2) Pictorial Example of Particles Deposition [11]

Fig. (1.3) Pictorial Example Solids Distribution in a longitudinal Pipe section [12]

1.4. Problem Statement

Slurry, by definition, is a mixture of solid particles and liquid carrier. This mixture is set to motion by the energy supplied to the fluid stream by some form of pumping equipment. In turn, the fluid stream imparts some of its energy to the solids. If the energy supplied to the fluid stream is stopped, the stream will gradually become stagnant. At the same time, the solids will take some form of trajectory motion until they loose their energy and settle at the pipe bottom. A static liquid column cannot move nor suspend solids for a considerable period of time. Thus, the solid-liquid system is a dynamic one and can be physically defined by its variables.

A single particle is dragged along by the fluid stream and is pulled downwards, due to gravity, by its submerged weight. In the existence of turbulent fluid, turbulent eddies produce upward forces that counteract part of, or all of, the settling effect of the submerged weight of the particle depending on the intensity of turbulence and size and shape of the solid particle. Thus, the particle experiences translational motion in some form of suspension. Due to the imperfections in the geometrical shape of the particle and the chaotic motion of the turbulent eddies, the particle starts to rotate and sway in a random manner. Statistically speaking, the combined motion of this single particle will lead it to sporadically collide with the pipe boundary and rebound away. The frequency and nature of collisions with pipe boundary under turbulent flow conditions is random. If one of these collisions is magnified, many probable patterns of contacts with the pipe wall may be observed. The particle may slide for some time on the boundary, may roll on it and (or) may just ricochet away from the pipe wall. Most probably, a combined form of contact may be observed. Furthermore, the particle has to squeeze away some of the liquid as it approaches the pipe wall.

For multiple of particles, the picture is more complicated. The particles move in a nebular like pattern and randomly interact with themselves and the boundaries. They contact each other while sliding or rolling over or around themselves. The frequency of these collision contacts is increased among themselves and the pipe boundary. They disperse and diffuse while dragged along with the fluid stream. Due to

increased number of particles, they experience motion in confined neighbourhood. Thus, introducing an even more complex motions and modifying the way they are dragged, uplifted, and collided within themselves and the boundaries.

Solids exist in various shapes and sizes in slurries. This further complicates the nature of contact collisions. Coarser and heavier particles will be reluctant to move after a collision in the same way that smaller and lighter particles would move. A larger particle blocking the way of a smaller one may captivate the smaller particle and stay attached to it. On the other hand, a larger particle gaining higher momentum may rollover a smaller one making the path easier for the larger particle. In case of high concentration of mixed sizes, layer movements may be expected with intricate motions. Smaller particles may serve as a smoother boundary for the coarser ones. The smaller particles are more prone to be carried upwards by turbulence and, thus, may give leverage to increased upward motion of the neighbouring coarser ones.

Added to this random state of motion are the effects of the fluid stream properties. Fluid experiences shear stresses of various intensities depending on its viscosity, velocity of flow, the disturbances due to solids and the roughness of the pipe boundaries. These stresses give rise to turbulence and the existence of solid particles disrupts the shape of an already random-turbulent fluid flow pattern.

The random motions of solid particles and their interactions with themselves and the pipe boundary (just described) consume additional energy when compared with the fluid alone in the form of increased pressure drop across a given pipe length. The only source of energy supply is the fluid stream that must continually maintain some kind of a flow. Industrially, flow has to be made steady as much as practicable.

The slurry flow problem just described is a multi variable extremely random one. As such, it is unthinkable to try to find an analytical solution. Instead, a well thought experimental work might offer a workable solution.

The existence of small and large particle sizes in slurry simultaneously is common in

industrial applications. As shown above, additional interactions take place due to the coexistence of more than one particle size. However, prediction of pressure losses for this kind of slurry (sometimes called polyfractional slurry) is much needed by pipeline designers.

Under the given conditions, it is required to set up an experimental program that correlates the pressure losses with the solid liquid flow system variables for polyfractional slurries. This program must highlight the impact of the added complexity, due to the existence of more than one particle size, in slurry flow.

1.5. The Aims

The aims of this research exercise may be summarized as follows:

a) To carry out a comprehensive literature review in order to understand the state of the art related to the problems of slurry flow.

b) To examine, experimentally, the relation between the slurry system variables through carefully designed experiments. The experimental program includes the synthesis of polyfractional slurry containing finer and coarser fractions at different concentrations and the measurement of pressure losses across a given length of a horizontal pipe, of 6" diameter, for a measured range of flow rates (50 to 200 cubic meters per hour).

c) To utilize a combined methodology embracing the prescription of a preset program of experiments and the use of dimensional analysis to reduce the number of variables to a fairly manageable size. This combined approach is expected to reduce the amount of experimental work and highlights the interactions between different variables.

d) To develop a pressure loss coefficient that leads to a more reliable prediction method for the pressure losses in horizontal pipelines for polyfractional slurry containing a finer fraction coexisting with a coarser fraction of solids.

Chapter 2

Literature Review

2.1. Introduction

2.2. Transport of Solids in Heterogeneous Regime

2.3. Transport of Solids Containing Moving Beds

2.4. Transport of Multi- Sized Solids as Polyfractional Slurries

2.5. Main Observations on the Reviewed Literature

2.6. Justification of Aims

2.1. Introduction:

Literature on slurries may be broadly classified into those treating *non-settling* slurries and those treating *settling* ones. The first category deals with rheology of pseudo liquids while the second category deals with mixture of solids of considerable particle size. The treatment of *non-settling* slurries as a separate category is considered out of the scope of this work, as it does not serve the goals of the sponsoring body of this research exercise.

Analytical solution of the solid liquid flow system requires defining the many variables involved and their functional relationships. The state of knowledge is still far from being capable to render the solid liquid flow system amenable to analytical solution. This has been reported clearly in literature and has become a common knowledge. Previous work was, by a vast majority, experimental and empirical in nature.

Much work was done for the prediction of pressure losses in slurry flow. The importance of the issue to industry, the complexity of the solid liquid flow problem and the various inconsistencies found in the developed empirical correlations could be enumerated as the main reasons for the continued interest in the pressure losses associated with slurry flow. It could be, theoretically, argued that empirical correlations have the shortcomings of their limited use to the experimental data for which they were developed, nevertheless, they still form the most convenient method for research work in the field of slurries. Dimensional analysis is, normally, used to reduce the number of variables to a reasonably manageable size and to correlate the pressure losses to physically meaningful parameters. Generally speaking, much of the reported experimental work on slurries pressure drop concentrated on single particle size, at various concentrations and of perfect particle shape (mostly perfect spheres). As such, polyfractional slurries (coexistence of more than one particle size) were not well represented in the previous work. Moreover, the general trend in research is invariably similar.

As a general observation, in a real hydraulic design problem of a pipe network conveying slurries, a designer is left to decide on a design velocity out of over sixty correlations [15]. Others reported similar comments about the diversity of results in obtaining pressure losses for slurries [16]. [17].

2.2. Transport of Solids in Heterogeneous Regime:

Heterogeneous regime is, statistically, the most suitable means of slurry transport in industry for the relatively coarser particles. It incurs reasonably lower pressure losses compared with bed flows on one extreme and homogeneous flows on the other. Bed flows need more energy to overcome the contact friction with the pipe boundaries and between the particles themselves while homogeneous flow requires high operating flow velocities, thus, higher energy to sustain particles in complete and evenly distributed pattern. Still, more importantly, bed flows pose the threat of blockages and operational instabilities in pipelines. Bed flows, in industry, may only be tolerated in the pure transport applications between a loading point and a reception/ piling facility of solids while in process applications where different production units are involved, solids can at best be allowed to flow heterogeneously.

A collection of some empirical correlations for predicting pressure losses associated with heterogeneous flow is shown in table 2.2.1. Among many investigators, Zandi, [1] Govier and Aziz [13] and later Pirie [4] and Turian *et al* [5] reviewed and tabulated many of the empirical equations pertaining to heterogeneous flow regime. These correlations, mainly, apply to slurries containing solids of uniform shape (perfect spheres) and single particle size.

To identify this flow pattern, a criterion was needed. Durand [2] took the particle size and defined an upper limit of particle size of 2 mm above which settling occurs while Zandi and Govatos [11] used the free falling velocity of the solid particle (terminal velocity) below 0.174 mm/sec instead. Further on, critical velocity was defined below which a crawling bed of solids appears at the pipe bottom indicating a change of flow pattern (regime).

The physical basis for these correlations attributed the excess pressure loss observed, due to the existence of solids, to the extra work needed to keep the solid particles in suspension (completely or partially). Thus, the pressure gradient in slurry is assumed to be that of liquid plus excess gradient due to solids, mathematically:

$$i_m = i_l + i_s \qquad (2.1)$$

Where i_m is the pressure loss for the slurry (mixture), i_l is the pressure loss for liquid alone and i_s the excess due to solids (all in meter liquid per meter of pipe length). Table (2.1) summarizes the empirical equations that were most frequently used. Universally, a pressure loss coefficient (ϕ) was functionally related to a non-dimensional flow number (ψ) (a combination of a modified form of Froude number and the coefficient of drag), thus:

$$\phi = k\psi^m \qquad (2.2)$$

Where $\phi = \dfrac{i_m - i_L}{C_v i_L}$ And $\psi = \dfrac{V^2 C_D^{0.5}}{gD(S-1)}$

Where C_v is the void that solids occupy as a percentage of a measured volume of slurry (volumetric concentration), V is the mean velocity of flow, C_D the coefficient of drag for a particle, D the pipe diameter and S the specific density of solids.

Experimental evidence showed poor degree of fit in these correlations. Zandi [11] compiled experimental data, calculated the pressure loss for the same conditions and concluded that a pipe designer may end up with a prediction of pressure losses that are too high or too low by as much as 67%. Another compilation by Pirie [4] indicated up to 83% . error. In an attempt to enhance the fit of the Durand correlation, Zandi and Govatos [1] attributed the inaccuracies to the inability of Durand to separate the settled part of the particles from the suspended part and proposed a dimensionless number (N_l) analogous to Reynolds as a separation criterion, thus:

$$N_J = \psi \quad , \qquad \text{for} \quad N_J < 40 \quad \text{all solids are in suspension}$$

$$\text{for} \quad N_J > 40 \quad \text{solids start settling} \qquad (2.3)$$

On the same issue, Babcock [18] reported N_J of 10 as a separating criterion. In both cases improvements in prediction were reported. Later on, Pirie [4] and Khan *et al* [19] collected a great number of experimental data from the published literature for various particle sizes, pipe diameters, carrier liquids, solid materials and concentrations. They made log plots of dimensionless pressure gradient versus a modified form of Froude number. The results showed poor fit indicating loss of correlation. According to Khan *et al* [19], a variation of 4 fold was observed. However, original data and their sources were not reported.

Another issue, that seems to have not been adequately resolved, is how to predict pressure losses for slurries with more than one particle size. Recommendations were made to employ an average size characteristic based on the coefficient of drag, summarized in table (2.2). But still the accuracy of prediction of pressure losses falls within the accuracy limits of the individual correlation used and in the absence of fine solids [1]. Noting that averaging methods did not yield satisfactory results, Wasp *et al* [20] used successive calculation of pressure drops for each size and sum up to obtain the total drop. The underlying assumption was that pressure drop due to each particle size is invariantly dependent on their corresponding sizes. Obviously, this assumption ignored the interaction that may exist between finer and coarser solids.

Experimental observations of Sobota [21] and Fangary *et al* [3] in two separate works showed that fine particles, when existing along with coarse particles, cause a reduction (or increase) of pressure drop depending on their ratio in the mixture. However, definitive ratios were not reported.

To resolve the discrepancy found in the their prediction method for the fine particles combining with liquid to form a pseudo liquid, Wasp et al [20] proposed a separating criterion in the form of a concentration distribution [20]. The following equation that represents a logarithmic relation was proposed:

$$\frac{C}{C_A} = \exp\left(-1.8U_t / kU_*\right) \qquad (2.4)$$

Where C is concentration near the pipe top (homogeneous part), C_A is the concentration at the middle of the pipe (heterogeneous part). U_t the terminal velocity. k von Karman constant and U_* ($(f/2)^{0.5}$) is the friction velocity (f is Fanning friction factor). No recommendations were given on how could the concentrations be measured or predicted or on what proximity of the pipe middle should the concentration C_A be considered. The work of Wasp *et al* concentrated on excluding the effect of fines by simply combining them with the fluid.

On the same lines, Charles and Charles [22] reported pressure drop decrease due to China Clay (extremely fine material) in sand of around 35% concentration while Kenchnington [23] reported pressure drop increase for virtually same material and concentration.

In a more recent review to delineate the different flow regimes, Turian *et al* [5] compiled published data and proposed an extended pressure drop correlation scheme that denotes a separate formula for each regime.

For the flow with stationary bed:

$$f - f_w = 12.127C^{0.7389} f_w^{0.7717} C_D^{-0.4054} \left[\frac{I'^2}{Dg(s-1)}\right]^{-1.096} \qquad (2.5)$$

For saltation flow (starting of moving bed formation):

$$f - f_w = 107.09C^{1.018} f_w^{1.046} C_D^{-0.4213} \left[\frac{I'^2}{Dg(s-1)}\right]^{-1.354} \qquad (2.6)$$

For heterogeneous flow:

$$f - f_w = 30.115C^{0.8687} f_w^{1.2} C_D^{-0.1677} \left[\frac{V^2}{Dg(s-1)} \right]^{-0.6938} \tag{2.7}$$

For homogeneous flow:

$$f - f_w = 8.538C^{0.5024} f_w^{1.428} C_D^{0.1516} \left[\frac{V^2}{Dg(s-1)} \right]^{-0.3531} \tag{2.8}$$

Where f and f_w are the Fanning friction factors for slurry and water, C is the volumetric concentration of solids, C_D is the coefficient of drag, V is the mean flow velocity, D is the pipe diameter, g is the gravitational acceleration and S is the ratio of solids to liquid density.

The study of these formulae reveals that, for the saltation regime, the numerical coefficient assumes a high value that decreases as the regime changes to heterogeneous and homogeneous (continued increase of flow rate) reflecting higher losses with bed formation. The exponent of solids concentration decreases indicating decreased effect at higher flow rates, which contradicts most of the correlations reported (see table 2.1). The exponents for the Fanning friction factor and the coefficient of drag show a marked increase with flow rate. Previous work [19] imposed limitations on the increase of the coefficient of drag. The coefficient of drag is less sensitive to flow changes for large particle size but this is not reflected in the above equations. Turian *et al* [5] extracted data for their review from numerous sources that were not reported, which gives no means of knowing what the different experimental conditions were or how they were interpreted.

Also, Turian *et al* [5] compiled correlations of critical velocities from many sources in tabulated form. The tabulated relations of critical velocity versus the different flow parameters showed substantial variations. They concluded that critical velocity is not particle size dependent but it corresponds to the square root of the pipe diameter; increases with the increase of concentration and then decreases. This was attributed

to hindered settling. As the mass of the solids increases, the settling is hindered due to increased particle interaction with concentration. The independence of the critical velocity from the particle size does not agree with the results of other workers. For example, Wilson [24] proposed a relation in which the particle size was represented in terms of the terminal velocity and appeared in the exponent of the exponential:

$$V_t = 0.6U_t\sqrt{\frac{2}{f}}\exp^{\frac{45d}{D}} \qquad (2.9)$$

Where V_t is the critical velocity for suspension, U_t is the terminal fall velocity and f is the fanning friction factor.

It is worth noting that nothing was mentioned in the work of Turian *et al* [5] about slurries with multi sizes (polyfractional slurries). Also, Pirie [4] restricted her investigations to slurries of single-sized particles.

More recently, previous empirical correlations were challenged on the basis of an increasingly emerging experimental evidence of their inadequacy to provide an insight into the flow structure [25]. Wilson [26] reported that Durand famous equation overestimates pressure losses at the lower range of operating velocities while the same equation underestimates the losses at higher velocities.

Table 2.1. Empirical Equations for Slurry Flow (Correlation form $\phi = K\psi^{M}$)

No	Investigator/Reporter	Ref	K	M	Remarks
1	Durand *et al*	[1]	180	-1.5	Experimental, F_L is a charted function of d_p and C_v up to 15%, $V_c > F_L\sqrt{2gD(S-1)}$
2	Newitt *et al*	[1]	$\phi = 1100\frac{gD}{V^2}\frac{U_t}{V}(S-1)$		Experimental, $1800gDU_t > V > 17U_t$
3	Zandi and Govatos	[1]	6.3 280	-0.35 -1.93	for $\psi > 40$, Analysis of published data for $\psi < 40$
4	Chhabra and Richardson	[19]	$0.3\ f_L$	-1	Experimental, Non-Newtonian carrier liquid (not reported)
5	Gaessler	[4]	$\phi = (f_s\ f_w)(S-1)$		Experimental, f_s, f_w are solids and liquid friction
6	Pirie	[4]	55.6	-1.08	Experimental, single sized, coarse
7	Fangary et al	[3]	$\phi = 131Fr^{-1.2}$ $\frac{i - i_f}{C_v(1-C_f)} = 96\left(\frac{V^2}{gD(S-1)}\right)^{1.18}$		Experimental, coarse particles Experimental, fine particles

$\phi = \frac{i_m - i_l}{i_l C_v}$ And $\psi = \left[\frac{V^2 C_D^{0.5}}{gD(S-1)}\right]$

Table 2.2 Averaging Methods of the Size Characteristic of the Particle

No.	Investigator	Ref.	Method	Remarks
1	Condolios and Chapus	[1]	$\sqrt{C_D} = \sum p_i \sqrt{C_{Di}}$	Where *Pi* is the weight percentage of the material of drag coefficient C_{Di}
2	Bonnington	[1]	$C_D = \frac{\sum C_{Di} p_i}{\sum p_i}$	
3	Fangary *et al*	[3]	d_{50}	The median particle size passing a sieve
4	Mishra *et al*	[27]	$d = \frac{\sum w_i d_i}{n}$	Weighted average of n particle sizes

2.3. Transport of Solids Containing Moving Beds:

Slurry flow with moving beds was investigated by many workers. The reason is, partly, to distinguish this pattern by identifying the velocity below which it is formed (critical or deposit velocity) so that the velocity of flow is kept reasonably higher than this value and partly because, in some applications not including centrifugal pumps as prime movers, it may be an economical alternative mode of slurry conveying for short distances if accompanied with extremely high solids concentration (single mode transport of solids in loading/ unloading and piling applications). To discern the existence of moving beds, many relations for the inception of bed formation were developed. Table 2.3 summarizes some of the critical velocity relations cited in the literature [1] [19] [4]. Televantos [28] reported results on moving beds at high solids concentration. Earlier works, reported by Televantos, [28] based on the measurements of Condolios and Chapus related the mean velocity above the moving bed to the hydraulic diameter of the pipe area above the bed, thus:

$$\frac{V'}{\sqrt{2gR_h}} = K \qquad (2.10)$$

Where V' is the mean velocity above the bed, R_h the hydraulic radius of the area above the bed and K is a function of the particle size and concentration. Televantos work [28] reported a 65% error in this relation. The same equation was used to detect inception of settling by substituting the full radius of the pipe in place of the hydraulic radius. In a previous work by Newitt *et al* (reported by Televantos), the pressure drop for moving beds was developed from the balance between the work done on the particles and the energy dissipation due to the excess pressure gradient, thus:

$$\frac{i_m - i_L}{C_v i_L} = 66(S-1)\frac{gD}{V'^2} \qquad (2.11)$$

Babcock [18] reported a correlation constant of 60.6 instead of 66 for 1-inch pipe and 6.6 for 6-inch pipe indicating dependence on pipe diameter. More recent experimental work on deposition by Gillies and Shook [29] correlated the deposition velocity (shown in table 2.3) to the carrier liquid properties, modified by the existence of fines, and the coefficient of drag as a replacement of the widely used Durand relation.

Newitt *et al* [30] were among the first to base their differentiation between solids contribution to pressure losses from that of liquid resistance on a physically based approach. Thus, pioneering what has come to be known as *mechanistic modelling*. Newitt *et al* divided the heterogeneous flow into two parts. The first is that of particles in suspension for which they attributed excess pressure gradient to re-suspension mechanism that overcomes the settling tendencies of solids as they approach their terminal fall velocity. Thus, their equation:

$$\frac{i - i_w}{i_w C} = 1100\left[\frac{V^2}{gD(s-1)}\right]^{-1}\frac{U_t}{V} \qquad (2.12)$$

The second part is that of particles moving at the pipe bottom for which they attributed excess pressure gradient to the force required to overcome the friction of the solids at the pipe wall. This mechanism balances the submerged weight of particles assumed transmitted to the pipe wall with the pressure gradient required for driving them. Equation (2.12) above gave this relation combined for both parts.

It was not until Wilson, and workers who followed, that mechanistic modelling took its shape. Wilson [31] used a force balance model for the determination of the limit deposit velocity for stationary beds. Further on, Wilson [24] developed his famous two-layer model. The basic features of the model lie in the assumption that solids divide themselves into a portion suspended by liquid (suspended load) occupying the upper part of the pipeline and a portion contacting the pipe wall (contact load) comprising the solids moving in continuous contact with the pipe bottom (moving bed) and solids moving in sporadic contact with the pipe wall (saltating solids). The concentration of solids was arbitrarily divided into two constant parts. The upper

concentration defines the suspended load while the lower concentration, contains most of the solids in a loosely poured form, and defines the contact load. Figure (2.1) shows the geometrical representation of the two-layer model. The geometrical representation shows an abrupt change of concentration at a single dividing line. This simplification can only be physically justified when all the particles move as one bed *en bloc*.

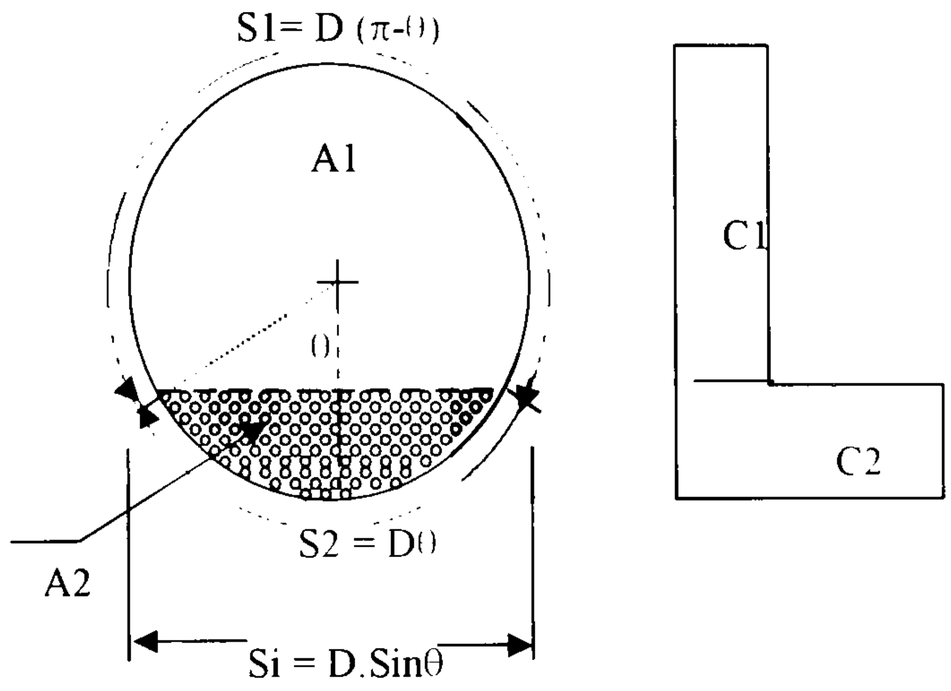

Fig. (2.1), Wilson Two-Layer Model Geometry

By conducting a force balance for the two layers, Wilson obtained the pressure drop for each layer in terms of the shear stresses experienced at the pipe perimeter of each area and at the virtual interface between layers. The set of equations are:

For the upper layer:
$$-\frac{dP}{dx}A_1 = \tau_1 S_1 + \tau_i S_i \tag{2.13}$$

For the lower layer:
$$-\frac{dP}{dx}A_2 = \tau_2 S_2 - \tau_i S_i + \mu_F \sum F \tag{2.14}$$

For the whole pipe:
$$-\frac{dP}{dx}A = \tau_1 S_1 + \tau_2 S_2 + \mu_F \sum F \tag{2.15}$$

Where A is the area, τ is the shear stress, S is the perimeter and $\mu_F \sum F$ is the sum of the normal forces exerted normally on the pipe wall leading to Coloumbic friction resistance and the subscripts denote the perimeters shown on fig. (2.1). The shear stresses are calculated using Fanning friction factor except for the shear stress at

transition that is calculated using rough boundary configuration. The normal forces are calculated from the submerged weight of the particles and the hydrostatic pressure of the fluid column.

The geometry of the two layers is determined by an empirical formula that determines the contact portion first and then the suspended portion is found by subtraction from the total solids concentration. The formula takes the form of a power law:

$$\frac{C_C}{C} = \left(\frac{V_i}{V}\right)^2 = \left(\frac{U_t}{V}\right)^2 \left(\sqrt{\frac{2}{f}}.0.6\exp(45\frac{d}{D})\right)^2 \qquad (2.16)$$

Where V_i is the velocity of incipient suspension and U_t is the terminal velocity and f is Fanning friction factor. Further on, Gillies et al [30] proposed a logarithmic empirical relation:

$$\frac{C_C}{C} = \exp(-0.0184\frac{V}{U_t}) \qquad (2.17)$$

Alternatively, Matousek [32] proposes to calculate the suspended fraction first and gave yet another formula. Khan and Richardson [33] report further formulas indicating disagreement between different authors on the method to separate the contact from the suspended load.

The second main flaw with the two-layer model is the calculation of the shear stress at the interface. The interface could not be as sharp as configured by Wilson but more realistically shall assume a gradual shape, which casts much doubt on this simplification physical significance. Also, the shear stress at the interface cannot be measured experimentally. Thus, the assumption of its friction behaviour cannot be based on measurable physical means. The only way possible for Wilson to overcome the inability to measure shear stresses at interface was through carrying out iterations of velocities of flow in both layers until an agreement between the pressure drops between layers was obtained. The process included the pre-assumption of a certain

friction factor at the interface (apparently for the sake of obtaining a converging solution of the iteration scheme rather than some solid physical justification). In an effort to assess the validity of the friction factor assumption at the interface, Riet *et al* [34] and Miedema *et al* [35] repeated the numerical iterations to solve the two layer model and concluded that the friction factor at the interface gives different results for different model input variables. In a recent work, Matousek [36] established experimentally in a series of lab tests on sand water mixtures the sensitivity of the friction factors at the pipe wall and interface to the suspension mechanism and concentration of solids. A closing remark on the two layer model, the flow velocity range in pipelines is well in the turbulent region, at least in industrial applications where considerable settling can not be tolerated and economical factors dictate smaller pipe sizes, thus the assumption of maintaining distinct layers is much in doubt. However, in open channel flow the layered model may gain more significance. Also, by definition, the two-layer model is for a flow with bed while in industry the pattern is more or less heterogeneous.

Doron *et al* [10] [37], in a series of papers, proposed a layered model based on that of Wilson's. The same problems apply to the division of the contact and the suspended load and the configuration of the transition layer (a layer added to the two layer model in an effort to extend the interface to a region rather than a line). Even more, Pirie [4] noted that Doron model was unstable when iterations were carried out.

Table 2.3 Deposit Velocity Criterion for Moving Beds

Investigator	Ref.	Criterion	Remarks
Durand	[1]	$V_C = F_L\sqrt{2gD(S-1)}$	F_L Is valid up to 15% concentration and is given by a family of curves. It is a function of concentration and particle diameter
Spell. K. E.	[1]	$V_c = \sqrt{\left[(2.53\times10^{-3})gd_p(S-1)\left(\frac{VD\rho_m}{\mu_m}\right)^{0.77}\right]}$	Valid for particle diameter (d_p) from 0.05 to 1.5 mm. ρ_m and μm are the density and viscosity of the mixture
Zandi and **Govatos**	[1]	$V_c^2 = \frac{40C_v Dg(S-1)}{\sqrt{C_D}}$	Babcock suggested coefficient of 10 instead of 40
Newitt *et al*	[1]	$V_c = 17\,U_t$	U_t is the particle terminal velocity. this relation is not verified extensively
Gillies and Shook	[29]	$F_L = \exp(0.165 - 0.073C_D - 12.5K_2)$. $K_2 = [K_1 - 0.14]^2$ and $K_1 = \left[\mu_L / \rho_L\sqrt{gd^3}\right]^{0.67}$	Obtained for particle size 0.15-4 mm. concentrations14-0.44 and pipe dia. 0.053-0.495 m
Turian *et al*	[5]	$\frac{V_c}{[2gD(S-1)]^{0.5}} = 8.948C^{0.4779}C_D^{-0.0272}\left(\frac{D\rho[gD(S-1)]^{0.5}}{\mu}\right)^{-0.1174}$	Wide range of collected data

2.4. Transport of Multi- Sized Solids as Polyfractional Slurries:

Literature reviewed so far did not give sufficient credit to polyfractional slurries Normally, the total concentration of solids is taken into consideration for only one particle size obtained by some averaging method. Several workers [3] [20] [21] [22] [23] [25] noted that mixed sizes of solids give rise to unexpected effects on pressure drop but, unfortunately, few made further investigations [3] [21]. However, Matousek [38] puts it clearly that little is known about the flow behaviour of mixtures composed of two or more sand fractions that differ in size.

Fangary *et al* [3] obtained experimental results that clearly showed that for the same total concentration, varying the ratio of coarse to fine particles gave different pressure drops. Their main observations were that increasing the content of finer particles increases the pressure drop while a mix of both fine and coarse tends to the behaviour of coarse particles. It is not to underestimate this experimental work, but it is difficult to infer reasonably accurate conclusions out of these results because the materials used in the experiments are widely graded, the finer particles were below 74 microns that, usually, combine with the fluid to form a fluid like behaviour, the upper range of particle sizes was limited to 250 microns (relatively fine size), the comparisons between different mixes were carried out at different total concentrations (ignoring the effect of the total solid content), the plots presented in the original paper of the experimental data and the proposed correlations are wide apart (correlations no. 7 in table 2.1).

Sobota [21] compiled data collected by others on polyfractional slurries and concluded that the fines combine with the liquid to form a carrier liquid of which the pressure drop is calculated by a fluid like model with modified density and viscosity. According to Sobota [21], coarse particles give an additional pressure drop contribution that is a function of their submerged weight, their concentration and the squared ratio of the flow to terminal velocities.

Thus:

$$\Delta P_c = f\left(\rho g(S-1), C, \left(\frac{V}{U_t}\right)^2\right) \qquad (2.18)$$

Where ΔP_c is the pressure drop due to coarse particles, C is the concentration of coarse particles and all other properties defined for coarse particles.

Algebraic form of the pressure drop relation was not reported. The division of particles in this manner separates only between the particles that combine with the fluid (usually smaller than 74 micron) and assumes the same characteristics to all the sizes above (reported particle sizes varied from 1 micron up to 50 mm). Experimental conditions and procedures were not mentioned.

Kazanskij *et al* [39] observed that the addition of fines to coarse dredged materials showed decrease of pressure drop but then an increase was observed at higher velocities. At lower velocities in the heterogeneous regime, they attributed the decrease to "lubrication effect" of the fine particles on the coarse particles. At higher velocities, they assumed that a pseudo-fluid was formed increasing the pressure drop. Only comments and a set of curves were given. No correlation or modelling was reported.

In a relatively more elaborate laboratory investigation on the economy of transporting broadly graded sand- water mixtures, Matousek and Ni [40] concluded that the addition of finer solids to the mixture decreases pressure losses in mixtures exhibiting partial stratification while increases the pressure losses in those having negligible stratification. Unlike other workers who attributed the behaviour of finer particles to either increased density of the carrier liquid or their lubrication effect, Matousek and Ni [40] divided the effect of fine particles between a reduction of mechanical friction and an increase in the viscous friction taking place at the same time. No quantitative relationships were shown. Deeper examination of their work reveals that two mixtures were tested (fine- medium and fine- coarse mixtures); the hydraulic gradient only decreased at lower flow velocities and increased markedly

higher with the fine- medium mixture at higher flow velocities. the concentration profiles showed more uniform distribution for the fine- medium slurry and the deposition velocity gave contradicting trends (lower for fine- medium and higher for fine- coarse slurries). On the same lines, Matousek [38] reported that near the pipeline wall, a liquid lift was observed that seemed to affect the coarser particles only.

Many researchers avoided dealing with the coexistence of finer and coarser particles in slurries. Ijadi and Streat [41] noted that the existence of fines in coarse coal resulted in head loss over prediction and left it as a safety margin in pipeline design calculations. Gillies *et al* [25] reported similar situation in which clay was removed from the mixture to avoid complicating their model unnecessarily. Pirie [4] limited her investigations to slurries having coarse single particle size.

2.5. Main Observations on the Reviewed Literature:

a) The vast majority of the literature reviewed conducted experimental work on single particle size slurries. Even when multi sizes existed, averaging of properties was carried out without supporting experimental evidence.

b) In the few examples, observed in the literature, the treatment of the interactions between the different sizes and their effect on the pressure drop was not the main aim of research. Instead, the separation of the sub 70-micron fraction was targeted so that it can be combined with the fluid.

c) It has been repeatedly reported that the existing empirical correlations suffered from the lack of fit while the improvements sought through mechanistic modelling did not yield reliable predictions due to the inherent difficulties in the prediction of shear stresses at the interface transition region and the drastic simplifications of the shape of the concentration distribution profile.

d) The physical understanding of the turbulent processes is still lacking and, thus, a reliable solution based on physical laws is not foreseen in the near future.

2.6. Justification of Aims:

a) The literature review revealed many observations on the previous work that casts more light on the complexity and the random nature of slurry flow. Under virtually similar conditions, numerous outcomes of pressure drops emerge when using different formulas reported in the literature (in the part on economical considerations, ch.1, these differences have been clearly illustrated through solving a typical example).

b) It is necessary to address the polyfractional slurry flow as it is not sufficiently covered in the previous work and because it bears significant importance in industrial applications.

c) A suitable method is needed to enable separation of the different interactions encountered in polyfractional slurry.

d) A fairly reliable design tool is still lacking due to the confusion on which prediction method to use. The available correlations to the pipeline designer are numerous without any means to select any particular one.

Chapter 3

Theoretical Background

3.1. Introduction

3.2. The Principle of Continuity (Mass Conservation)

3.3. The Force Balance on a Control Volume for a Clear Liquid

3.4. The Force Balance on a Control Volume for Solid- Liquid Flow

3.5. Physical Description of Solid- Liquid Flow

3.1. Introduction:

The governing relations controlling fluid flow in general and slurry flow in particular are elucidated by theories that explain their nature. A representative control volume is chosen on which mass and momentum balances are derived. Due to the complex nature of fluid flow problems, simplifying assumptions are unavoidable. Also, alternative physical representations are sometimes employed to further simplify the problem. Moreover, empirical correlations become necessary to develop functional relations for pressure losses associated with flow. Under all cases, a theory is needed to form the ground of work.

The following treatment summarizes some of the more general theoretical issues, critically discusses the underlying assumptions, highlights the difficulties from a physical point of view and ends up with a working physical description that forms the basis for experimental work.

3.2. The Principle of Continuity (Mass Conservation):

The flow of a liquid in a horizontal pipeline is described by the properties of liquid (density and viscosity), flow velocity and pipeline boundary (pipe diameter and pipe roughness). The basic assumption in this flow problem is that flow is continuous. Taking a control volume and following a flow path in space and time, the continuity principle (mass conservation) can be described mathematically:

$$\frac{\partial \rho}{\partial t} = -(\nabla \rho V) \qquad (3.1)$$

The rate of change of mass per unit volume ($\frac{\partial \rho}{\partial t}$) is described by the mass flow rate per unit area in space ($\nabla \rho V$). For liquids, it can be safely assumed that the control volume is inelastic and the density is constant (incompressible under normal working velocities). Under steady flow conditions, transient pressure surges are assumed nonexistent.

Thus, the continuity equation reduces to:

$$(\nabla V) = 0 \tag{3.2}$$

The representation of flow as a continuum is basic to the solution of flow problems for single fluids. For slurries (liquids carrying solids under motion), the continuity assumption holds physically true for the carrying liquid only. The solid particles travel as discrete entities within the body of the liquid continuum (they have their own density and do not deform the same way as liquids). However, as the interest is concentrated on the global effect of slurry flow on the pipeline (as a pressure drop), it can be assumed that slurry is, also, a continuum. Thus, the continuity equation per unit volume for constant densities of liquid and solids becomes:

For Liquid fraction:

$$\frac{\partial}{\partial t}(1-C)+\nabla[(1-C)V_L]=0 \tag{3.3.a}$$

For Solids fraction:

$$\frac{\partial C}{\partial t}+\nabla(CV_s)=0 \tag{3.3.b}$$

Where C, V_L, V_S and (∇) are the fractional volumetric concentration of solids (solids fraction), the velocity vectors for liquid and solids and ∇ is the three-dimensional space operator respectively. Under the assumption that the rate of change of concentration is time invariant, the time related differential vanishes.

3.3. The Force Balance on a Control Volume for a Clear Liquid:

The next step in the description of the physical nature of the control volume, following the path of liquid flow, is considering the forces acting on it. The control volume gains energy from the flow and expends it to overcome the pressure and

viscous forces as experienced on its boundaries and, still, the control volume falls under the effect of its own weight.

Mathematically, the force balance follows the steps of Newton's second law of motion:

$$\begin{pmatrix} Rate\ \ of\ \ Change \\ of\ \ Momentum \end{pmatrix} = -\begin{pmatrix} pressure \\ force \end{pmatrix} - \begin{pmatrix} viscous \\ force \end{pmatrix} + \begin{pmatrix} gravity \\ force \end{pmatrix}$$

$$\rho \ \frac{Dv}{Dt} = -\nabla \ \ p - (\nabla \ \tau) + \rho \ . g \qquad (3.4)$$

For steady flow conditions, external forces (accelerating and decelerating flow) do not exist under the assumption that the flow is fully developed, thus,

$$\nabla p + (\nabla \tau) = \rho g \qquad (3.5)$$

This indicates that the force balance within the flow is a competing mechanism between the pressure forces experienced across a pipe length and viscous forces developed within the flowing medium. Turbulent flow regime is marked by the formation of turbulent eddies, that are random in nature. The intensity of turbulence depends on the effect of viscosity on velocity of flow. This is translated in velocity variation in a given pipe cross section. Also, due to inertia, the flow continuum is reluctant to velocity changes. Under turbulent conditions, the relationship between the velocity distribution and viscous shear stress (τ) cannot be found analytically due to the random nature of turbulence and the complexities with the inertial- viscous interactions. Thus, analytical solution does not exist for this basic and relatively simple flow problem. Instead, Reynolds developed his famous inertial to viscous forces empirical relationship that uniquely marks the flow number expressing the changes from laminar to turbulent.

$$\mathrm{Re} = \frac{\rho V D}{\mu} \qquad (3.6)$$

Where Re is Reynolds number, ρ is the liquid density, V is the average flow velocity, D is the pipe diameter and μ is the liquid viscosity.

Furthermore, the interaction of liquid with the pipe boundary results in pressure loss expended on the account of the kinetic energy of the flow. This, in turn, can only be empirically determined through the formulation of a pressure loss coefficient as a non-dimensional parameter f (commonly known as Fanning friction factor), thus,

$$\frac{\Delta p A_c}{\frac{1}{2} A_l \rho . V^2} = f \tag{3.7}$$

Where A_l is the wetted surface area for a given pipe length

If the pipe boundary enclosing the liquid is not completely smooth, the effect of surface texture roughness of the pipe wall (ε) will further complicate the friction factor.

Summing up, an empirical relation (Colebrook-White equation) [*] is drawn up to relate the turbulent flow regime in terms of Reynolds number and the friction factor so that the pressure losses can be predicted for a pure liquid (water) under turbulent conditions, thus,

$$\frac{1}{\sqrt{f}} = -4 \log \left\{ \frac{\varepsilon}{3.71D} + \frac{1.26}{\mathrm{Re}\sqrt{f}} \right\} \tag{3.8}$$

[*] Munson, B.R.,Young, D.F. and Okiishi, T.H. "Fundamentals of Fluid Mechanics". Third Ed. John Wiley and Sons. Pp. 494 (1998)

As Reynolds number tends to infinity, friction factor becomes a function of the pipe diameter D and pipe wall roughness (ε) only and the friction factor becomes less dependent on Reynolds number. For design purposes, Moody constructed a log-log

plot of the friction factor against Reynolds number for clear water at different pipe roughness to diameter ratios.

Up to this point, only the empirical advent of Reynolds number (marking the flow regimes), the formulation of the pressure loss friction factor and their coupling for turbulent conditions made it possible to empirically solve the problem of clear liquid flow.

In a pipeline design problem, usually, either the flow rate or the permissible pressure drop is given; liquid properties and pipe geometry are known. Then Reynolds number is calculated and the friction factor is found iteratively from Colebrook-White equation. Thus, pressure drop (or flow rate) is determined and hydraulic power is found. The final design may include optimisation between the cost of the pipe size and power consumption.

3.4. The Force Balance on a Control Volume for Solid- Liquid Flow:

Following the assumption that slurry flows as a continuum, momentum balance formally describes its motion in the form of a force balance on a given control volume. The main assumption, *apriori*, is that mass is conserved in the control volume. Momentum balance per unit volume is carried out for the liquid fraction and then for solids fraction. Mathematical representation using Cauchy [27], [42], [43], [44], [45] momentum equation is as follows:

For Liquid Continuum is:

$$\underbrace{\rho_L \frac{\partial}{\partial t}(1-C)V_L}_{\text{Rate of change of Momentum}} = \underbrace{-\rho_L V_L \cdot \nabla[(1-C)V_L]}_{\text{Convective term}} - \underbrace{\nabla[(1-C)P_L]}_{\text{pressure force}} - \underbrace{\nabla[(1-C)\tau_L]}_{\text{viscous force}} + \underbrace{(1-C)\rho_L g}_{\text{Gravity force}} + \underbrace{M_L}_{\text{interactio term}} \qquad (3.8.a)$$

For Solid Continuum is:

$$\underbrace{\rho_s \frac{\partial}{\partial t} CV_s}_{\text{rate of change of momentum}} = \underbrace{-\rho_s V_s \cdot \nabla[CV_s]}_{\text{Convective term}} - \underbrace{\nabla[CP_s]}_{\text{pressure force}} - \underbrace{\nabla[C\tau_s]}_{\text{viscous force}} + \underbrace{C\rho_s g}_{\text{Gravity force}} + \underbrace{M_s}_{\text{interaction term}} \qquad (3.8.b)$$

For steady flow conditions, the rate of change of momentum with respect to time is zero.

Interaction terms represent the transmission of forces between liquid and solid particles, which are equal in magnitude and opposite in direction. Viscous force terms represent the shear stresses due to liquid viscous friction, particles collisions and particles friction with each other and with the boundaries. Body forces reflect the effects of gravity.

The momentum balances, given above, treat solids as if they are of the same nature as the liquid carrying them. Thus, in literature, they are termed liquid phase for the liquid fraction and solid phase for the solids fraction. Physically, such terminology applies to the same matter in different states (e.g. ice is the solid phase of water and steam is its gaseous phase). More correctly, instead of phases components should be used, thus, liquid component and solids component . The difference is not in terminology but in the physical nature of liquids and solids. Liquid is a pack of molecules having the same microscopic size , cohesive bonding and dynamic characteristics in terms of resistance to shear forces and influence of turbulence. Solids have totally different molecular structure ; their cohesive bonding is much higher than liquids and can stand much higher shear forces when compared to liquids. In particle form, solids keep a certain granular size and shape while liquids keep size and shape on molecular scale only. Obviously, the scale of measurement is totally different. Also, when examining a control volume to study the behaviour of slurries it is assumed that this control volume is homogeneous in representing the various properties of flow. In reality, a control volume in slurries is composed of two

components that possess substantial differences in their properties. The momentum balances do not give credit to these differences; instead solid particles are treated as if they were of the same nature as liquids (molecules of the same size, shape and dynamic properties).

Thus, momentum balance equations for slurries do not give information about the interactions of solid particles as separate (discrete) entities and liquid as a continuum and do not account for momentum exchange between the particles themselves. These issues greatly affect how shear stresses are viewed.

As stated earlier, the random nature of flow renders the equations of motion unsolvable analytically under turbulent conditions. Introducing solids into flow problems makes the analytical solution even more distant. To solve equations (3.8.a) and (3.8.b) it is necessary to know the concentration distribution, velocity distribution and pressure distribution as functions of space coordinates under effects of viscosity and turbulence. The distribution functions must take into account the effects of solid particle size and shape, their interactions with liquid and their collisions. These tasks can only be fulfilled under drastic simplifications (like assuming a certain concentration distribution, turbulence model and velocity distribution). Apart from the random nature of turbulence, which is closely related to liquid properties, energy imparted to solid particles most probably produces even more randomness in modelling turbulence. Also, the profiles that concentration distribution may assume are strongly dependent on the difference in densities between liquid and solids, the size(s) and shape(s) of the particles. Except under totally dispersed solid particles (homogeneous slurries of very low solid fraction) or mostly settled particles (bed flows), an assumption of a certain concentration distribution profile could hardly be justified from a physical point of view.

In the special cases where solids can be viewed as freely moving within the liquid continuum, the kinetic theory is employed to describe the motion of solid particles. The kinetic theory, as originally applied on gases, defines the equilibrium state of gas molecules as the statistical average state of balanced collisions among the molecules themselves [43], [46]. By analogy, equilibrium state has been extended to slurries to

include balanced collisions among the solid particles themselves and their interactions with liquid fraction (in statistical average sense). Adapting Boltzman equation to slurries, their motion can be mathematically expressed [43], [46]:

$$\frac{\partial f(V)}{\partial t} + v_i \frac{\partial f(V)}{\partial x_i} + \frac{\partial (F_i f(V))}{\partial v_i} = \left(\frac{\partial f(V)}{\partial t} \right)_c \tag{3.9}$$

Where $f(V)$ describes a velocity distribution vector function for the solid particles with respect to time and space, v_i is the stochastic velocity, x_i is the position vector in space and F_i is a particle body force vector per unit mass representing the combined gravity and liquid effects on a particle. The r.h.s. represents the collisions between the particles themselves. Wang and Ni [43], [46] suggested to ignore the collision term for dilute suspensions (assuming a particle path free from particle collisions) and proposed a numerical solution that combines the theory of continuum for the carrying liquid and the kinetic theory for solids.

The physical analogy between the motion of slurries and gases on the basis of the kinetic theory emphasizes the dynamic difference between the liquid as a continuum and the particles as separate entities obeying the laws of solid mechanics. In the analogy shortcomings arise, firstly, from the fact that liquid modifies the motion of the particles greatly (due to the viscosity turbulence interaction). Secondly, the no-particle collisions assumption cannot be physically justified (most slurries have solids fraction that is too high to avoid inter particle collisions).

In an effort to simplify the momentum balances under the theory of continuum, a partial explanation of the motion of slurries is given by the settling dispersion model. The model states that particles fall under two competing mechanisms; their tendency to settle due to gravity on one side and disperse from higher to lower concentration regions due to random motion on the other side (settling- dispersion model)[14].

Mathematically the equation is:

$$\underbrace{\nabla(-D\nabla C)}_{\text{Dispersion term}} + \underbrace{\nabla|V|C}_{\text{Convection term}} = 0 \qquad (3.10)$$

Where dispersion vector D and velocity vector V are found empirically in terms of concentration at boundaries. The applicability of this model is limited to finely dispersed particles (homogeneous fine particles at relatively low concentrations). Fundamentally, this model treats slurry motions from kinematical point of view (nothing in the model gives insight into the dynamics of the problem.)

To conclude, solid liquid flows may be successfully described by a set of partial differential equations that reflect the physical reality to a certain extent. Also, these equations may be formulated to embed even more terms (e.g. shape, size...etc). Nevertheless, the lack of adequate physical models that describe the random nature of slurry flows under the effects of turbulence makes an analytical solution unthinkable and drives research work to simplifying assumptions mainly needed for numerical solutions. In principle, all the dynamically changing physical quantities (e.g. velocities and stresses in vector form) have a steady component and a fluctuating component, thus, in the absence of their analytical form empirical correlations are needed and then an averaging method must be employed to quantify them in preparation to a solution numerically.

It is not to underestimate this direction of research, but the degree of accuracy of numerical solutions cannot be readily estimated for a real solid liquid flow problem (especially when noting the successive simplifications in each step of these solutions).

3.5. Physical Description of Solid- Liquid Flow:

In horizontally oriented pipelines, slurry is set in motion by an external energy source, in fully developed steady flow; liquid drag imparts energy to solid particles along the pipeline axis. Liquid density counteracts solid particles weight by their buoyancy. Liquid turbulence interacts with drag to form a complex and random mechanism by which solids are sustained in partial suspension. As solid concentration (volumetric fraction) increases, inter-particle collisions increase. Liquid drag, liquid turbulence and particle collisions form an extremely random momentum exchange mechanism that contributes to suspension and possibly diffusion of solids fraction. Particle shape and size further modifies this mechanism. Coexistence of particles of different sizes and shapes produces heterogeneity in the way each size and shape is dynamically affected and possibly in their disposition within the liquid carrier.

As the term random implies, isotropic dynamic effects are expected in time and space. Thus, solid liquid interaction (as a global resistance to flow) can be safely assumed to be evenly distributed when transmitted to the pipe wetted boundaries. The assumption of isotropy of random motion shall be restricted to the effects rather than the properties of slurries. This can be physically justified due to the macro scale of effects (the pressure drop experienced on the pipeline boundary) while the case is different on micro scale. The latter is related to the structure of turbulence-drag-diffusion mechanisms.

Dynamic effects (drag, turbulence, diffusion due to collisions...etc) can be viewed, in a global sense, as resistances to flow. Existence of solids in various sizes, densities and shapes add more resistances to flow than it would be experienced for liquid flowing alone. For fully developed steady flow, resistance increases with pipe length. In a thermodynamically isothermal system for incompressible fluid, the energy balance for a horizontally oriented pipeline manifests resistance to flow as a pressure loss on the account of kinetic energy available due to the action of an external device. A minimum energy is expected below which solids cease to be carried hydraulically by the liquid.

Although, the above theoretical representation may well describe the motion of slurries, in the absence of analytical solution, the best that can be done is to carry out experimental work. Experimental work has to reflect a real slurry flow problem and that is not easy. For pressure losses associated with slurry flow in a horizontally oriented pipeline, functional relation must be established, mathematically:

$$\Delta P = f\left(\rho_L, \rho_S, V, L, D, \varepsilon, C, PSD, g, \mu, particleshape\right) \tag{3.11}$$

Where $\Delta P, \rho_L, \rho_S, V, L, D, \varepsilon, C, PSD, g, \mu,$ are the slurry pressure drop, liquid and solids densities, average velocity of flow, pipe length, pipe diameter, pipe wall roughness, volumetric concentration (solids fraction as the percentage that particles occupy in a given slurry volume), particle size distribution, gravitational acceleration, liquid viscosity and particle shape respectively. It is difficult to run experiments with all the variables in equation (3.11). In order to reduce the number of variables to a manageable size, non-dimensional parameters have to be introduced.

Pressure drop can be safely assumed to distribute evenly along a given pipe length for fully developed turbulent flow due to isotropy of random motion. If slurry pressure drop can be assumed to be a sum of resistances to flow, then it can be decomposed to liquid and solids resistances respectively. Because it is difficult to measure these resistances separately, a pure additive relation has to be assumed. Various interactions in a slurry containing more than one particle size (multi-fractional slurries) may possibly distort the assumed mathematical sum relation. However, in the absence of alternative method, it will be left to the other terms in the correlation to mitigate any possible inaccuracies. Pressure loss coefficient can be formulated:

$$P_{coeff.} = \frac{i_m - i_L}{i_L C} \tag{3.12}$$

Where $i_m = i_S + i_L, \quad i_m = f_{slurry} \cdot \frac{V^2}{2gD}, \quad i_L = f \cdot \frac{V^2}{2gD}$, *(i)* is the pressure drop in metres liquid per meter of pipe length and subscripts $_T$, $_S$ and $_L$ denote slurry, solids and liquid respectively.

Liquid drag force on particles can be formulated through a coefficient that balances the apparent weight of a particle against resisting forces due to viscosity and particle shape at the state of equilibrium in a stagnant liquid column. This has the advantage of defining Reynolds number in terms of particle diameter. However, due to the existence of more than one particle size, some average method must be employed. In practice, coefficient of drag is normally defined for perfect spheres. These assumptions, if adopted, are too simplistic. First, the equilibrium state at free fall velocity in a stagnant liquid column does not translate the dynamic nature of drag in slurry. Second, averaging of drag coefficient is not mathematically justified. Third, significant effects of shape are difficult to quantify. Finally, drag may be affected by the total solids content. To account for these discrepancies, a relation must be established that takes away the possible inaccuracies that may affect calculating the drag coefficient. The candidate physical quantity that allows for such correction is the terminal fall velocity. Thus, the terminal fall velocity must be determined experimentally to reflect the combined effects of mass, shape and concentration. Consequently, drag calculation will emerge (in the form of a drag coefficient). For the purpose of accounting for shape and mass imperfections before concluding drag coefficient, mass ratios equating masses of particles to equivalent spheres have to be deduced and equivalent diameters of particles (sand particles in this exercise) have to be obtained depending on how they are packed as compared with perfect spheres. Then, drag coefficient can be formulated:

$$C_D = f\left(\rho_L, \rho_S, PSD, \mu, g, U_t\right) \tag{3.13}$$

It is commonly assumed that particle transport in slurries is due to drag and lift forces. This statement needs deeper examination, as lift will take place only under certain conditions. Alternatively, it can be stated that, physically, drag in slurry flow is the driving force that eventually transfers a particle from one point to another. Collectively, this includes the effects of turbulence, weight in fluid, collisions and diffusion. Unlike an aerofoil in air, for example, lift cannot be physically separated as a perpendicular companion to drag for smaller particles practically encountered in real solid liquid flow. For lift to develop pressure difference must be experienced across the lifted body in the direction of the lift and a singular point must exist that acts as a wall to prevent venting of this pressure difference. In particular, pressure

difference is disrupted due to turbulence leading to venting the aerofoil and eventually failure of lift. In slurries, the existence of solids by itself is a source of turbulence and practically laminar regime is not a feasible means for hydraulic transport due to increased friction factor, inability to develop suspension for particles at low velocities of flow and economical considerations of cost of pipelines and pumping devices. Thus, in a turbulent stream of fluid, it is the drag that imparts energy to solid particles without distinctive existence of lift (turbulence, collisions of particles and possibly diffusion are the possible accomplices to prevent lift forces taking place). Thus for the type of particles considered, lift is likely to be insignificant.

Some form of Froude number may best describe the relation of inertial forces with gravitational forces on particles. Defining Froude number based on solids weight in liquid, basically, defines the densimetric disturbances of solids on liquid. Thus Froude Number:

$$Fr = f(V, g, S, D) \tag{3.14}$$

Where S is specific weight of particles and D pipe diameter

A tentative functional relation that is suitable for conducting experiments may be summarized:

$$\frac{i_T - i_L}{i_L} = f(C, Fr, C_D) \tag{3.15}$$

The existence of mixed particle sizes in slurries necessitates the design of experiments to find out the effect on pressure drop. Most suitably by selection of particle sizes that are closely graded, classification of different populations. In this work, two different populations of particles are employed. Coarser and finer populations that have particle size distribution that are wide apart are intentionally selected. The main aim is to compare their behaviour for the same concentration. If the pressure losses in slurries vary only due to variation in total concentration

(regardless of the particle size distribution and shape) then the pressure losses correlation shall be invariantly the same for any particle size population as far as the total concentration is maintained constant. The theoretical basis of this work is that pressure losses associated with slurry flow are affected by the differences of the particle sizes proportions, nature (shape, mass and distribution) as well as the total concentration and the other system variables (fluid and geometrical boundary properties). The experimental program will examine the possible differences in pressure losses due to variations of shapes and sizes as populations of poly-fractions for virtually similar total concentrations.

Chapter 4

Design of Experiments

4.1. Introduction

4.2. Experimental Programme

4.3. Offline Experiments

4.4. Non Dimensional groups

4.1. Introduction:

In view of the literature review and the examination of the underlying theoretical considerations, it is unthinkable that a reliable analysis whether theoretical or semi theoretical (that is analytical in nature) can be produced for slurry flow. The reason is that slurry flow is a multi variable and highly random problem. Slurries cannot be defined by the properties of fluid alone and cannot be considered multiphase in which the same matter takes different states. It is a multi component mixture comprising liquid and different sizes of solids. Each has its own physical properties. The result, under dynamic flow conditions, is an extremely complex flow pattern.

An empirical approach is the best can be done. The author does not under estimate the difficulties related to the proposal of the empirical approach in data acquisition and interpreting results to build up a pressure loss model in slurries. This program of experiments aims at highlighting some of the ambiguities related to slurry flow and produces yet another empirical correlation.

In particular, a carefully designed experimental program shall be developed that highlights the effects of the existence of two particle size fractions (two distinct populations) on the pressure losses.

4.2. Experimental Programme:

Experiments outlined below are designed to measure the pressure drop across a horizontally oriented pipe length (6" diameter and 14.59 m test length) at various flow rates. Mainly, they are divided into two sets (the first is for the coarser population Sand (A) and the second is for the finer population Sand (B)). The reason for this strategy is to enable the author carry out comparisons (paired comparisons) between these two populations. Each comparison shall take one pair of trend lines from each set of experiments under the condition that they have the same concentration. So that the comparison does not measure the effect of concentration but the structure of each pair of curves in terms of the constituting particle size distribution and its effects on pressure losses. Table 3.1 illustrates this strategy:

Table 3.1. Program of Experiments

Coarser Population (Sand (A))		
	Experimental Measurement Points	
% Volumetric Concentration	Differential Pressure Across 6" pipe length of 14.59m (in mm H_2O)	Flow Rates In m^3/Hr (Max. 200 m^3/Hr)
1	1 2 3 4 5	1 2 3 4 5
2	Repeat same as for concentration (1)	
3		
Finer Population (Sand (B))		
Repeat same as above		

Paired comparisons are repeated for all concentrations in the program in the same manner.

4.3. Offline Experiments:

Offline experiments were conducted to:

- Separate sufficient quantities of sand populations in preparation for carrying out the main experimental program. This included the selection of the suitable screeners and meshes to exclude the unwanted sizes. The purpose was to obtain two sand populations. Each of them is closely graded while their particle size distribution is not the same or near to each

other (the cut sizes are wide apart).

- Terminal velocity measurements were carried out in preparation for the coefficient of drag calculation. Care has been taken to time the fall of each particle in a liquid column without interaction with its boundaries.

- Viscosity measurement of the carrier liquid. Although viscometer calibration was carried out successfully on a standard fluid (as shown in chapter 5), the viscosity measurements of the carrier liquid were not satisfactory and had to be discarded. The reason is that separation of liquid from small sized particles of solids proved to be much of an arbitrary selection rather than physical behaviour. Leaving what is supposed to be carrier liquid including some portion of fine particles for different time periods gave different carrier liquids containing different amounts of particles. In the absence of a physical means to assess which combination of liquid solid carrier to be the correct carrier liquid, the best that can be done is to take the properties of the pure liquid as it is invariantly definitive in properties. Moreover, viscosity can only be defined for liquids and liquid like fluids. In the latter case, the fluid must possess a consistent and time invariant viscosity.

- Calibration experiments of the differential pressure transducer, the magnetic flow meter, the chart recorder and the viscometer.

It is important to mention that an introductory part in the experimental work is dedicated for solids characterization (particle size distribution PSD, mass of particles equivalent to perfect spheres to pronounce the shape imperfections and measurement of terminal velocities for actual sand particles).

This introductory part proved to be useful in achieving the main aims of this exercise, because it paved the way to quantify the basic corrections needed to improve the prediction of the drag coefficient and consequently the pressure loss correlation. It is more often than not that these basic corrections have not been given

due attention in the literature. Instead, they were considered minor leaving a significant source of error unsolved.

4.4. Non Dimensional groups:

The number of variables in a solid liquid mixture flow is too much to conduct an experimental program without reducing to a manageable size. The grouping in non-dimensional parameters serves this purpose. Moreover, non-dimensioning serves to remove the effect of dimensions so that the non-dimensional groups are more general. The variables are divided into separate categories that all contribute to the prediction of the pressure drop:

- Fluid properties (density ρ_l and viscosity μ)
- Solid properties (density ρ_s, particle diameters d_1, d_2, d_3, etc. and concentrations C_1, C_2, etc and total concentration C_t)
- Flow velocity V
- Pipe geometry (pipe diameter D, pipe roughness ε and pipe length)

Other properties such as compressibility, chemical activity and electrical properties are not accounted for because they are not considered to significantly exist for the solids (sand) and liquid (water) used in this exercise. In a functional form:

$$\Delta P = f(\rho_l, \mu, \rho_s, d_1, d_2, .., C_1, C_2, .., C_t, V, D, \varepsilon, L) \qquad (4.1)$$

It is convenient to put the pressure drop in a more compact form as a pressure gradient so that the pressure drop is found as meters of fluid per metre of pipe length:

$$\frac{\Delta P}{L} = \rho.g.\frac{\Delta h}{L} \qquad \text{Denoting } \frac{\Delta h}{L} = i \qquad (4.2)$$

Where i is the pressure gradient in meters of water per meter of pipe length.

Further, the pressure gradient for water or other Newtonian fluid is a function of

Fanning friction factor, pipe diameter, pipe roughness and flow Reynolds number.

Thus, the pressure drop for the mixture can be put in the following form:

$$\frac{i_m - i_w}{i_w} = \phi \tag{4.3}$$

Where m and w denote mixture and water and ϕ is a function of non-dimensional parameters to be defined below.

Physical definition of particle motion may be considered as taking place in a gravity field, dragged by the viscous nature of the flow and affected by the inertia field due to fluid velocity. Archimedes fluidisation number (Ar) [*] summarizes these competing effects on a particle. It is a measure of keeping the particles suspended. Thus, in a standard form for a perfect spherical particle:

$$Ar = \frac{4}{3} d^3 g \frac{\rho_l(\rho_s - \rho_l)}{\mu^2} = C_D \,\mathrm{Re}^2 \tag{4.4}$$

[*] Douglas, J.F., Gasiorek, J.M. and Swaffield, J.A. "Fluid Mechanics".

Third Ed. Longman. Pp 371 (1996).

Where Ar is defined for a particle of diameter d, solid and liquid properties (ρ_l, ρ_s, μ), gravitational acceleration g, and Reynolds number defined for a particle.

It is apparent from equation (4.4) that a direct relation can be established between Archimedes number and the coefficient of drag. However, the coefficient of drag is a function of the terminal fall velocity of a particle (defined as the velocity which a particle resumes under equilibrium of forces acting on the particle when falling in a column of fluid). Thus:

$$C_D = \frac{4}{3} dg \frac{(\rho_S - \rho_L)}{U_t^2 \rho_L} \qquad \text{Appendix (A), (A.1)}$$

Where U_t is the terminal fall velocity.

In experiments, it is relatively easier to measure the terminal fall velocity as compared to the coefficient of drag due to the small particle size used in this experimental work. Moreover, the above functional relationship indicates that the terminal velocity is the only variable resembling all the dynamic effects of drag mechanism (shape imperfections and turbulence). In this work, terminal fall velocity will be measured experimentally and, subsequently, the coefficient of drag calculated as a function of the experimentally obtained data. The terminal fall velocity for an actual particle can be obtained in a non-dimensional form (as a ratio of the corresponding terminal velocity of a perfect sphere) and related functionally to Archimedes number. Thus:

$$\frac{U_t}{U_{ts}} = f(Ar) \tag{4.5}$$

Also, interaction between the flow and the solids can be defined by an additional non-dimensional parameter that reflects the competing effects of fluid flow inertia and the submerged weight of solids. A modified form of Froude number *(Fr)* is used for this purpose:

$$Fr = \frac{V}{\sqrt{gD(s-1)}} \tag{4.6}$$

Where S is the specific gravity of solids.

Thus, the final relationship for pressure losses associated with slurry flow in a horizontally oriented pipeline may be developed with all the variables included.
Thus:

$$\frac{i_m - i_w}{i_w} = f(C, Fr, C_D) \qquad \text{Ch. 3 (3.15)}$$

An algebraic form for the above relationship would be:

$$\frac{i_m - i_w}{i_w} = K \cdot C^a \cdot Fr^b \cdot C_D^c \qquad (4.7)$$

Where K, a, b and c are curve fitting constants. By carrying out the tests in the experimental programme and including the results in the non-dimensional relationship (4.7), a model will be developed that covers the aims of this work. Statistical testing for curve fitting adequacy is employed (details are in chapter (6)).

Chapter 5

Design of the Test Rig

5.1. Introduction

5.2. Sand Screening Rig

5.3. Test Loop Description

5.4. Instruments Description and Calibration

5.5. Terminal Fall Velocity Test Rig

5.1. Introduction:

The test rig was designed to be of industrial scale size in an effort to reflect the results of the experiments directly to industrial applications. The test rig comprises slurry holding tank (15 cubic meter capacity), a centrifugal circulating pump (nominal capacity 0- 200 cubic meter per hour flow rate) and a long pipe loop leading to a horizontal pipe test section (152 mm diameter and 14.59 meters long). The test loop was so designed to allow for the possibility of varying flow rate through adjusting isolating valves at the discharge side of the test section. Controlling the flow rate at the downstream of test section allowed for minimal disturbances before the pressure test points. The whole system is drainable to allow for cleaning and dumping of any slurry mix at the end of a series of experimental runs. Air venting is facilitated at the cardinal points of the system to prevent fluctuations of measurements due to air entrapment. The instruments for pressure drop and flow rate measurement are lead to a chart recorder for simultaneous recording of both the pressure drop and the flow rate. Yet the test loop configuration is simple and easy to manipulate. Figure (5.1) is a pictorial view of the test rig.

In the course of preparation for conducting experiments, the need arose for sand preparation in accordance with the specifications required for achieving the objectives of this research exercise. The screening and classification of sand proved to be indispensable in obtaining the required sand sizes that are not readily available. The selection of sand for this research work is partly due to its availability, its shape characteristics (non spherical) and its fairly good resistance to attrition (disintegration during conducting experiments).

5.2. Sand Screening Rig:

A multi deck vibrating screening machine was built to classify the raw sand used in this exercise (valley sand) into reject cut sizes and desired size distributions. It is required that two sand populations be prepared that are wide apart in their range of sizes (details of sands particle distributions, their benefits to experimental work and

results obtained are extensively illustrated in chapter 6). The main aim of the separation of these sand populations is to reveal the differences in pressure losses associated with slurry flow due to differences in solids particle distribution while maintaining the same concentrations.

Figure (5.2) shows the details of the screening machine. At the top entry, raw sand of wide particle size distribution is led to the top of an inclined screen mesh to scalp the particle sizes of sand exceeding 4.75 mm sieve size. Scalped sizes are piled in a reject pile. Particle sizes below 4.75 mm sieve size pass through the top screen mesh to the second screen deck that is of 1.7 mm sieve size. A second pile is formed for sizes ranging from 4.75 mm to 1.75 mm as a product of the sizes retained on the top of mesh of sieve size of 1.75 mm (denoted Sand (A) that is the first and coarser population to be used in experimental work). Remaining sand of size less than 1.7 mm passes through to the top of a third stage screening deck having a mesh size of 0.6 mm. Sand size range from 1.7 mm to 0.6 mm is retained on the top of the 0.6 mm mesh and piled separately to a second reject pile. The last screening deck has a mesh size of 0.15 mm and retains at its top sizes between 0.6 mm to .15 mm (denoted Sand (B) that is the finer population to be used in experimental work). Sand particle less than 0.15 mm are piled below the last stage of screening as a reject pile (full investigation of sand characteristics forms the introductory part of chapter 6).

5.3. Test Loop Description:

Figure (5.3) shows the process and instrumentation diagram of the test rig. The circulating pump (Denver HG 100/100) circulates slurry from the slurry holding tank into a 4" inch discharge pipe. The slurry is kept under agitation to prevent settling in the holding tank. The bottom of the tank is conical in shape and is dished at its bottom end to ensure smooth and homogenous flow. Reliability of this tank configuration was proven to be adequate during experimental work (i.e. pulsating flow at low frequencies indicated frequent choking of tank discharge with improperly mixed slurry which was observed each time the system was started but disappeared shortly afterwards).

The circulating pump discharge is led to a 152 mm pipe that is vertically oriented to allow correct installation of a 152 mm magnetic flow meter (Pulsmag V DMI 6532). The selection of this pipe size was dictated by the size of the magnetic flow meter so that a correct matching of size is obtained to prevent abrupt size changes in the neighbourhood of the flow meter. A straight vertical run exceeding ten times the pipe diameter was maintained to allow correct operation of the flow meter. The pipe size is then reduced after the flow meter to 100 mm diameter to eliminate the possibility of solids settling and system instability. At the top end of the 100 mm pipe, an air vent was installed to purge the system of entrapped air. The pipe connects to the test section through a steep inclination to reduce the possibility of solids settling and ensure adequate air purging.

The pipe test section is enlarged to 152 mm diameter to allow for relatively gradual change of flow velocity. A straight uninterrupted horizontal run of approximately 3 meters from the last pipe enlargement is maintained before the upstream test point (piezometric ring) to eliminate end effects on the pressure signal at test point. The pipe test section length was maximized to a length of 14.59 m to obtain higher differential pressure readings. The down stream test point is kept 2 meters from the next pipe direction and pipe size change. An inverted U- shaped final 100 mm pipe section is led back into the slurry-holding tank. This configuration ensures backpressure on the test section to prevent it from running partially filled

The flow rate is changed by a pair of valves at the discharge end of the test section. The slurry is prepared by measuring a quantity of water and a quantity of solids to give the desired concentration. Short test runs are conducted to minimize attrition of the sand particles due to repeated circulation in the pump and piping. Every time the concentration was changed, the slurry tank was emptied and thoroughly washed. A by pass is provided for discharge of the used slurry and introducing a fresh charge

Figure (5.4) shows the instrumentation arrangement on the test rig. The magnetic flow meter signals are directly led to the chart recorder. The chart recorder allows for recording on 4 channels simultaneously. The Differential pressure transducer (Rosemount 1151 DR) takes pressure signals from two piezometric rings that are

14.59 meters apart. Both the flow rate (0-200 meter cubes per hour) and the pressure drop (0-3500 mmH2O) are recorded on a separate channel on the chart recorder. Readings of corresponding signals of flow rate and differential pressure are marked on the recorder chart paper.

Figure (5.5) shows the details of the testing points (piezometric rings). The pipe test section is surrounded with a 250 mm pipe section welded to it to form a plenum between the test section and the outer boundary of the larger cross section. Three holes are drilled on the circumference of the test section of 5 mm diameter at equal spacing. The reason for drilling these holes was to ensure non-blockage of the test point and to absorb small pressure surges that helps in obtaining steady pressure signals and reduces ripples. The spacing (plenum) between the inner and outer pipe sections served well in collecting any escaping particles that may otherwise have entered into the pressure test tubing and may have blocked it. Air vent and drain cocks are installed to allow frequent cleaning and air release. This configuration of test pressure points operated up to expectation and helped much in obtaining fairly stable pressure signals. On many occasions when abnormal signal pulsations were observed, draining and venting of the test points restored the pressure signals back to acceptable limits.

The test rig was first commissioned on plain water to verify stable operation and capability to control of flow rate as needed.

5.4. Instruments Description and Calibration:

It was decided to include the instrument description and calibration procedures and results in an appendix (Appendix (D) at the end of this work).

5.5. Terminal Fall Velocity Test Rig:

A separate test rig was built to measure the terminal fall velocity of the sand particles. This is important to distinguish the drag behaviour of the sand particles

The test rig comprises a 2" diameter transparent tube of 10 meters length. The tube was vertically fixed and the terminal velocity measured by noting the time taken by a particle to pass through the last meter of the tube length. The measurement of terminal velocity at the end of the tube length ensures that an equilibrium state is reached. Visual observation of the falling particles during conducting the experiments verified equilibrium state by comparing the results with the results obtained for the next one-meter length up the measurement length (results obtained from this rig are reported in chapter 6).

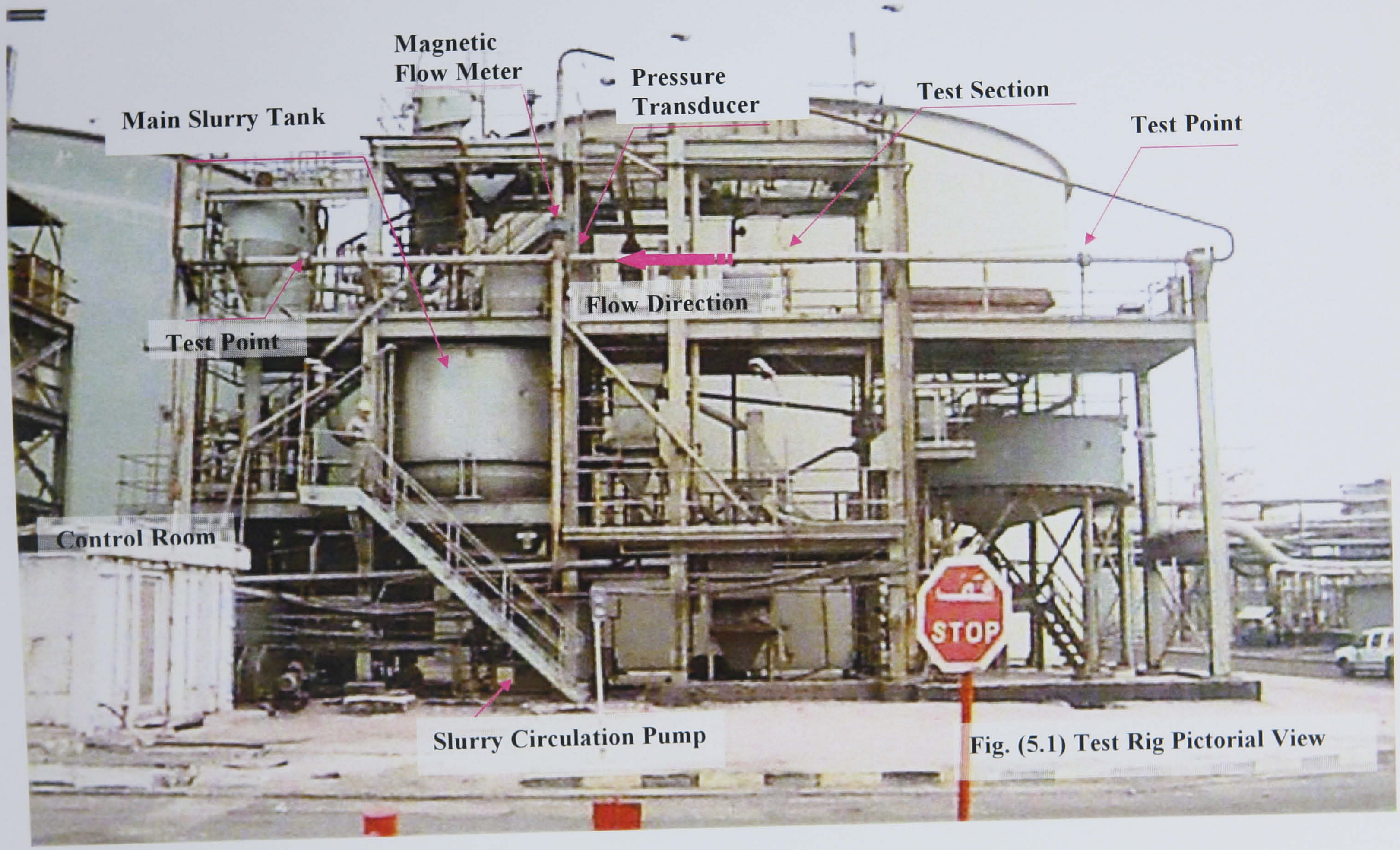

Fig. (5.1) Test Rig Pictorial View

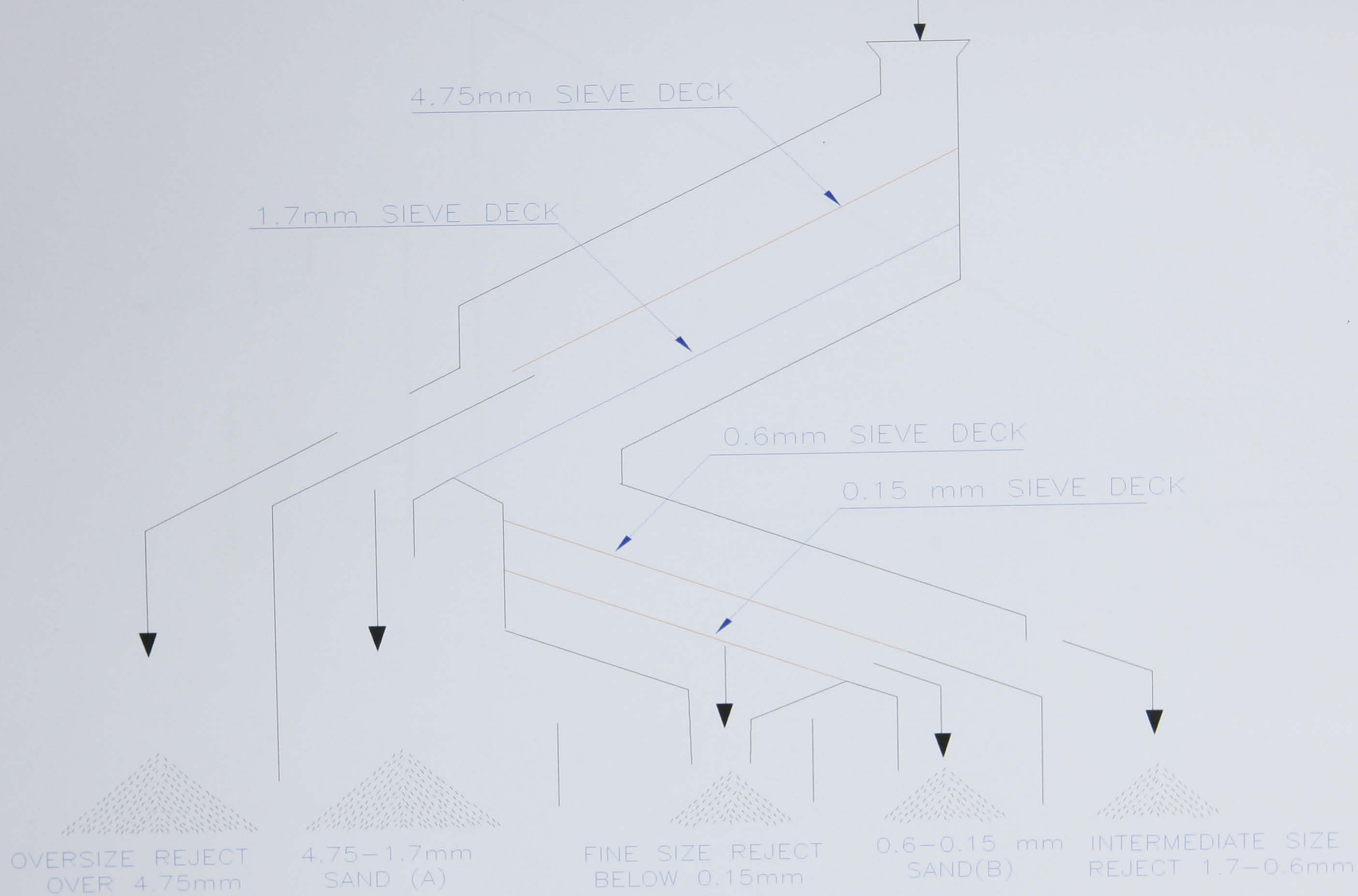

Fig. (5.2), Multi Deck Screening Machine

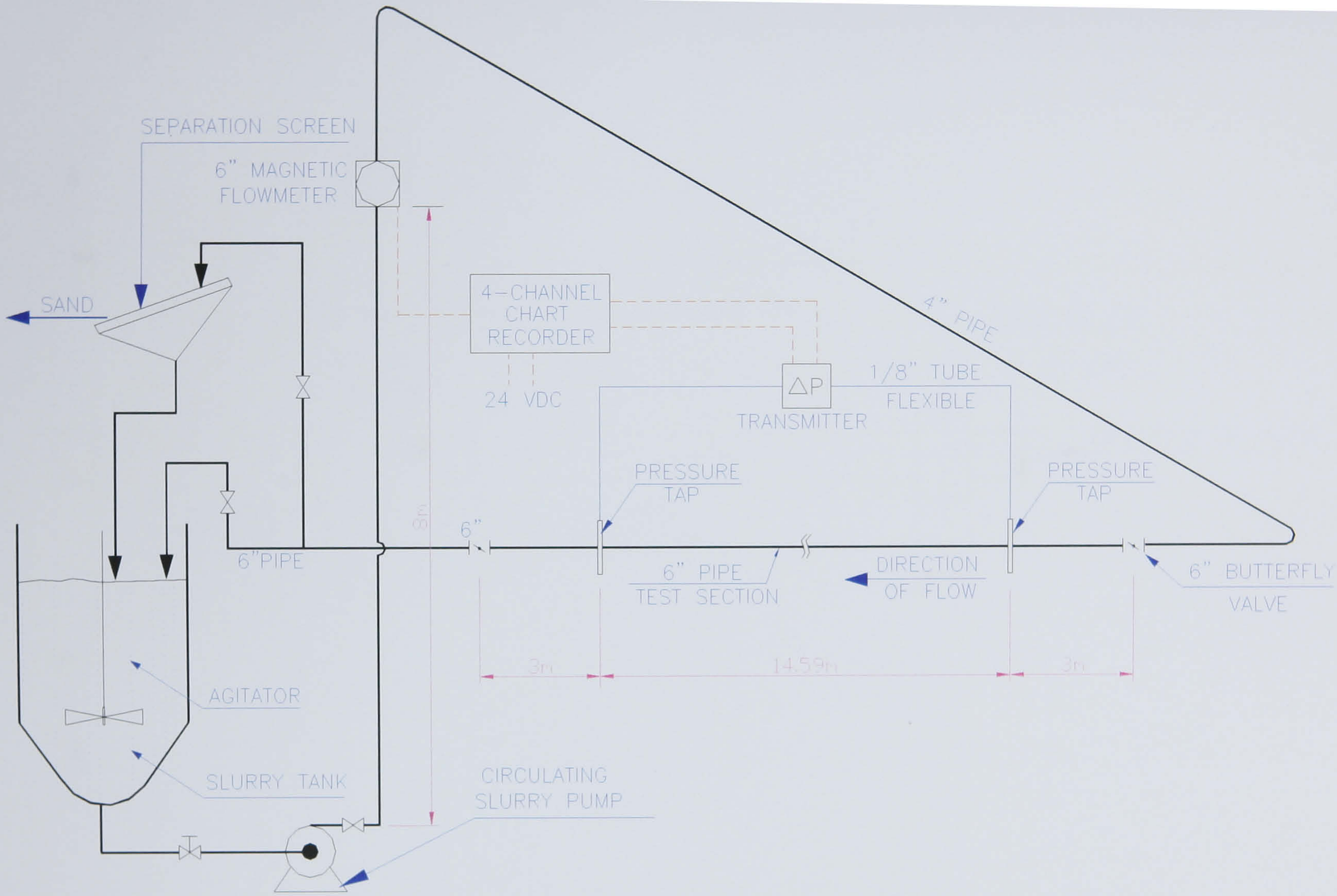

Fig. (5.3), Test Rig Process and Instrumentation Diagram

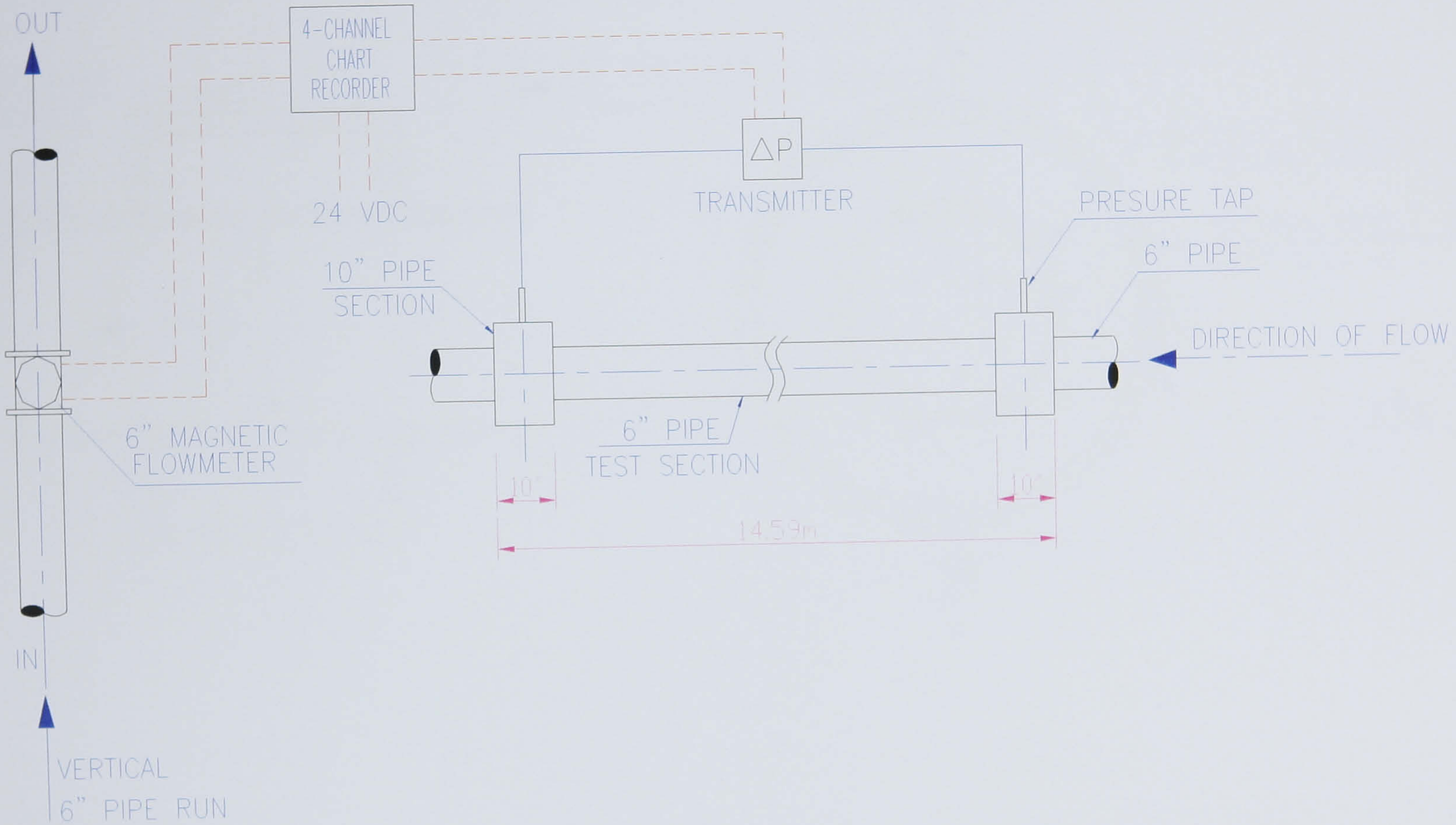

Figure (5.4), Instrumentation Disposal Diagram

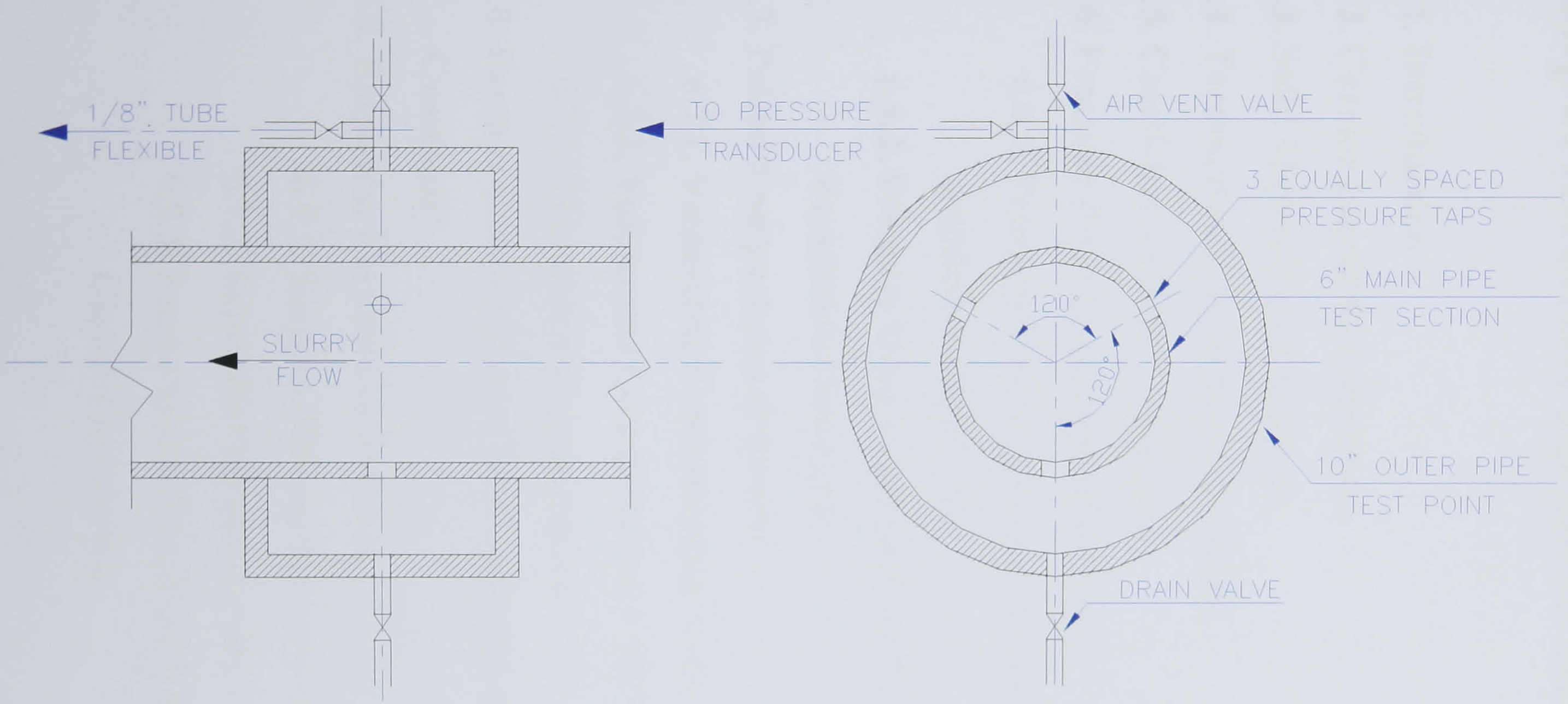

Figure (5.5), Details of Test Points (Piezometric Rings)

Chapter 6

Experimental Results and Discussion

6.1. Introduction:

The experimental results, reported hereinafter, start with an examination of the solids specifications used in experimental work, obtaining their drag characteristics as compared with standard spheres on the basis of equal mass. and then reporting the experimental results of the pressure drop in the selected pipe dimensions. Finally, the pressure drop correlations are derived and results discussed.

Due to the importance of drag mechanism in a slurry system, it is a prerequisite (for obtaining a pressure drop correlation) to evaluate critically the existing correlations and compare them with the experimental data obtained in this work. Appendix (A) reviews the drag characteristics for standard spheres, their terminal fall velocity and notes the differences in the reported predictions. For this purpose three of the mostly used correlations were examined. Special emphasis is given in this chapter to the deduction of the coefficient of drag as it embraces the combined effects of turbulence, diffusion and viscous drag of liquid on solids. Although these flow mechanisms are physically inseparable in a real slurry flow problem, they can be best described by a global coefficient of drag. The most important parameter in the deduction of the coefficient of drag is the free fall terminal velocity because it can be readily measured.

However, because the solids used in experiments are not perfect spheres and contain more than one particle size it was necessary to devise a procedure by which the effects of shape and multi- sizes are accounted for. This twofold procedure assigns a weighted average diameter for the multi fractions of solids used in experiments and then extends the treatment to mitigate the differences in masses and compares the shape imperfections to the standard spherical shape.

Experimentally obtained results for the pressure drop are for an industrial scale test rig so that they can be readily applicable for hydraulic design of piping systems of similar nature.

6.2. Carrier Liquid Specifications:

Carrier liquid is plain water at 30 C, having density of 995.7 Kg/ m^3 and dynamic viscosity of 0.000798 N/m^2. Water is known for its Newtonian viscosity relationship. It is taken as such in this work because of the absence of extremely fine solid material (e.g. mud, silt etc.) that may modify viscosity.

6.3. Solid Material specifications:

Solids employed in the experiments are washed natural sands of roughly prismatic shape. The prismatic shape is due to the attrition process on natural sand by the passing of time. Sands are intentionally selected in two distinctive populations (mixes of various sizes proportions). The first is fairly coarse mix of sand (Sand A), while the second is fairly fine mix (Sand B).

The sand populations were selected to be wide apart so that their behaviour in slurry may be distinct from each other. A standard sieve shaker was used to separate the different particle sizes. A certain particle size is that size passing the bigger mesh square opening and retained on the next smaller one below it. By this way, a particle retained above a certain sieve is assumed to have a sphere diameter equal to that sieve opening dimension. Thus, two issues have to be resolved; first, an average diameter (for an equivalent perfect sphere) has to be assumed for sands having more than one particle size and the second is to deduce a relation that equates the mass of the hypothetical sphere to the true mass of equivalent sand particle.

Due to the fact that particle sizes, in a given particle size distribution, do not exist in equal proportions; a simple average will not reflect a true average. Instead, a weighted average is more appropriate as it accounts for the relative weight percentage of each size fraction (proportion) in the particle size distribution. Thus:

$$d_{av} = \sum (w_i d_i) \qquad (6.1)$$

where w_i is the weight percentage for the *ith* fraction and d_i is the sieve opening dimension in mm (sieves are of square opening) denoting an equivalent sphere diameter for the corresponding sand particle.

It is worth noting that, up to this end, the true mass of a sand particle is not accounted for. In the literature, despite its importance, a solution to the issue is not concentrated on. It was observed by the researcher that this could be partly attributed to the use of single particle size (either a perfect sphere or assumed as such) or apparently it was assumed not important. It could be a reasonable assumption to ignore mass differences between a single particle size and a sphere but this could hardly be overlooked in a more complicated case were multi sizes are considered.

The procedure will be applied to each sand material in turn as follows:

a) Sand (A), Coarse Sand:

The nominal sizes obtained from the sieve analysis range from 4.75 mm to 1.7 mm as accumulated above the corresponding mesh. Table (6.1) summarizes the results.

Table (6.1), Particle Size Distribution of Sand (A)

Sand (A) Coarse: Measured Density: 2600 Kg/m^3, Sample Size: 467.1 gm.

Sieve Opening		% Cumulative	Weight (gm)
U.S. Mesh No. to ASTM E-11-87	Mesh Square Opening (mm)		
4	4.75	1.73	8.1
5	4	27.66	129.2
6	3.35	58.64	273.9
12	1.7	100	467.1
Weighted Average Dia.	2.861	mm	

b) Sand (B), Fine Sand:

The nominal sizes obtained from the sieve analysis ranges from 0.6 mm to 0.15 mm as accumulated above the corresponding mesh. Table (6.2) summarizes the results.

Table (6.2), Particle Size Distribution of Sand (B)

Sand (B) Fine: Measured Density: 2650 Kg/m^3, Sample Size: 340.7 gm.

Sieve Opening		% Cumulative	Weight (gm)
U.S. Mesh No. to ASTM E-11-87	Mesh Square Opening (mm)		
30	0.6	30.79	104.9
40	0.425	49.55	168.8
50	0.3	71.76	244.5
70	0.212	93.16	317.4
100	0.15	100	340.7
Weighted Average Dia.	0.387	mm	

Figure (6.2) shows the particle size distribution for (A) and (B) respectively. Main observations on the figure are:

i. Sand (A) is widely graded compared with Sand (B).

ii. The axes, around which the sizes are distributed, are sufficiently wide apart (forming two distinctive populations).

iii. Constituent sand sizes, for the finer population (Sand (B)), are in fairly similar proportions compared with the coarser sand population (steadier rise of the curve for Sand (B)).

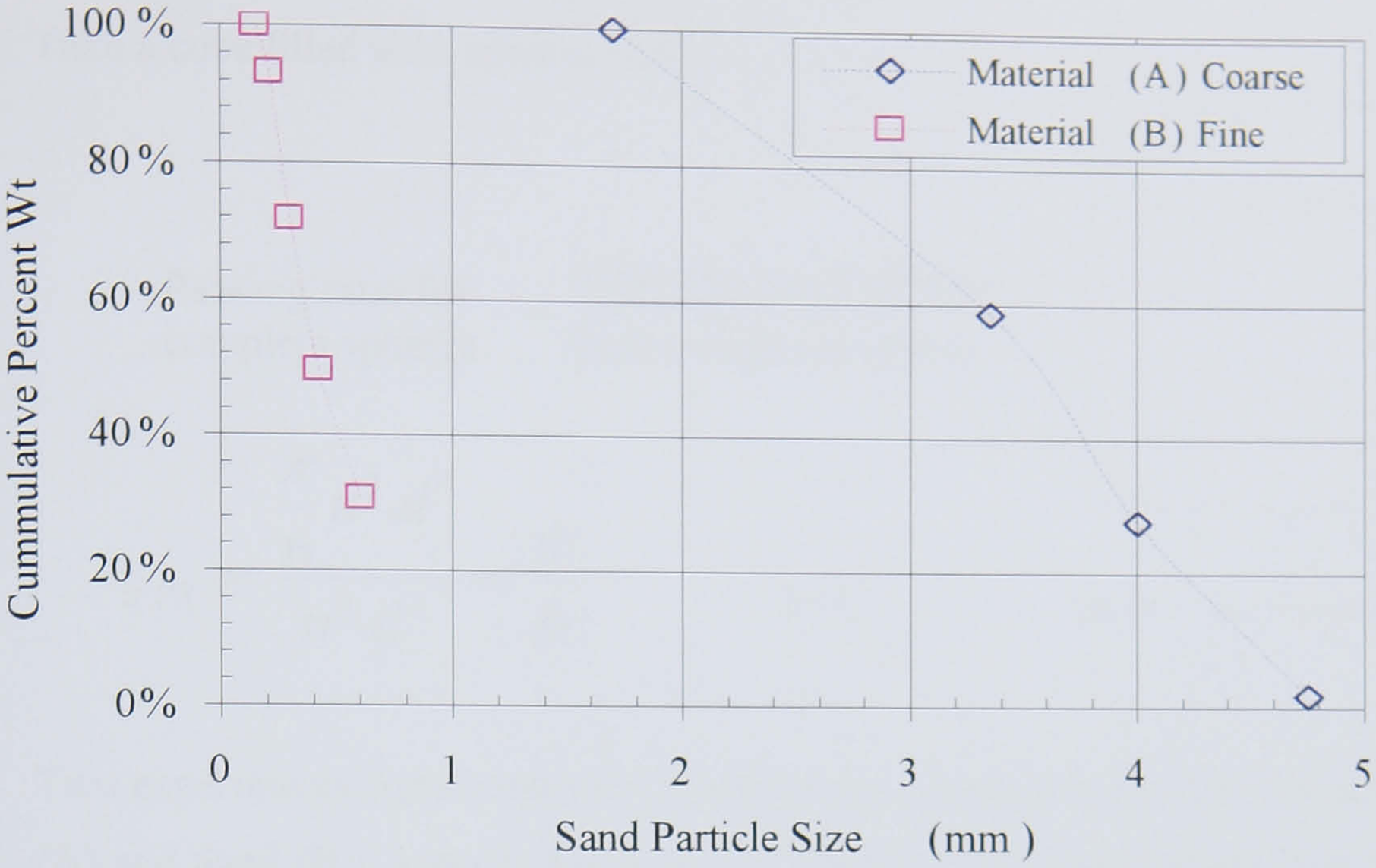

Fig. (6.2), PSD of Sand Used in Experiments

6.4. Terminal Fall Velocity Correlation:

Terminal fall velocities of complete spheres were investigated in Appendix (A) and three of the mostly used correlations were examined along with the coefficient of drag in each case. Relative errors ranging from ± 5% to ± 10% were observed for the same physical conditions.

For non-spherical particles, nominal (equivalent) diameters are usually assumed bringing in complexities of how to equate masses of particles and, moreover, shape departures from spherical necessitate devising a suitable shape factor. Thus:

a) Mass Ratio:

In order to separate the effect of the adoption of an equivalent diameter in the sieve analysis and the existence of more than one particle size, a mass ratio (ψ_{mass}) is deduced that is used as a correction factor in finding the terminal velocity for a mix of non- spherical particles in terms of standard correlation for spheres. The procedure is as follows:

Take a cube filled with spheres then,

$$\text{Packing ratio for complete spheres} = \frac{\text{True volume of spheres}}{\text{Bulk volume of spheres}}$$

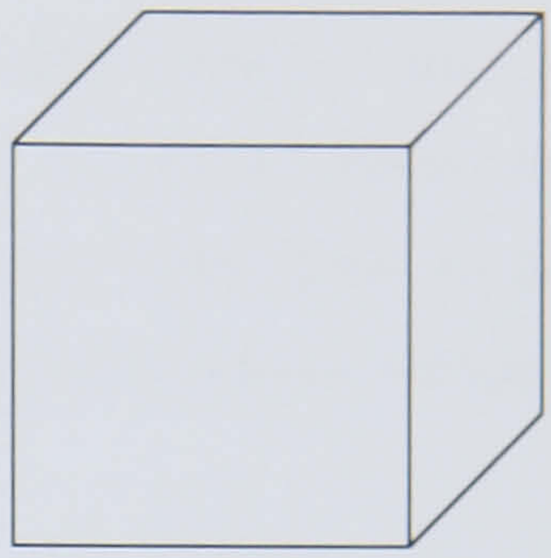

$$\varsigma_{PR} = \frac{\frac{\pi}{6} n^3 . d^3}{n^3 . d^3} = \frac{\pi}{6} \qquad (6.2)$$

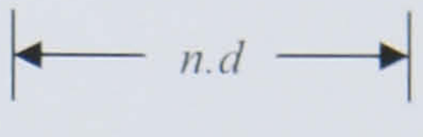

Two experiments were conducted to obtain the actual packing ratio for both Sand (A) and Sand (B). A graduated tube was filled with a measured quantity of each of the materials in turn, a known quantity of water was added and both the bulk volume of the solid materials and their true volume were observed. Applying equation (6.2) for the true sands and rearranging, the mass ratio (ψ_{mass}) is obtained:

$$\psi_{mass} = \frac{\varsigma_a}{\varsigma_{PR}} \qquad (6.3)$$

where (ψ_{mass}) is the mass ratio, ς_a is the true sands packing ratio and ς_{PR} is the packing ratio for sand as if it was complete spheres

The mass ratio inflates the equivalent sphere by its value to obtain equal mass with the corresponding prismatic sand particle. This is necessary for calculating both the terminal velocity and the coefficient of drag.

Table (6.3), Actual Packing and Mass Ratios (ψ_{mass}) for experimental Sand

Sand	True Volume (ml)	Bulk Volume (ml)	Packing Ratio	Mass Ratio
(A)	195	330	0.59	1.126364
(B)	237	365	0.65	1.240909

Table (6.3) summarizes the results. It is clear from these results that the mass ratio exceeds unity (a given sand particle is heavier than an equivalent sphere of sand), which is physically justified because of the prismatic nature of sand. A direct benefit of obtaining a mass ratio is that it can be utilized to convert the equivalent diameter of a given material population (multi-sized sand) to an equivalent sphere diameter for the employment in finding the terminal velocity and the coefficient of drag. Thus:

$$M_{particle} = \psi_{mass} \times M_{sphere}$$

$$\frac{\pi}{6}\left(D_{eq}\right)^3 = \psi_{mass} \times \frac{\pi}{6}\left(d_{sphere}\right)^3 \qquad (6.4)$$

$$D_{eq} = d_{sp} \times \left(\psi_{mass}\right)^{\frac{1}{3}} \qquad (6.5)$$

where D_{eq} is the equivalent sand particle diameter accounting for equal mass with a true sand population and d_{sp} is the weighted average diameter for a sphere for a given sand population.

This procedure is an improvement on assuming equivalent diameter by averaging only. It was illustrated earlier (in the literature review) that many averaging methods were used on purely mathematical manipulation but none appears to have extended the treatment further to allow for physical equivalence with particles true mass. The concept of devising a mass ratio helps in reducing the differences between the coefficient of drag for different shapes of particles to those related to shape only by maintaining the masses of these particles similar to equivalent spheres. In this work, the weighted average diameter, combined with mass ratio, is used in the conclusion of the terminal velocities and consequently the coefficients of drag.

b) Terminal Velocity Correlation:

In this work, terminal fall velocities were determined experimentally for each particle size. The measurement of terminal velocity is relatively simpler than measuring the coefficient of drag directly due to the small size of the particles. Terminal fall velocity, when determined experimentally, allows for the calculation of the coefficient of drag on experimental basis. Also, terminal velocity is a unique value for a given particle that determines drag particle-liquid interaction. By conducting simple dimensional analysis, the experimental terminal velocity can be related to the standard terminal velocity for a sphere of equal mass. The correlation for the latter may be readily obtained from literature (Appendix (A) reviews some of the most commonly used). Thus:

$$\frac{U_t}{U_{ts}} = f\left(d_{sp}, \rho_P, \rho_L, \mu_L, g, \psi_m\right) \qquad (6.6)$$

Rearranging by finding non-dimensional groups by inspection,

$$U_t = K\left[\frac{g(\rho_s - \rho_L)\psi_{mass}.d_{sp}^3}{\frac{\mu_L^2}{\rho_L}}\right]^n U_{ts} \qquad (6.7)$$

Where the non-dimensional group between the braces of the RHS is a modified form of Archimedes number to take into account the mass ratio. Physically, Archimedes number relates the apparent weight of a mass falling at terminal velocity in an inertial- gravitational field to the resisting viscous forces of the liquid. In this work, it is employed to mark the behaviour of a falling sand particle in terms of an equivalent mass for a corresponding sphere. However, Archimedes number is employed here in a modified form to allow for mitigating mass differences between a sand particle and an equivalent sphere. Thus, enabling direct calculation of a sand particle terminal velocity as a function of

that for a sphere of equal mass. Shape differences between a sphere and a sand particle of equal mass are partly accounted for by the constant ***K*** and the correlation exponent ***n***. It is expected that these two quantities change for different shapes. Differences in shapes of sand particles employed in this exercise are considered minor because their shapes are nearly prismatic (natural sand from the same source valley) due to fairing of sharp edges through long-term attrition.

Using a power law regression function, best fit is obtained for minimum error in the form:

$$\frac{U_t}{U_{ts}} = 0.7941[Ar]^{-0.0333} \qquad (6.8)$$

Table (6.4) summarizes the results for the above correlation. While terminal velocity (U_t) is found experimentally, (U_{ts}) is calculated according to a standard correlation (in this case Turton and Levenspiel [47] correlation according to the algorithm reported in Appendix (A)). Instead, any suitable correlation for sphere terminal velocity could be used provided that its sensitivity is pre-examined compared with other correlations (fig. 5.A in appendix (A) compares three of them). The correlation fits fairly well with the experimental data. The relative error between the experimental points and the correlation is rather distributed in the range of ± 8% while the average for all points is less than 1%.

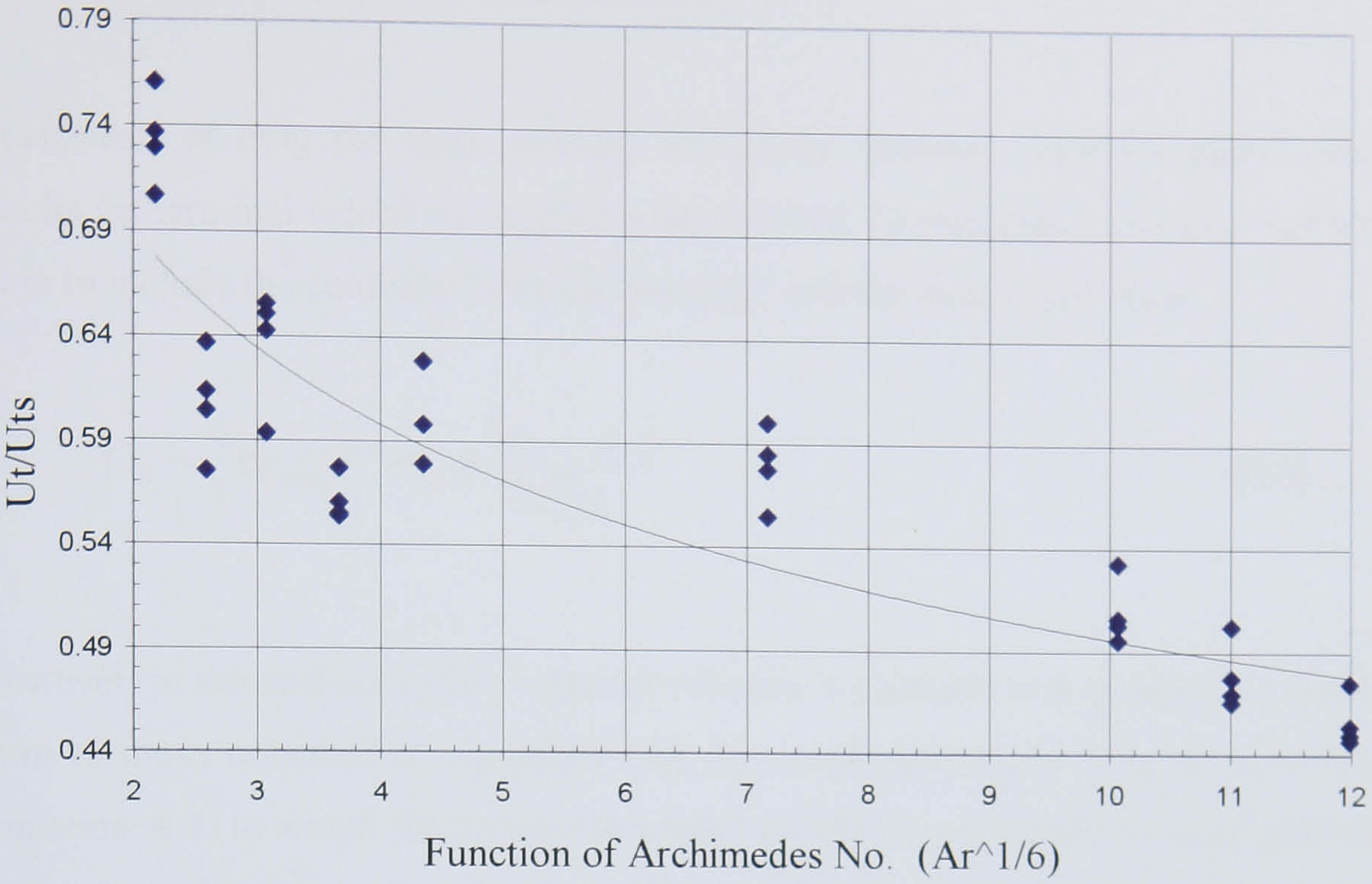

Fig. (6.3), Terminal Velocity Correlation for Experimental Sand (A) & (B)

Table (6.4), Results of Terminal Velocity Correlation for Sands (A)& (B)

Particle Dia. (mm)	Terminal Velocity (m/s)			% relative error
	Sphere (Uts)	Particle (Ut) (experimental)	Correlation (Utcorr.)	
0.15	0.0183	0.0134	0.0124	-7.9%
0.212	0.0303	0.0184	0.0199	7.48%
0.3	0.0474	0.0295	0.0301	1.97%
0.425	0.0709	0.0365	0.0398	8.3%
0.6	0.1019	0.0613	0.0603	-1.71%
1.7	0.2562	0.1484	0.1372	-8.18%
3.35	0.4169	0.2124	0.2086	-1.81%
4	0.463	0.2216	0.2276	2.62%
4.75	0.5081	0.2319	0.2455	5.55%
		%Average Rel. error		0.755%

6.5. Coefficient of Drag Correlation:

Coefficient of drag for sand particles is directly obtained from the experimental results for terminal velocities. Applying equation (A.2) (Appendix (A)) in a modified form to include the equivalent particle diameter and the mass ratio. Thus:

$$C_D = \frac{4}{3}(\psi_{mass})^{1/3} d_{sp}\, g \frac{(\rho_S - \rho_L)}{U_t^2 \rho_L} \qquad (6.9)$$

However, in the absence of the terminal velocity, a correlation is needed in a similar form to those reviewed in Appendix (A). The procedure starts with standard form (equation A.3) in which the particle Reynolds number is calculated for sand particles (equivalent diameter and mass ratio), the coefficient of drag is found according to equation (6.9) and then correlating the coefficient of drag as function of particle Reynolds number. Thus:

$$C_D = K(X)^n \qquad (6.10)$$

where X is the R.H.S. of Turton and Levenspiel [47] standard correlation for spheres but modified by equivalent particle diameter and mass ratio, K and n are correlation coefficients. Using a power law best-fit regression function the final form of the correlation is:

$$C_D = 3.4531(X)^{-0.7862} \qquad (6.11)$$

Table (6.5) summarizes the results. Relative error percentage is in the range of ±12%. Bearing in mind that terminal velocity correlation contributes by about ±8% of the error. However the error is fairly distributed as indicated by the low value of the average error, which is less than 1%.

Table (6.5), Results of Coefficient of Drag Correlation viz. Experimental

Particle Diameter (mm)	Coefficient of Drag		%Relative Error
	Correlation	Experimental	
0.15	23.06714	25.36403	-9.96%
0.212	13.87792	14.06768	-1.37%
0.3	9.04107	8.691358	3.87%
0.425	6.317335	5.896437	6.66%
0.6	4.687121	4.323112	7.77%
1.7	2.479875	2.213472	10.74%
3.35	1.865424	1.886899	-1.15%
4	1.776578	1.892622	-6.53%
4.75	1.713546	1.931269	-12.71%
		Average	-0.30%

Figure (6.4) exhibits a comparison between a standard correlation for spherical shape and that of the true sand experimented on in this work. The general trend is the same. At lower Reynolds number, both curves come closer indicating that finer particles are relatively near to round shape compared with the coarser ones. As Reynolds number increases, the correlation slope reduces until toward the highest values it becomes nearly asymptotic to horizontal. This agreement is in conformity with the well-known dependence of the coefficient of drag on the Reynolds number only at higher values of the latter. However, the curve for sand particles is shifted up higher than that for perfect spheres. Its decrease is rather less steep than that for spheres. These differences may be attributed to the shape imperfections of sand giving rise to drag specially at higher particle sizes (associated with higher Reynolds numbers). This is to be expected, as the larger sand particles are more of a prism than a sphere.

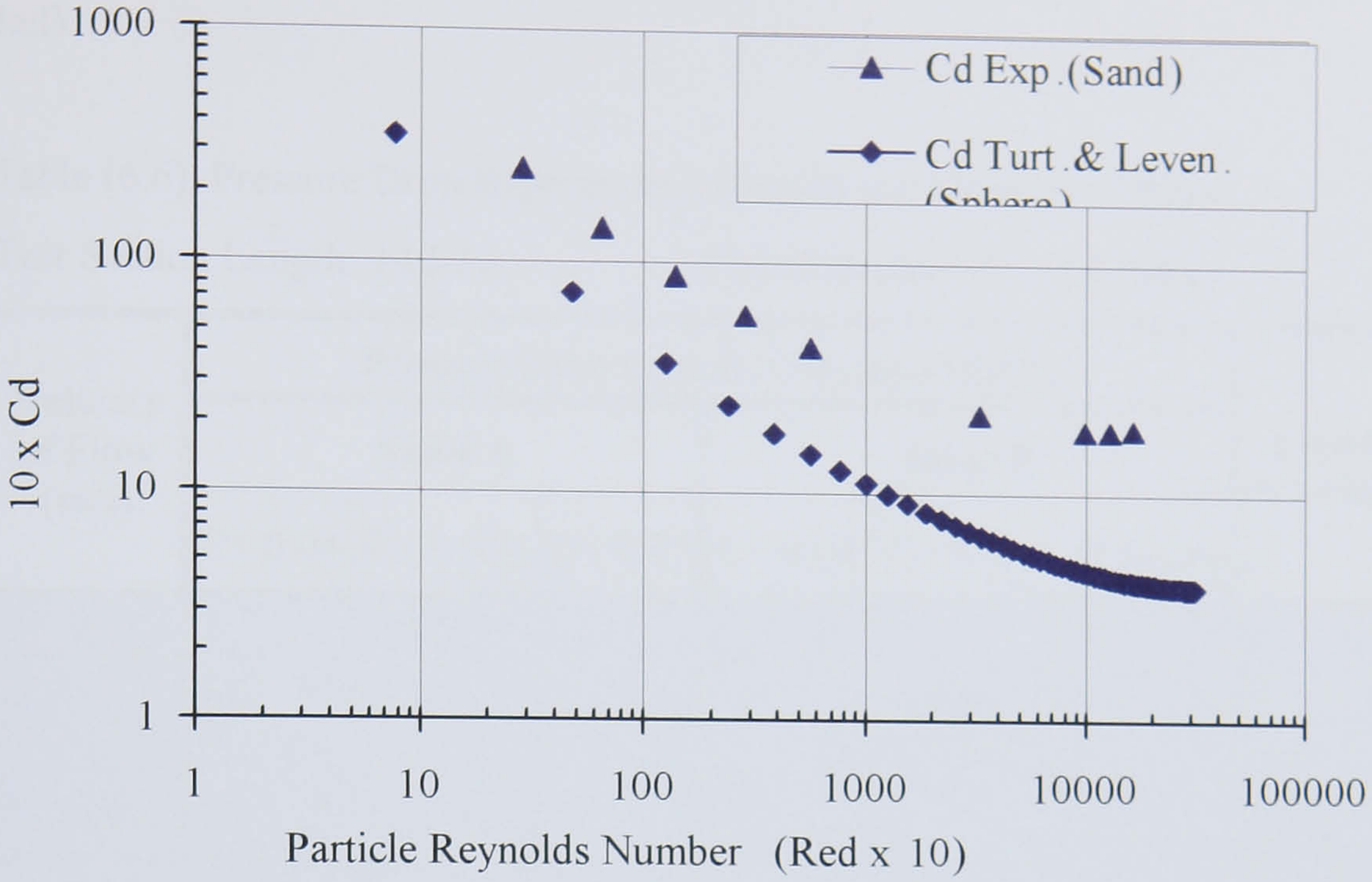

Fig. (6.4), Cd for Sand (A&B) and Sphere viz Red

6.6. Pressure Drop Experimental Results:

Table (6.6) summarizes the experimental results obtained for the various concentrations and flow rates (in terms of the average velocity of flow in m/s). The sand used was pre washed so that to eliminate contamination with dust or mud. The pressure drop readings are quoted in terms of mm H2O per meter of pipe length. The data clearly indicate that for the same concentrations the pressure drop is not equal for the two sand populations (Sand (A) and Sand (B)). Also, it was not possible to obtain higher flow rates for the test runs at higher concentrations and the coarser particles. The reason is that it was necessary to obtain stable readings, which was not achievable due to the care that was taken to discard the readings that produced wavy unstable signals. At higher flow rates for coarse or high concentrations the pump started producing higher vibrations. Moreover, the control of flow rate was restricted to the valve at the outlet of the pipe test section to eliminate any possible turbulence due to restricting the incoming flow at the entrance of the pipe entrance (entrance effects). This may explain the relatively lower number of settings of flow rates. However, the data points are distributed over a reasonable range of flow rates sufficient to represent the relation between pressure losses and flow rate with a fair

degree of accuracy (as will be seen further on in discussing the results in more detail).

Table (6.6), Pressure Drop Experimental Results viz. Velocity of Flow

Test Section Length: 14.59 m Pipe Diameter: 6" (154 mm)

Velocity of Flow (m/s)	Pressure Drop (mm H2O/m pipe length)						Liquid Carrier
	Sand A			**Sand B**			
	C= 0.04	C= 0.056	C= 0.09	C= 0.04	C= 0.056	C= 0.09	
2.0292				71.967			
2.0143					95.956		
1.9000	73.350						
1.8800							31.528
1.8502				48.389			
1.8203				57.574			
1.8200		55.520					
1.7888							27.416
1.7590							28.239
1.7300		79.781					
1.6711				52.776			
1.6300							25.017
1.6263					52.913		
1.6200			89.788				
1.6114	35.888						
1.5816				43.660			
1.5667					69.568		
1.5503							23.989
1.5200							17.409
1.4921						125.840	
1.4921		38.590					

../ Continued … Table (6.6),

Velocity of Flow (m/s)	Pressure Drop (mm H2O/m pipe length)						Liquid Carrier
	Sand (A)			**Sand (B)**			
	C= 0.04	C= 0.056	C= 0.09	C= 0.04	C= 0.056	C=0.09	
1.4622					50.377		
1.4473					57.300		
1.4324	26.000		59.973				11.926
1.4175			66.278				
1.3714							19.740
1.3279			53.256				
1.2981						95.956	
1.2384						81.563	
1.2300	21.614						
1.1936						71.282	
1.1600		29.472					8.773
1.1340					34.407		
1.1329							15.833
1.1200		23.715					7.814
1.1100			30.158				
1.0584							16.175
1.0444						62.371	
1.0146						57.916	
0.9848						58.602	
0.9698					28.650		
0.9541							12.543
0.9400				13.228			
0.9251				16.175			
0.9000	11.652						

../ Continued …Table (6.6),

Velocity of Flow (m/s)	Pressure Drop (mm H2O/m pipe length)						Liquid Carrier
	Sand (A)			**Sand (B)**			
	C= 0.04	C= 0.056	C= 0.09	C= 0.04	C= 0.056	C=0.09	
0.8800		14.393					
0.8795							11.857
0.8654				14.393			
0.8646							11.995
0.8505			18.917				
0.8400							5.003
0.8356						54.832	
0.8050							10.350
0.7162						43.180	
0.7013					24.674		
0.6565			14.051				
0.6416				8.019			
0.6112							8.088
0.6100	3.633						2.193
0.5968		7.197	9.321				
0.5814							7.471
0.5521				6.717		23.989	
0.5217							4.798
0.4770							3.564
0.4625				3.427			
0.4178				5.346			
0.3730						20.836	
0.3700							0.960
0.3600		2.399					
0.3581					8.088		
0.1940			4.798				
0.1800	1.234						

6.6.1. Pressure Drop Experimental Results for Coarser Population (Sand (A)):

Figure (6.5) is a plot of the pressure drop against the average velocity of flow for the coarser population (Sand (A)). Preliminary examination reveals that as the concentration increases the pressure drop increases. The curves seem to represent the trends fairly well (the curves of 0.04 and 0.056 concentrations are closer to each other while the curve of 0.09 concentration is situated further above). At the lower end of flow rate the curves approach the carrier liquid curve and become closely spaced indicating inception of accelerated settling. However, the readings at the lower end were stable and repeated themselves well during tests. Much lower values were not achievable due to severe vibration of the pump (indicating significant failure of suspension of solids). The velocities within this failure range fall consistently around 0.2 m/s.

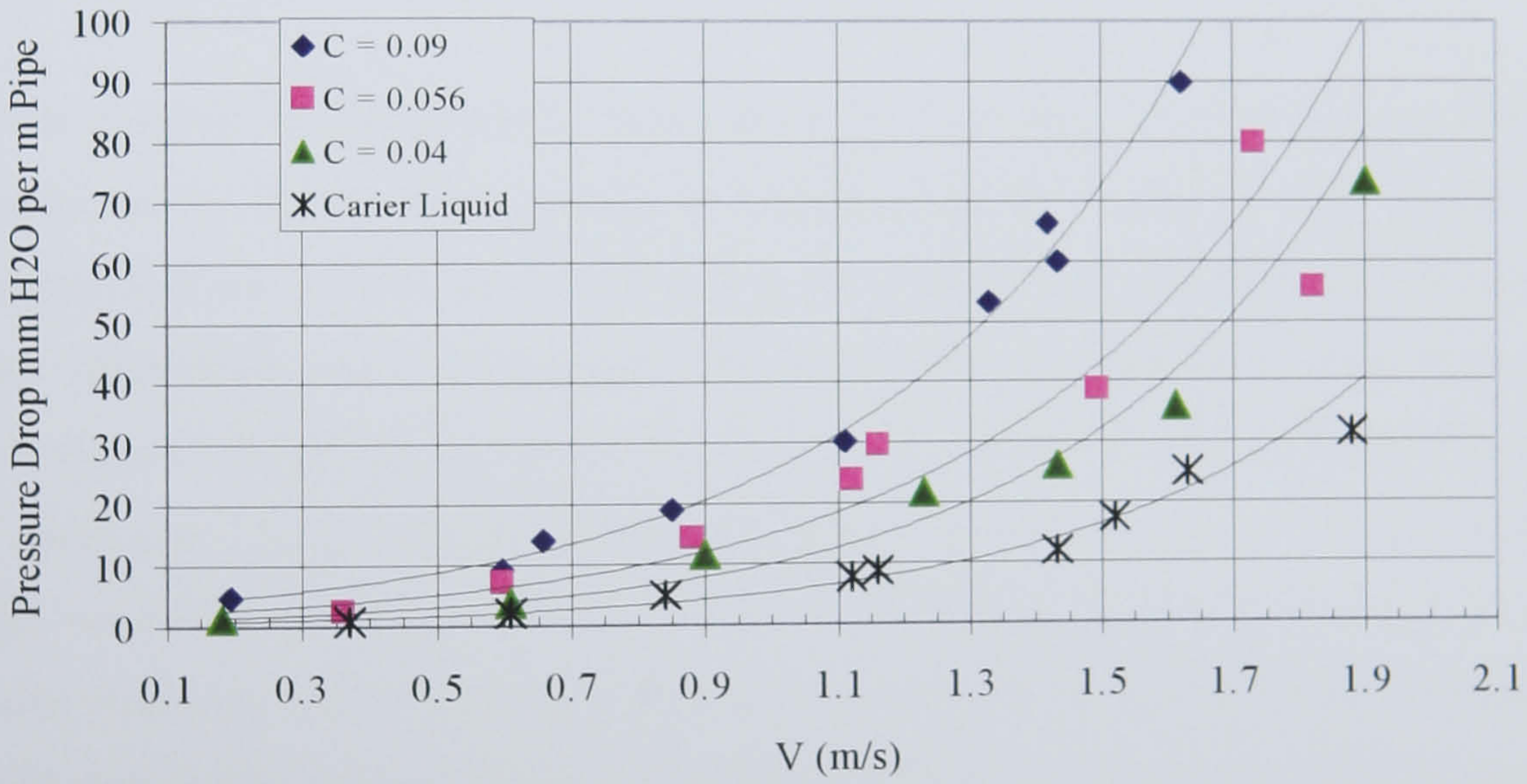

Fig. (6.5), Pressure Drop viz Velocity of Flow for Sand (A) at Different Concentrations

At higher velocities of flow (higher flow rates), the trend indicates greater rise compared with carrier liquid. The trend is fairly similar for the lower concentrations and significantly higher for the higher concentration. Even less scatter of the data points is observed at the highest concentration. This may suggest that the drag

mechanism becomes more effective as the concentration increases (in terms of imparting more energy to particles by fluid stream). The explanation is in two parts. first, suspension is increased due to increased turbulence and second, more energy exchange takes place between particles due to increased frequency of mutual collisions (being confined within the same boundary but with increased number of particles). Moreover, better degree of homogeneity is expected due to accelerated diffusion as a result of repeated collision (particles tend to follow the lowest energy path towards some form of equilibrium state). This may be confirmed by the greater rise of the trend line for the highest concentration as compared with the other lower ones.

In the intermediate region of the trend lines it seems common behaviour for all of them to have lesser rise than at the higher end. This could be attributed to increased heterogeneity of the concentration distribution due to relatively lower turbulent suspension and less severity of mutual collisions. However, the drag mechanism seems to work well as may be observed by the continual rise of the trendlines.

In the absence of experimental results about the exact degree of heterogeneity of the concentration distribution (being considered out of scope of this work), the commonly known relations for the starting of heterogeneity and formation of moving beds (departing from homogeneity of concentration distribution) were examined. Correlations of table (2.1) reviewed in chapter (2) were solved for the particle sizes of Sand (A). All proved unrealistic indicating either formation of moving beds at high velocities of flow exceeding 4 m/s or indicating full suspension at extremely lower velocities below 0.2 m/s. However, the relation given by Wilson [24] seems to yield reasonable estimation of onset of suspension for the lower range of particle sizes. The equation is:

$$V_t = 0.6U_t\sqrt{\frac{2}{f}}\exp^{\frac{45d}{D}} \qquad \text{Ch. 2 (2.9)}$$

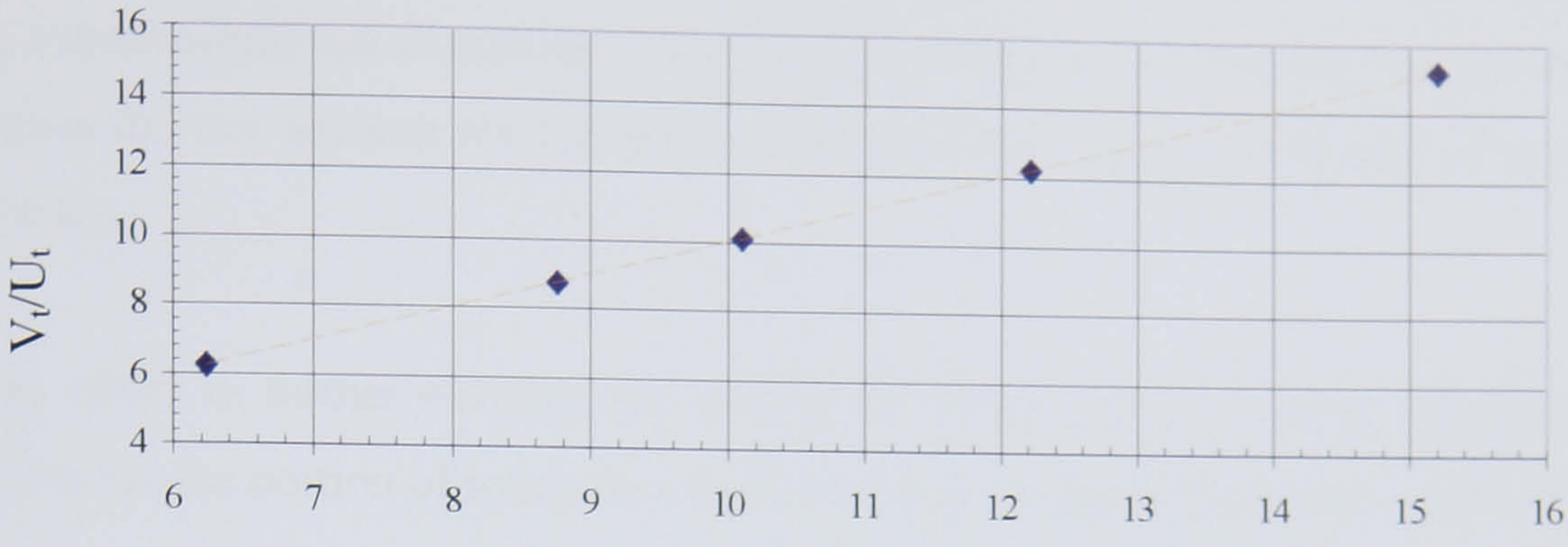

Fig. (6.6), Incipient Suspension Velocity (Sand (A))

Figure (6.6) depicts a linear relation between the deposition to terminal velocity ratio and the exponential of the R.H.S. and suggesting higher velocities for incipient suspension at higher multiples of terminal velocities (ranging from around 6 to 15). In its non- dimensional form, Inception of suspension is initiated at higher suspension number (the exponential quantity at R.H.S. of above equation). In conjunction with data in table (6.7), it can be seen that at higher sand particle diameter, suspension starts at a velocity near 3.7 m/s while at the average particle diameter for Sand (A) the value falls to around 2 m/s. However, applicability of Wilson's relation is much in doubt for polyfractional sand (such as Sand (A)). In this work, visual observation indicated significantly higher degree of suspension than may be predicted by the above relation. Observing the effluent coming out of the test section showed all particle sizes to discharge virtually simultaneously.

Table (6.7), Incipient suspension Data for Sand (A)

d. (mm)	(Vt) m/s	(Ut) m/s	Suspension No.	(Vt/Ut)
2.86	2.08000	0.23758	8.75496	8.75496
1.70	0.85553	0.13719	6.23618	6.23618
3.35	2.10663	0.20858	10.09975	10.09975
4	2.77925	0.22758	12.21232	12.21232
4.75	3.73278	0.24550	15.20465	15.20465

Also, it was possible to filtrate out almost all the sizes of sand during switching from one experimental run to another. This could be explained by the fact that the above relation did not account for the accelerated suspension due to existence of smaller particles.

In an effort to further examine the validity of equation (2.9), another relation that determines the portion of solids moving in contact (creeping) load was examined.

The relation of Gillies *et al* [30] is:

$$\frac{C_C}{C} = \exp(-0.0184 \frac{V}{U_t}) \qquad \text{Ch. 2 (2.17)}$$

This relation is built on equation (2.9). Table (6.8) summarizes the results of this relationship. As it can be seen, it could hardly predict the existence of suspended part of Sand (A). Actually, it suggests that all the solids move as creeping bed. In this work, visual observation and the ability to filtrate virtually all the solids out of the test loop gives an evidence of its poor validity to polyfractional slurry similar to Sand (A) mixture. Also, the relatively higher rise of the trend lines in fig. (6.5) when velocity of flow was increased further suggests that suspension higher than predicted by the above relations is taking place (probably due to more efficient drag mechanism embracing turbulent suspension and dispersive diffusion due to collisions).

Table (6.8), Contact Load for sand (A)

Velocity (m/s)	Sand A Contact Load (C_C)		
	C= 0.04	C= 0.056	C= 0.09
0.1	0.0397	0.0556	0.0893
0.3	0.0391	0.0547	0.0879
0.5	0.0385	0.0539	0.0866
0.7	0.0379	0.0530	0.0853
0.9	0.0373	0.0522	0.0839
1.1	0.0367	0.0514	0.0827
1.3	0.0362	0.0506	0.0814
1.5	0.0356	0.0499	0.0801
1.7	0.0351	0.0491	0.0789
1.9	0.0345	0.0483	0.0777

6.6.2. Pressure Drop Experimental Results for finer Population (Sand (B)):

Figure (6.7) is a plot for Sand (B) of pressure losses in meters H2O per meter of pipe length versus average velocity of flow in m/s. The general rising trend is observed for all concentrations. The same precautions discussed for Sand (A) apply; the range of velocities was dictated by the stability of the pump operation. At the lower end of the curves, they converge to the carrier liquid curve indicating the same trend as for Sand (A). However, convergence is significantly less than for Sand (A). The trend lines rise more rapidly as the velocity is increased; indicating greater influence of drag due to turbulent suspension taking place at lower velocities of flow. At the higher end, much divergence is observed in excess of that observed for Sand (A). In general, all the set of curves of Sand (B) are shifted higher up on the pressure loss scale for the same flow velocities compared with the set of Sand (A). Moreover, the trend is much pronounced for the higher concentration. The same reasoning apply as for Sand (A); more efficient drag mechanism is observed due much higher drag coefficient for smaller particles than for relatively coarser ones and the effect of more frequent particle collisions is even more due to the increased number of particles of smaller size filling the same void of coarser ones (for corresponding similar concentrations). The effect of divergence is specifically higher for the highest concentration confirming increased diffusion and inter-particle collisions. In the intermediate range, the rise is seemingly consistent and at a rate higher than observed for Sand (A). This may be directly attributed to the relative ease with which smaller particles are suspended. To validate the latter case, the same application of equations of incipient suspension and contact load determination were repeated (equations 2.9 and 2.17).

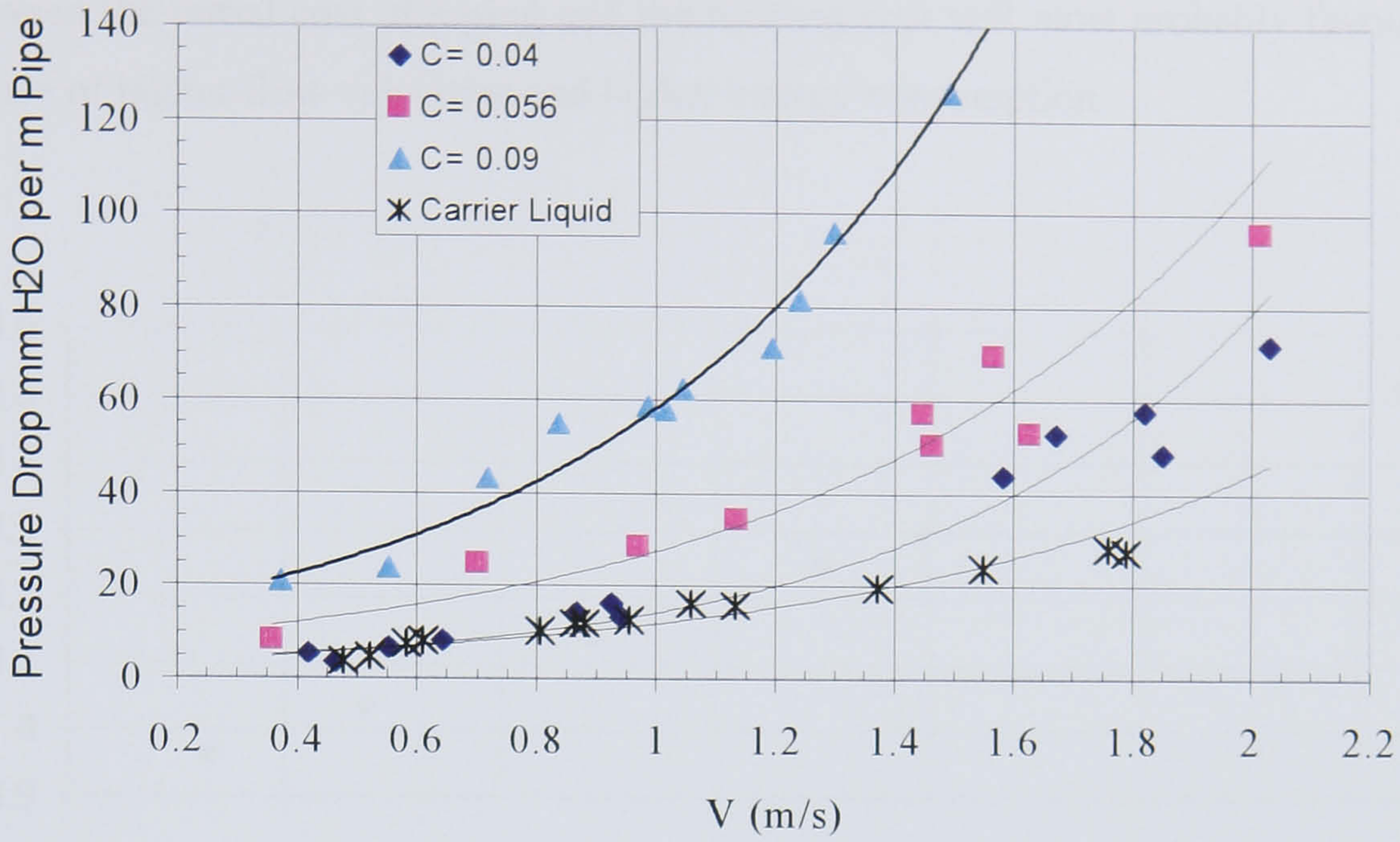

Fig. (6.7), Pressure Drop viz. Velocity of Flow for Sand (B) at Different Concentrations

Figure (6.8) shows clearly that suspension starts much earlier than for Sand (A). For even the larger particle sizes, the suspension is clearly taking place at a reasonably lower velocity in the range of 0.27 m/s. The full range of suspension velocities is in good agreement with the visual observations in this work. Re-examining the lower end of fig. (6.7) further confirms that almost all constituents of Sand (B) go into suspension within the proximity of the tabulated velocities. Although, unstable operation of the pumping device prevented further investigations at much lower flow velocities. Suspension number is much lower than for Sand (A). One of the main differences observed thus far between Sand (A) & (B) is the more accelerated suspension of Sand (B) at the lower range of measured velocity of flow, which further indicates that Sand (B) assumes more homogeneous behaviour. The consequence of this observation explains why the pressure drop curves for Sand (B) are shifted vertically higher up for the same concentration as compared with Sand (A). This is supported by the fact, commonly stated in the literature, that homogeneous suspension consumes much more energy than heterogeneous pattern. The homogeneous pattern is marked with even concentration distribution that renders particles to move in a nebular form. Although homogeneous suspension is not practically sought in industrial applications due to excessive energy consumption, in

case of Sand (B) it is readily attainable and seems to be unavoidable. The balance between the initial cost of piping and the running cost will most probably favour the choice of higher flow velocities and higher energy consumption.

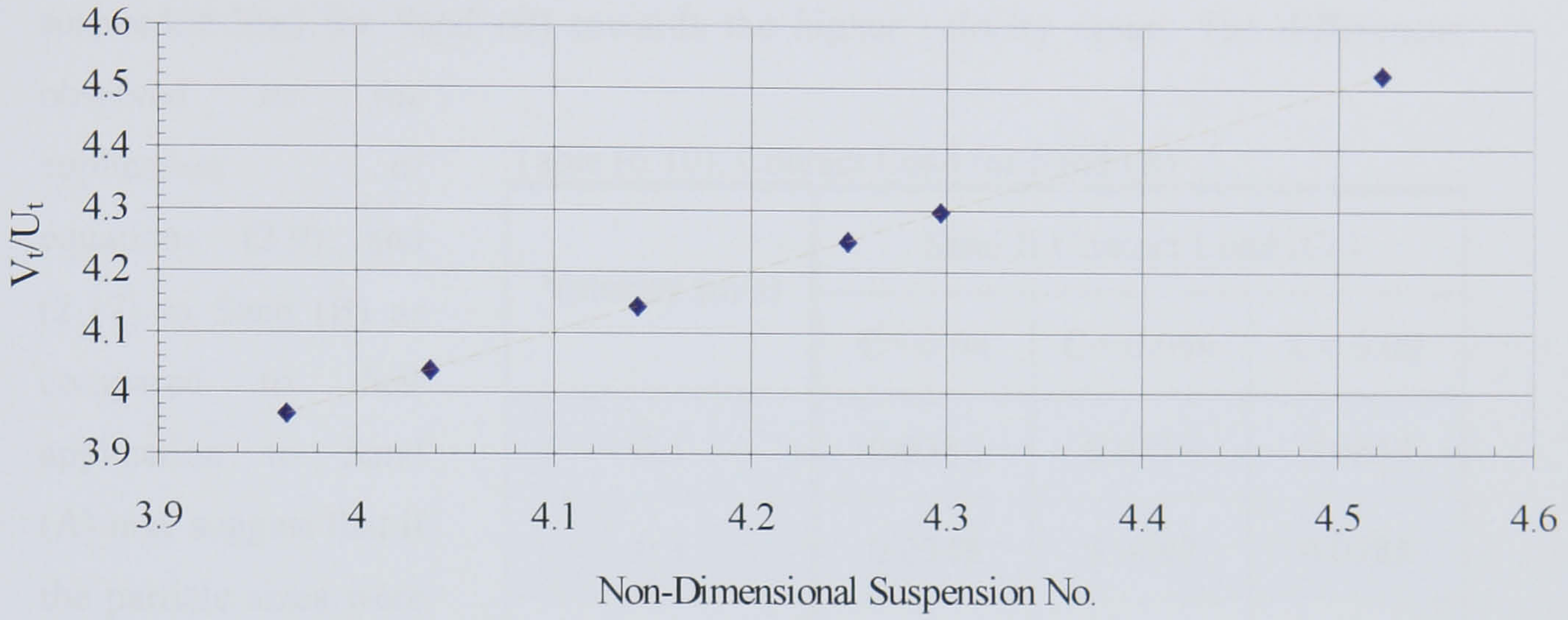

Fig. (6.8), Non- Dimensional Incipient Velocity (Sand (B))

Tables (6.9) and (6.10) show clearly that suspension of Sand (B) is more pronounced than that of Sand (A) for the same concentration. However, contact load prediction using equations (2.9) and (2.17) seems to suffer the same inadequacy except at the higher end of the flow velocities. This suggests, again, that the effect of mixed sizes and the possible increased suspension due to smaller particles are not accounted for. Visual observation coupled with the increased pressure losses for Sand (B) for the same concentrations of Sand (A) and the prediction of lower contact load (table (6.10) higher end) are strong evidences that drag mechanism is remarkably more efficient for lower particle sizes and possibly

Table (6.9), Incipient Suspension for Sand (B)

d. (mm)	(Vt) m/s	(Ut) m/s	Suspension No.	(Vt/Ut)
0.39	0.16784	0.03950	4.24906	4.24906
0.15	0.04933	0.01244	3.96476	3.96476
0.21	0.08019	0.01986	4.03724	4.03724
0.30	0.12453	0.03006	4.14240	4.14240
0.43	0.18664	0.04344	4.29651	4.29651
0.60	0.27258	0.06028	4.52193	4.52193

gains leverage by inter-particle support due to smaller fractions in Sand (A). Inter-particle support holds true for both Sands (A) & (B) but its effect is much pronounced for the smaller particle sizes (sand (B)).

Table (6.10), in particular, depicts somewhat better prediction of contact load and suspended load for Sand (B) towards the higher velocity range. The differences observed by the application of equations (2.9) and (2.17) to Sand (B) as compared to their application to Sand (A) may suggest that if the particle sizes were very much smaller, the ability of these equations to predict suspension may be enhanced. However, no reservations were reported in the literature concerning limitations on their applicability.

.

Table (6.10), Contact Load for Sand (B)

Velocity (m/s)	Sand B Contact Load (Cc)		
	C= 0.04	C= 0.056	C= 0.09
0.1	0.0382	0.0535	0.0859
0.3	0.0348	0.0487	0.0783
0.5	0.0317	0.0444	0.0713
0.7	0.0289	0.0404	0.0650
0.9	0.0263	0.0368	0.0592
1.1	0.0240	0.0335	0.0539
1.3	0.0218	0.0306	0.0491
1.5	0.0199	0.0278	0.0447
1.7	0.0181	0.0254	0.0408
1.9	0.0165	0.0231	0.0371

6.7. Paired Comparisons of Results:

Further examination of pressure drop results is necessary by examining each pair of curves representing the same concentration. If the differences in particle sizes are insignificant, then pressure drop for similar concentrations shall invariantly be the same regardless of the changes in particle size distribution. Preliminary examination

of results in figs. (6.5) and (6.7) confirmed existence of significant differences in pressure drops. The treatment to follow will concentrate on highlighting these differences. Each pair of curves representing same concentration will be taken in turn and further examined.

6.7.1. Volumetric Concentration = 4%:

Figure (6.9) compares the trend lines for Sands (A) & (B) at concentration of 0.04 and clearly shows approximately similar results for both sands.

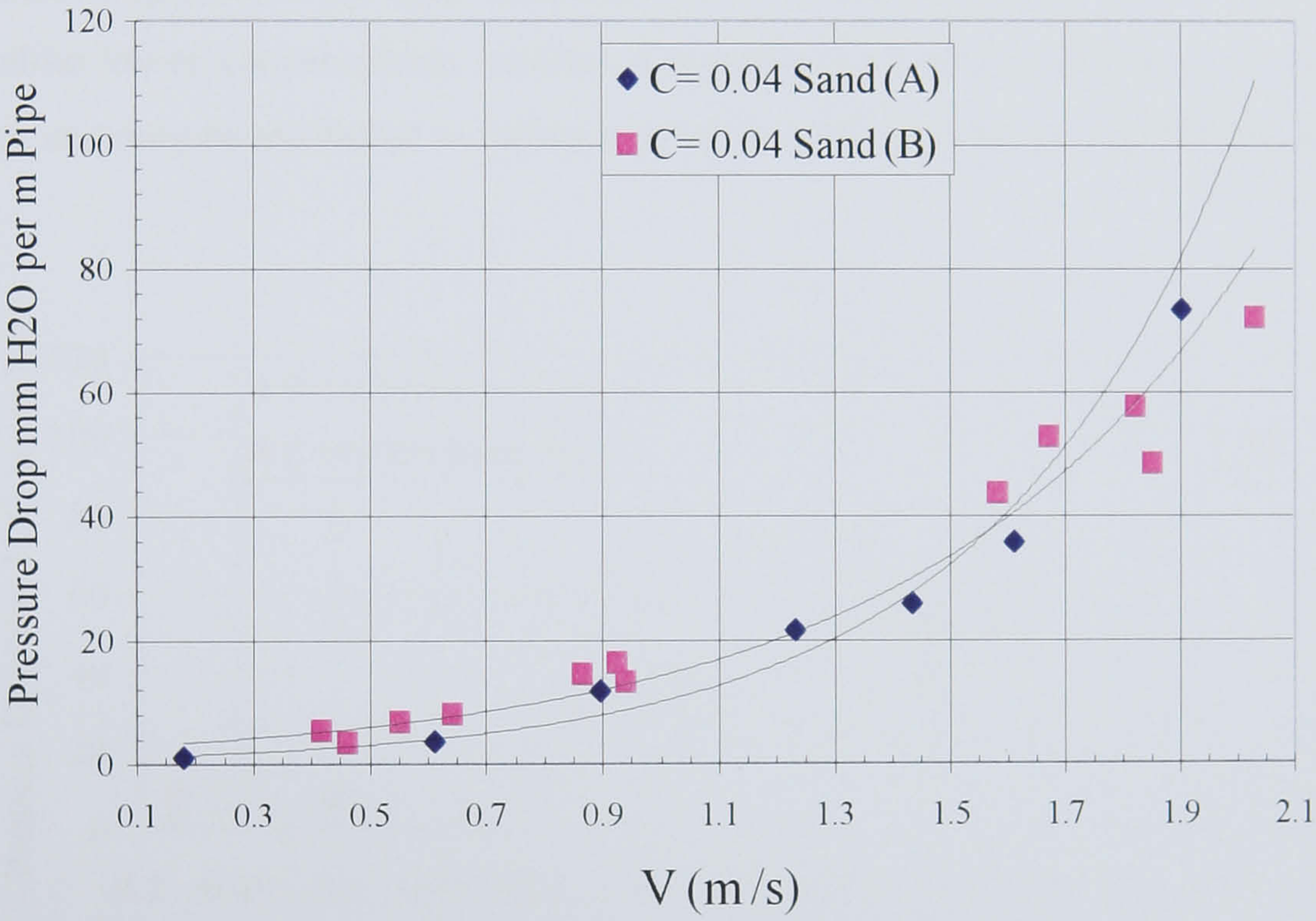

Fig. (6.9), Comparison of Pressure Drops for Sands (A) & (B) at Same Concentration (C = 0.04)

This may be explained that at such low concentration, the dominant factor in determining pressure losses is the total solids content rather than the constituent particle sizes. However, at the lower velocity range the pressure drop of Sand (B) is higher and the rate of rise of Sand (B) trend line is less while at higher velocities the rate of rise of Sand (A) is higher. In view of comparison between these two curves, it may be concluded that suspension of Sand (B) occurs earlier than Sand (A) while Sand (A) starts going into suspension increasingly at a velocity in excess of 1 m/s.

However, pressure drop is less affected by sand type than is observed in the following comparisons.

6.7.2. Volumetric Concentration = 5.6%:

Figure (6.10) shows that pressure drop for Sand (B) is markedly higher for the whole range of flow velocities and that the rate of rise for Sand (B) trend line is less than that for (B). This may reflect the idea that Sand (A) possibly has a higher degree of heterogeneity at lower velocities while Sand (B) maintains invariantly similar degree at the whole range. Smoother curve rise and higher pressure drop for almost the whole range, Sand (B) may be thought of as nearer to homogeneous flow pattern. Unlike lower concentration, marked difference is observed between the two sands that can only be attributed to differences associated with particle size structure.

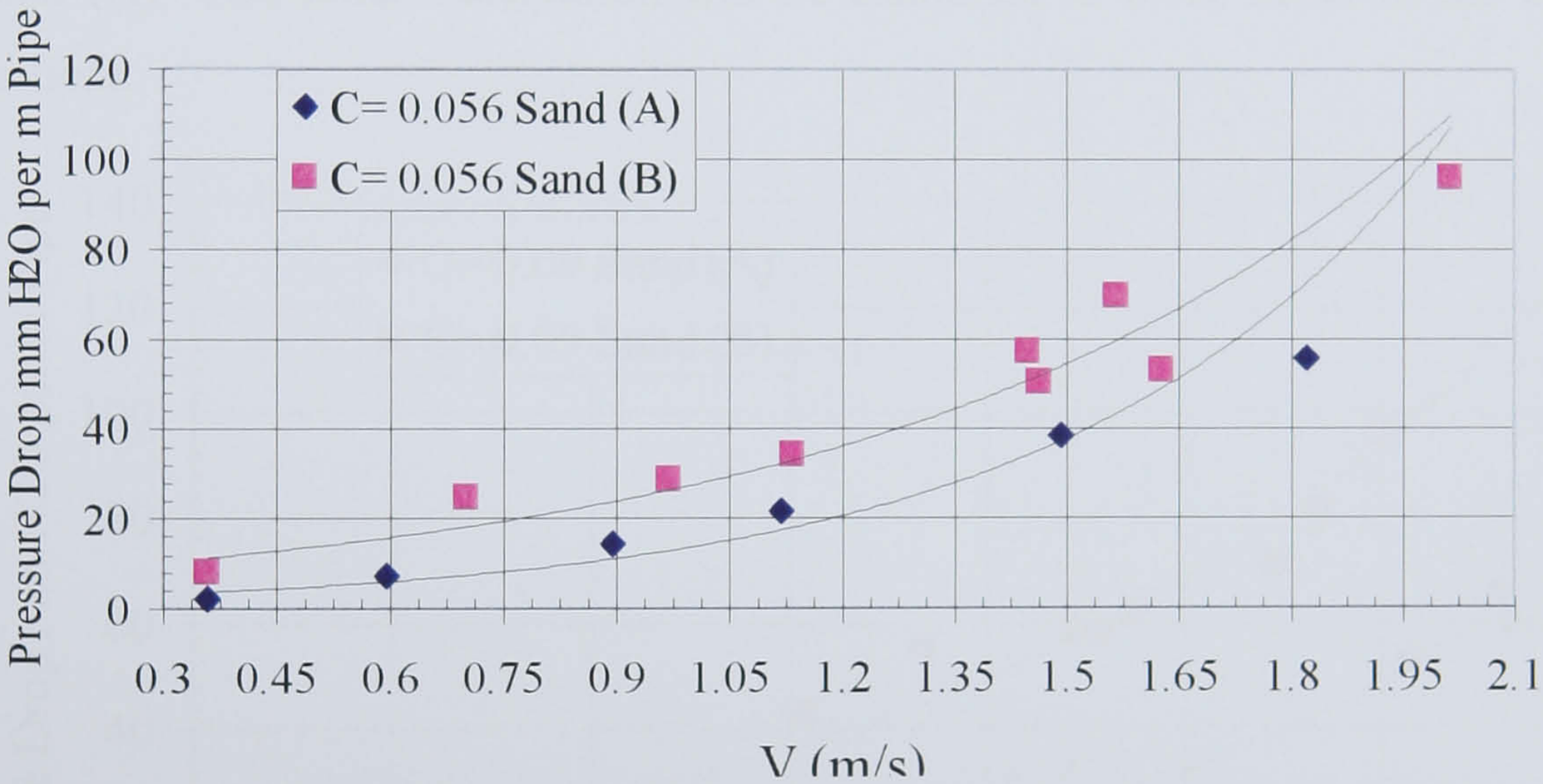

Fig. (6.10), Comparison of Pressure Drops for Sands (A) & (B) at Same Concentration (C = 0.056)

6.7.3. Volumetric Concentration = 9%:

Figure (6.11) shows clear differences between Sands (A) & (B). The trend observed for 5.6% concentration is accentuated more. The pressure drop is higher for the whole range of Sand (B). This indicates that increased concentration pronounces the effects of differences in sand populations giving evidence that inter-particle support becomes higher. Probably through increased collisions leading to increased drag due to efficient suspension of smaller particles which in turn give leverage to suspending larger particles. This explanation concord with observations and in the same manner it can be concluded that at lower concentrations the probability of collisions between particles is less. Thus, leaving the drag mechanism less affected by inter-particle interaction. The consistent trend of less rate of rise for sand (B), observed in all the paired comparisons, is also applicable to this pair of curves. This is an indication that drag mechanism has a similar nature for Sand (B) and it probably changes roles in Sand (A). This latter observation will be examined in more detail in the coming sections.

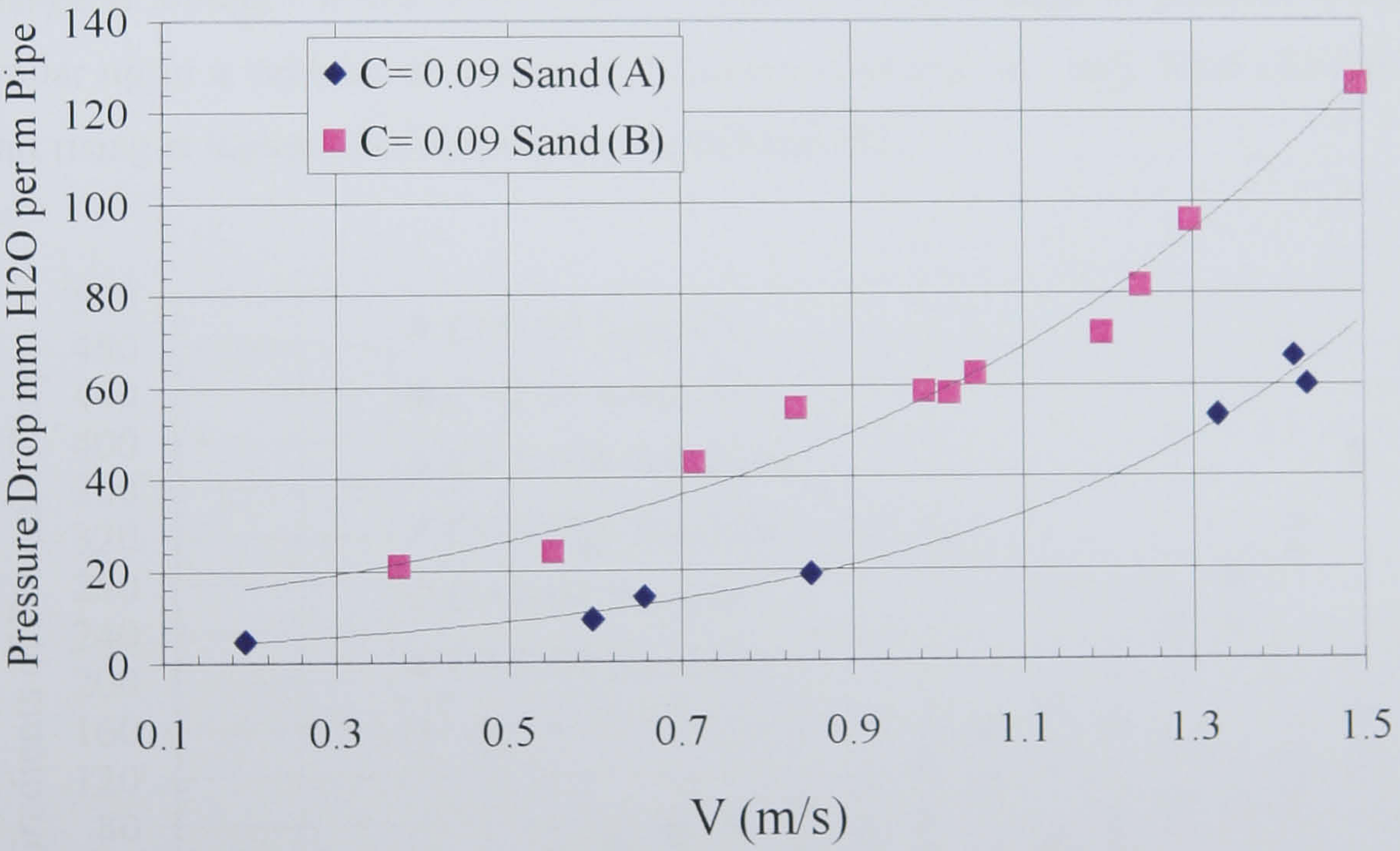

Fig. (6.11), Comparison of Pressure Drops for Sands (A) & (B) at Same Concentration (C = 0.09)

6.8. Further Examination of Results (Comparison of Trend Lines Gradients):

Figure (6.12) is a plot of the rate of change of the trend lines with respect to the velocity of flow $\left(\frac{\partial P}{\partial V}\right)$. The purpose of obtaining the gradients of the trend lines with respect to velocity is to compare the rate of rise of the curves for the different cases. To the knowledge of the author, this method was not cited in the literature. In general, as the velocity increases the gradient increases remarkably. This feature in itself is purely mathematical and commonly known for a power law relationship. However, the interesting features are the differences between the various curves, which should be related to physical reasons.

At the highest volumetric concentration (9%), Sand (B) trend line change is markedly higher for the full range while for Sand (A) the change in gradient increases at around a velocity of 1 m/s and approaches Sand (B) curve gradient change at around 1.8 m/s. For the other trend lines, the change in gradient is fairly similar up to a velocity of 1 m/s. At velocities in excess of 1 m/s, Sand (A) curves start rising at higher rates as compared with Sand (B).

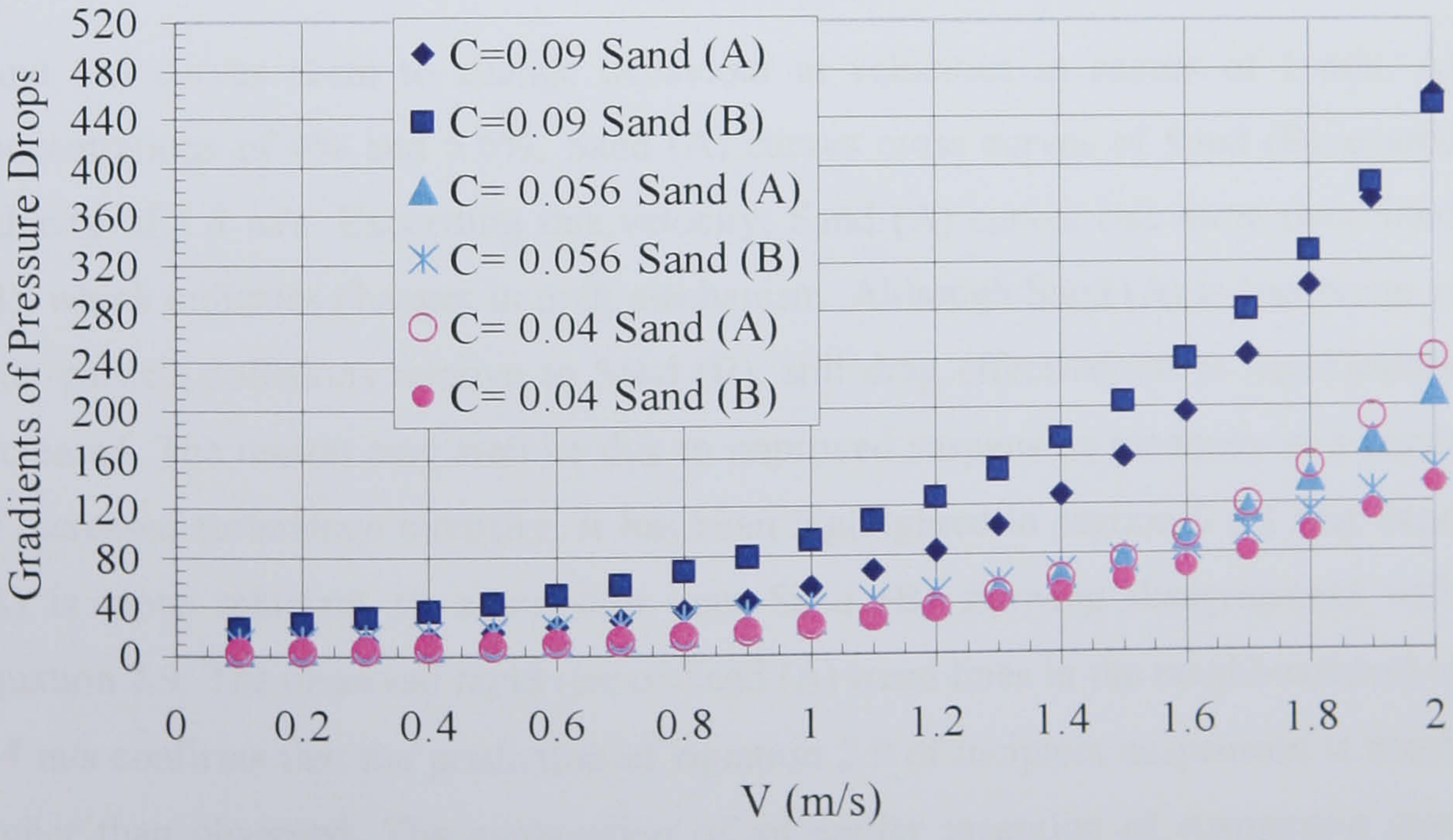

Fig. (6.12), Gradients of Pressure Drops Trend Lines for Paired Comparisons at the same Concentration

The highest change in gradient is that for Sand (A) at the lowest concentration (4%). These observations suggest that changes in concentration influence the rise of the curves. Also, the differences in particle sizes and particle size distribution in each population influence the rise of the curves. In all cases, rise of curves increased with increased concentration (although to a lesser extent below 1 m/s). This indicates that drag effectiveness (translated as more resistance to flow) increases due to increase in concentration. For the same level of turbulence intensity, being a strong function of velocity, the mechanisms of dispersion and diffusion may have increased due to existence of more particles in the same space which results in more inter-particle collisions (due to confinement). This is supported by the observation that, generally, Sand (B) curves start rising earlier than Sand (A) due to more particles in Sand (B) than in Sand (A) for the same concentration. Coupled with the previously mentioned observations (section 6.6.2) that showed suspension to take place in Sand (B) at much earlier flow velocities than for Sand (A), the rather lower rise of Sand (B) curves towards the higher end can be explained. Sand (B) trends seem to include a combined and effective drag mechanism that does not seem to change its nature throughout the range of velocities. Increased drag mechanism effectiveness may be attributed to easier suspension due to turbulence for the smaller particles of Sand (B) (probably enhanced by the existence of much smaller particles) and greater degree of homogeneity due to diffusive-dispersive forces.

Sand (A) curves seem to change behaviour at velocities in excess of 1 m/s. At concentrations of 4% and 5.6%, Sand (A) curves cross curves of Sand (B) around velocity of 1.4 m/s. Exceeding this velocity; Sand (A) curves rise more than Sand (B), which indicates changes in drag mechanism. Although Sand (A) is less prone to inter-particle collisions relative to Sand (B), still drag effectiveness is significantly increased. The reason may well be due to improved suspension tendency as a result of increased turbulence intensity. It has been highlighted in section 6.6.1 that Sand (A) is more reluctant to suspension than Sand (B) showing disagreement with equation 2.9. The observed rapid rise of Sand (A) trend lines in the neighbourhood of 1.4 m/s confirms that the prediction of equation 2.9 of incipient suspension is much higher than observed. The explanation of an earlier inception of suspension than expected (by equation 2.9) could only be explained by the existence of smaller

particles in Sand (A) population that play an assisting role in suspending the larger ones.

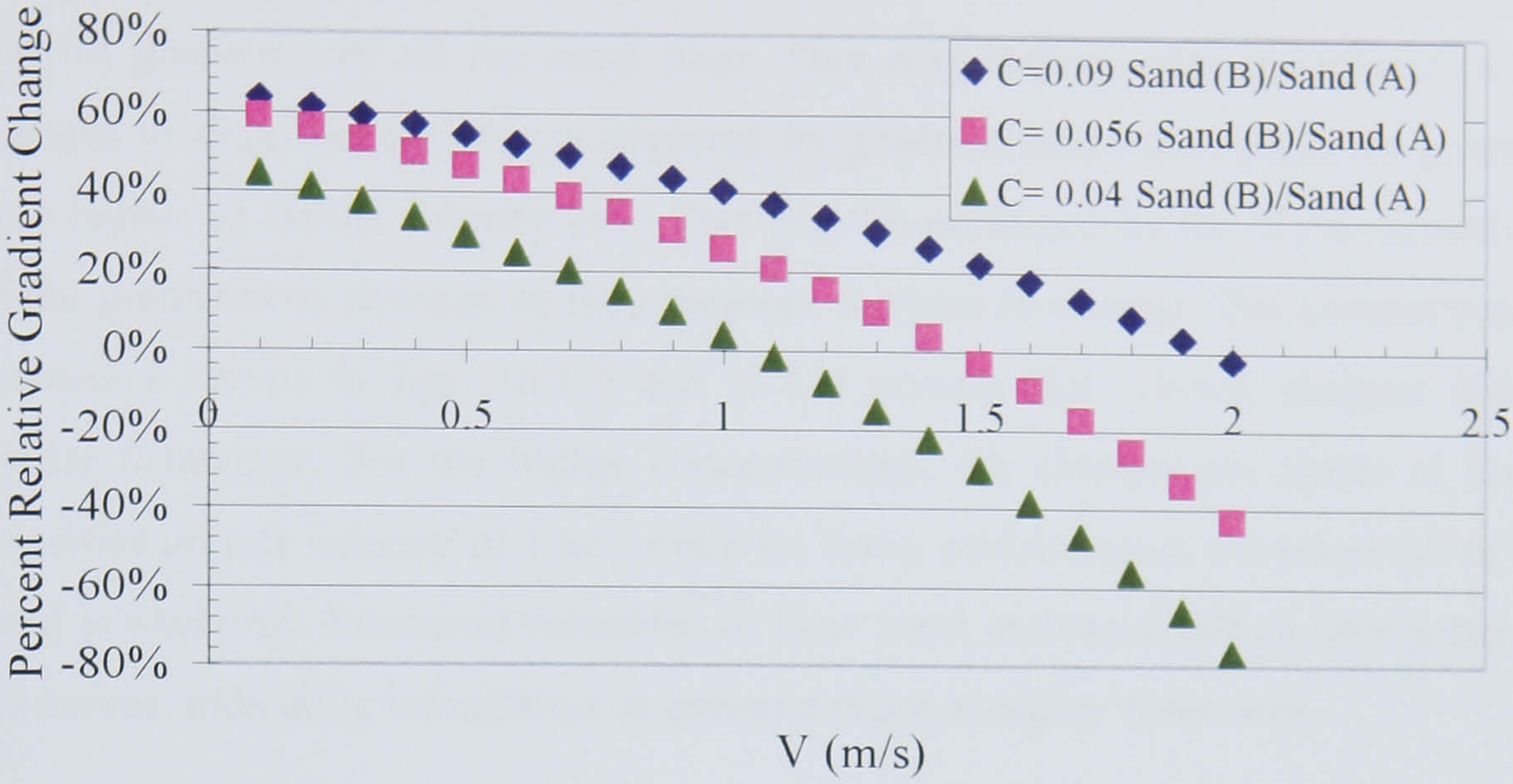

Fig. (6.13), % Relative Gradient Change viz Flow Velocity

Further investigation of the trend lines behaviour is through plotting the relative change of gradients as shown in fig. (6.13). It is clearly observed that relative changes in trend lines are sensitive to concentration. Reversal of relative changes to negative start from 1 m/s for 4% concentration to 1.5 m/s for 5.6% and near 2m/s for 9%. This further confirms that Sand (A) is incurring more pressure losses at higher velocities due to more particles going into suspension. Figure (6.7.5) is constructed using percent relative change relationship in Sand (B) gradient relative to Sand (A). Thus:

$$\%\ \text{Relative Change} = \frac{\text{Gradient (B)} - \text{Gradient (A)}}{\text{Gradient (B)}} \times 100\%$$

The same relationship is used to construct a similar plot for the relative values of pressure drops of Sand (B) to Sand (A) as shown in fig. (6.14). It is necessary to examine the changes in pressure drops for different concentrations and sands in a relative sense. It is not only that the gradient of pressure drop with respect to velocity of flow is important to examine, but also the relative changes of pressure drops themselves. The examination of the gradients highlights the milestones where the various compositions of sand experience changes in drag mechanism. Further

examination of pressure drops for the various trend lines show a shift in the relation towards higher flow velocities. Zero percent relative change of pressure drops occurs higher up on the velocity of flow axis at a shift of approximately 0.5 m/s relative to that for gradients for all the trend lines. This may indicate that the effects of the changes in drag mechanism (as depicted by gradient lines) take place on pressure drop higher up on the velocity axis. This may be explained by the higher sensitivity of the gradients to changes as they measure the rate of change. The comparison of respective curves in figs. (6.13) and (6.14) reveals that relative changes follow similar behaviour. For the higher concentrations, the changes are closer at lower velocities up to a velocity of 1 m/s while for lower concentration a marked fall of the trend is observed. Increased velocities of flow mark increased falling divergence of the curves; indicating less change in pressure drops at higher flow rates.

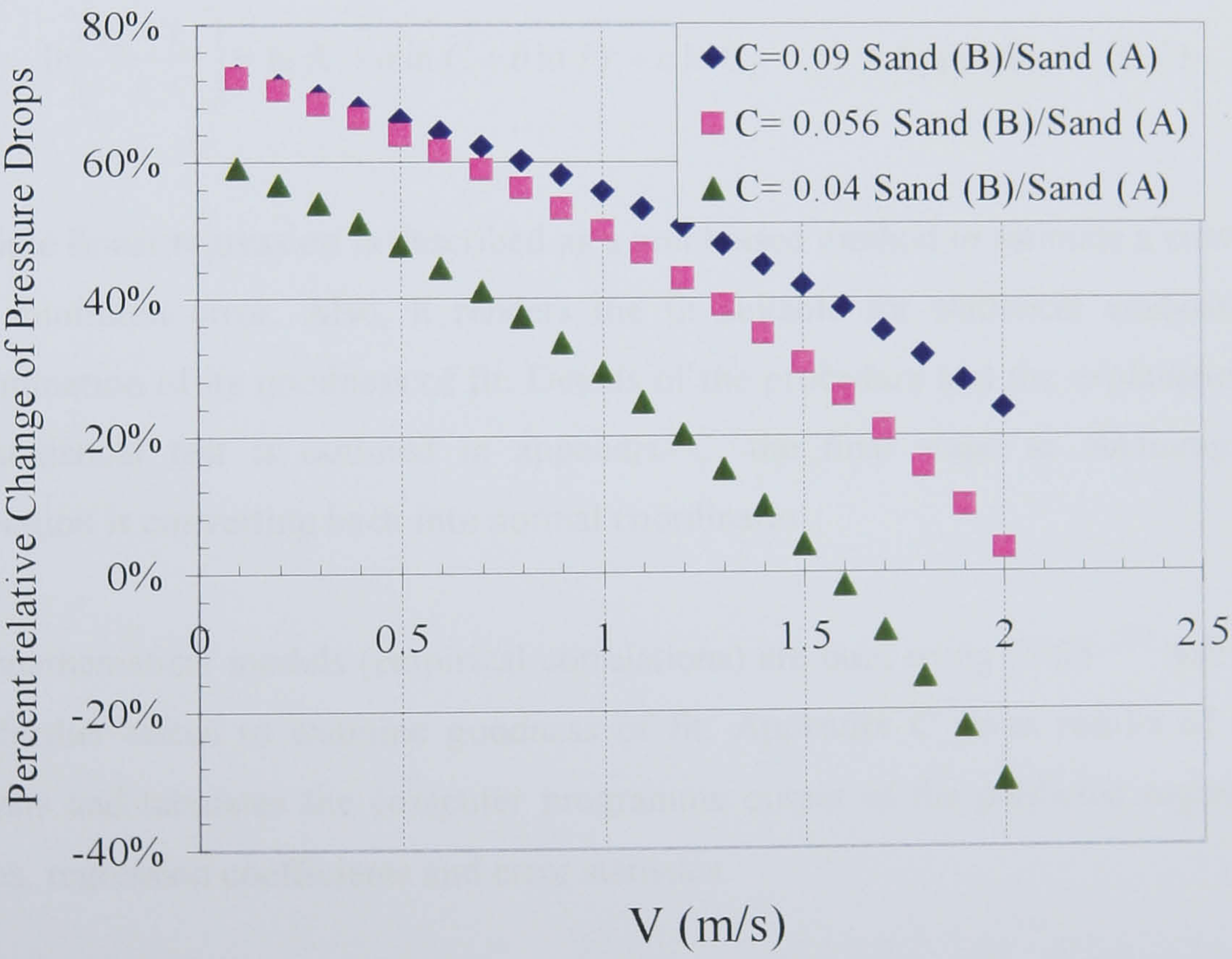

Fig. (6.14), % Relative Change of Pressure Drop Trend lines viz Velocity of Flow at Different Concentrations for Sand (B) Compared to (A)

6.9. Empirical Correlation Building:

The final results of experimental results are needed in a correlation that relates the pressure loss coefficient to the variables controlling the solid liquid flow. The general algebraic form for such correlation was suggested earlier (ch. 4. eqn.4 7):

$$\frac{i_m - i_w}{i_w} = K \cdot C^a \cdot Fr^b \cdot C_D^c \qquad \text{ch.4 (4.7)}$$

For curve fitting purposes multiple linear regression was employed. As such, it was necessary to put the above equation in a linear form by converting it into logarithmic coordinates, thus:

$$\ln\left(\frac{i_m - i_w}{i_w}\right) = \ln K + a \ln C + b \ln Fr + c \ln C_D \qquad \text{Appendix C (C.2)}$$

Multiple linear regression is described as a non biased method to estimate a curve fit with minimum error. Also, it renders the fit suitable for statistical analysis for determination of its goodness of fit. Details of the procedure and the explanation of the statistical test is outlined in appendix C. the final stage in obtaining the correlation is converting back into normal coordinates.

The mathematical models (empirical correlations) are built using SPSS [52] software and further tested to examine goodness of fit. Appendix C gives results of such analysis and tabulates the computer programme output of the predicted regression values, regression coefficients and error statistics.

In principle, ability of the correlation to explain the dependent variable in accordance with changes in the independent variables is measured as a percentage value (the higher the value the better is the fit of the regression). Furthermore, ascertaining that changes in the values of the independent variables are not due to chance but due to significant changes that are correlated to the dependent variable is measured by the

test of significance. Error serial propagation from one measured value to the next is also measured. The following sections give the correlations for Sand (A), Sand (B) and a global correlation for both Sand (A) and (B).

6.9.1. Sand (A) Pressure Losses Correlation:

Figure (6.15) plots the final results of the pressure loss correlation for Sand (A) in logarithmic form. The measured values of the pressure loss coefficient are plotted against the values predicted by the mathematical model (empirical correlation). The linearity of the model is reasonably good. Thus:

$$\frac{i_m - i_w}{i_w} = 1.2523 \cdot C_A^{4.3623} \cdot Fr_A^{2.692} \cdot C_{DA}^{15444} \qquad (6.12)$$

As shown in appendix C, about 86% of the set of experimental results are explained well by the above correlation.

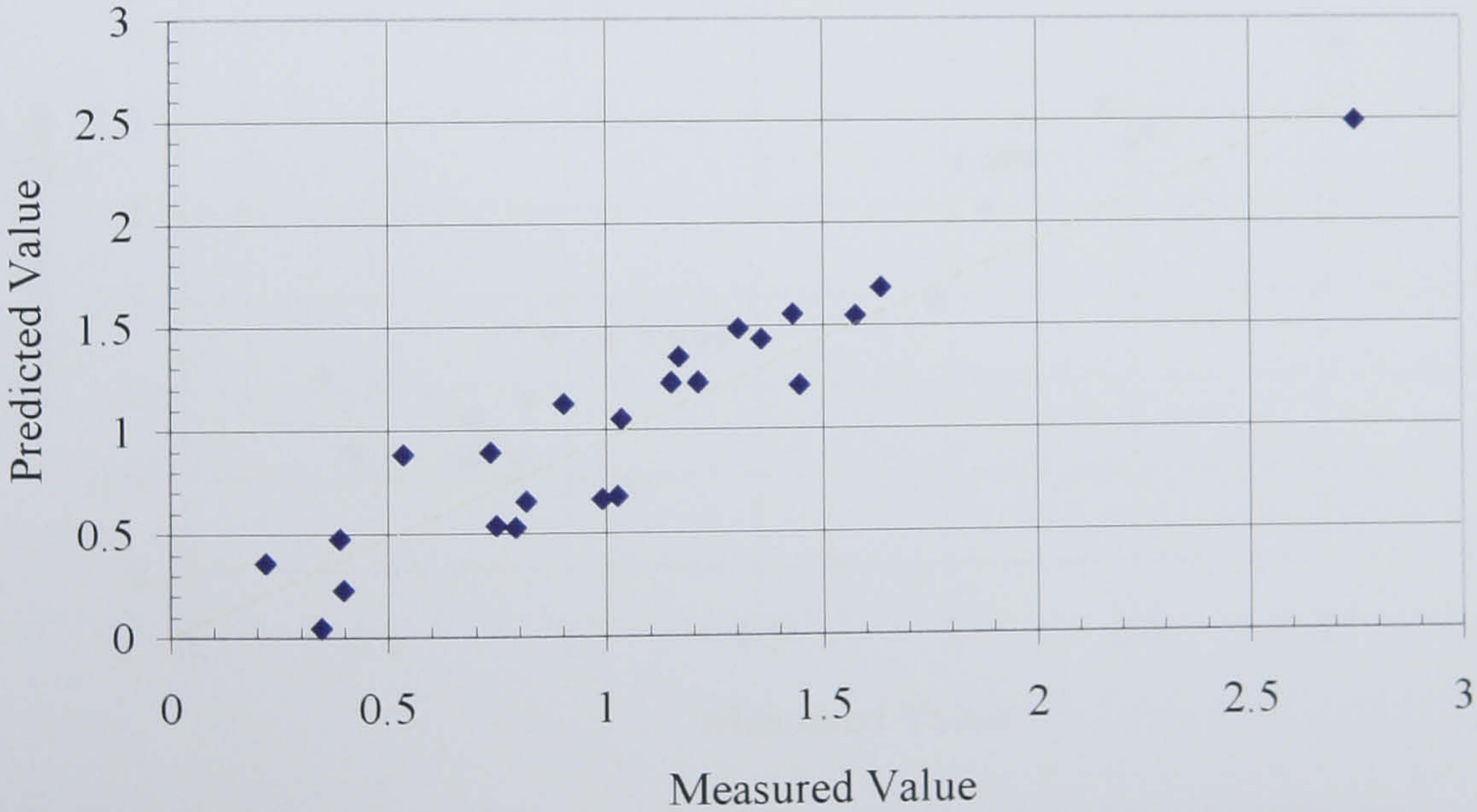

Fig. (6.15), Predicted viz Measured Values for Pressure Loss Coefficient Correlation for Sand A in Logarithmic Form

6.9.2. Sand (B) Pressure Losses Correlation:

Figure (6.16) plots the final results of pressure drop correlation for sand (B). A strong linear relationship is obvious between the measured values versus the values predicted by the empirical correlation. Thus:

$$\frac{i_m - i_w}{i_w} = 1.2789 \cdot C_B^{7.367} \cdot Fr_B^{6.6} \cdot C_{DB}^{12594} \qquad (6.13)$$

About 92% of the experimental results are well explained by the above equation. Comparing the correlation for Sand (A) with that of Sand (B), the effects of densimetric waves and concentration are much pronounced for Sand (B) than for Sand (A). Coefficient of drag is less different in both cases. This supports the previous discussions on differences in pressure drops due to changes in solids content composition. Due to the relatively smaller particle sizes of Sand (B), confinement effects increase the contribution of turbulence and concentration.

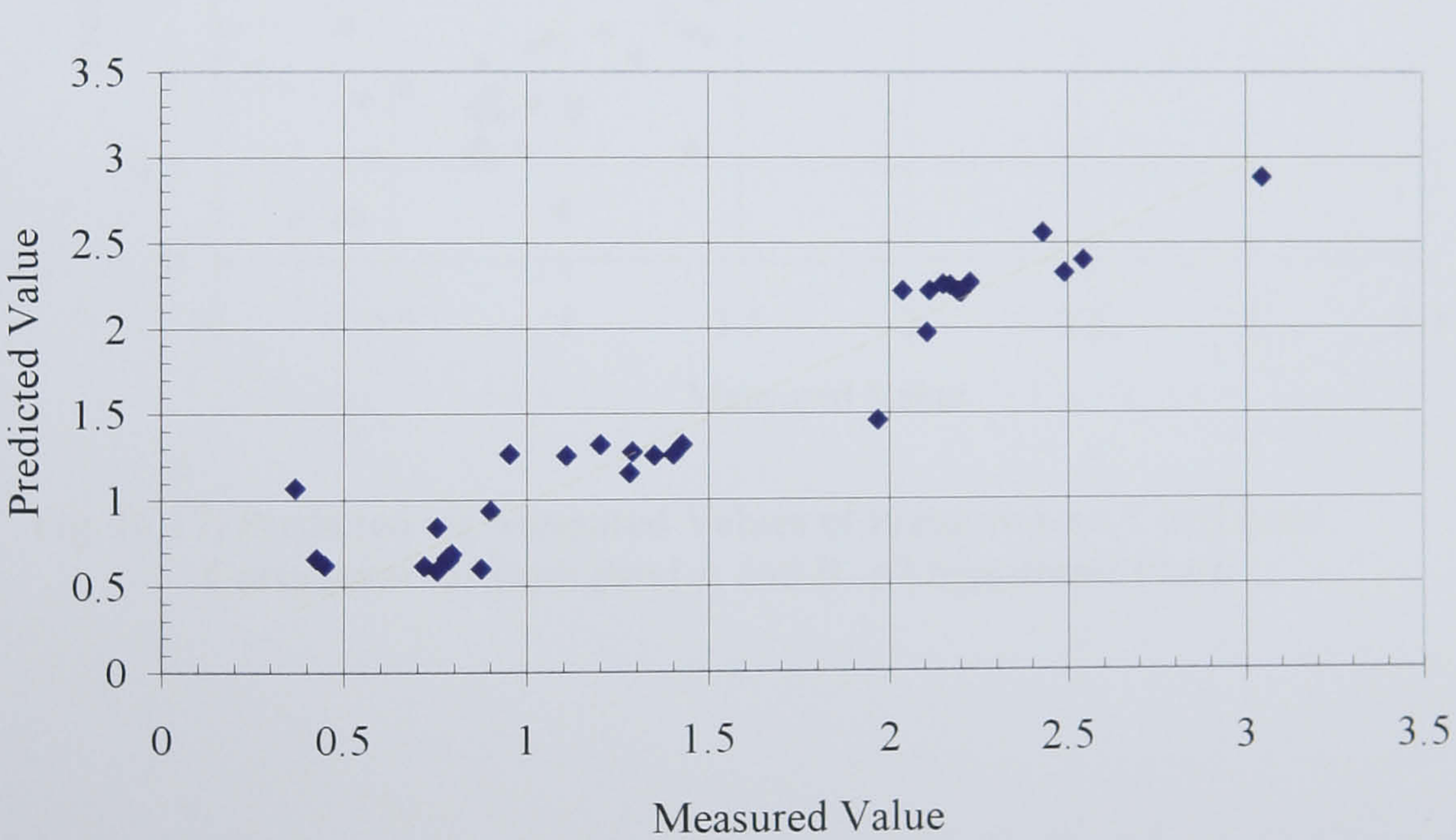

Fig. (6.16), Predicted viz Measured Values for Pressure Loss Coefficient Correlation for Sand B in Logarithmic Form

6.9.3. Sand (A) and Sand (B) Pressure Losses Global Correlation:

Figure (6.17) plots the results of the correlation for all the experimental results collectively for Sands (A) and (B). The relationship exhibits strong linear tendency. Thus:

$$\frac{i_m - i_w}{i_w} = 110.83 \cdot C^{5.398} \cdot Fr^{2.043} C_D^{6.514} \qquad (6.14)$$

About 82% of the values of the experimental results are well explained by the correlations.

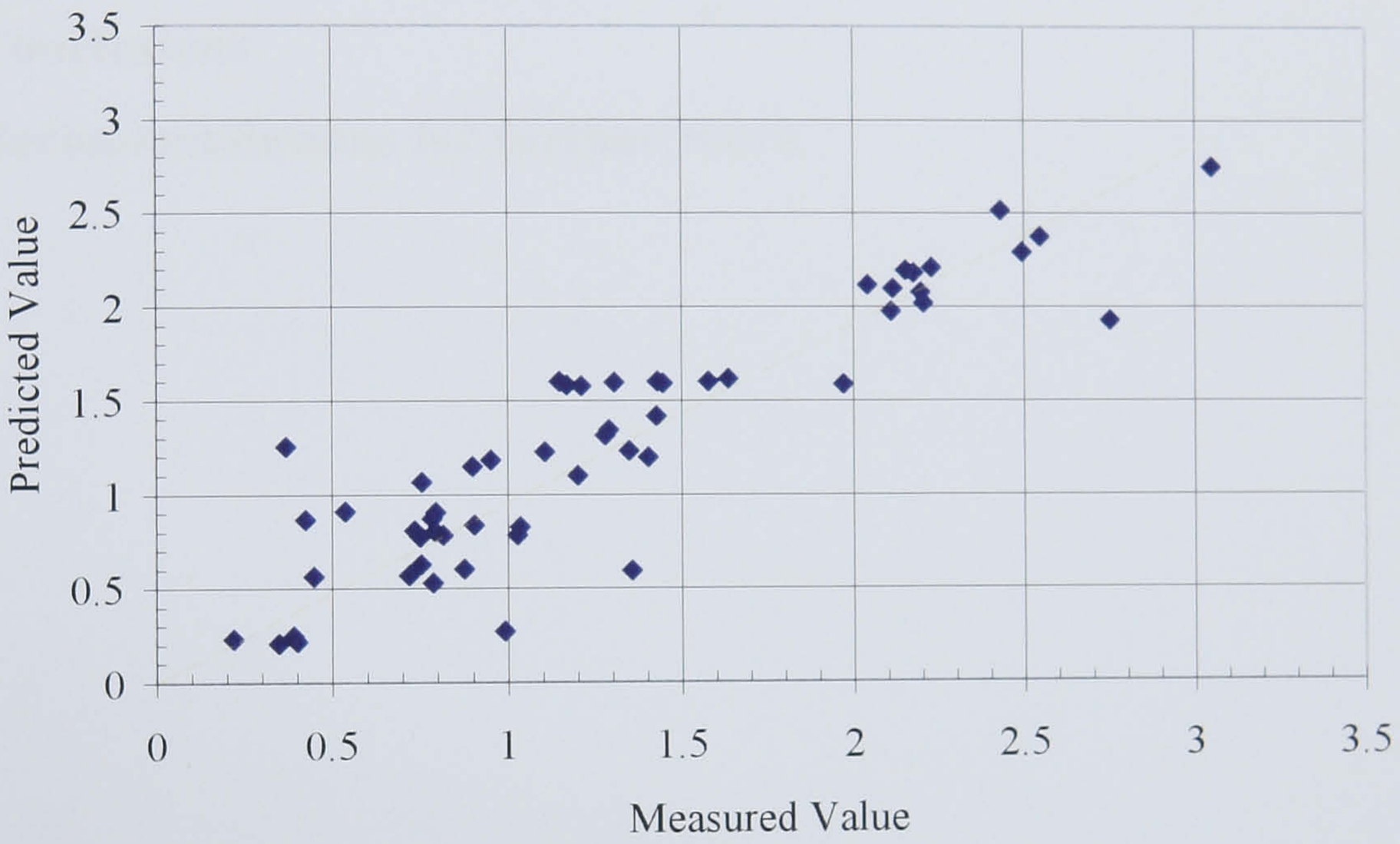

Fig. (6.17) Predicted viz Measured Values of Pressure Loss Coefficient Correlation for Both Sand A and B in Logarithmic Form

Chapter 7

Conclusions and Recommendations for Further Work

7.1. Conclusions:

The problem of solid liquid flow is a multi variable one. Existence of solids in a form of a mixture with liquid introduces more complications to the ordinary fluid only flow problem. In this work, the definition of this problem highlighted the difficulties in the prediction of the pressure losses associated with slurry flow. the added complexity of the existence of solids in more than one particle size was further concentrated on and the subsequent literature review showed that multi particle size slurry (polyfractional mixture) was not well represented in the literature.

Examination of the theoretical principles of solid liquid flow further suggested proceeding with conducting experimental work to determine with fair accuracy a suitably formulated pressure loss coefficient in the absence of an analytical solution. Experimental schedule was developed that allowed for the differentiation between the effects of particle size composition in given slurry by synthesizing two separate mixes of solid particles. The particle size distribution of each of these mixes is centred on a mean that is separated from the other by an order of magnitude (Sand (A) of coarser particle size distribution while Sand (B) of finer particle size distribution). The purpose was to observe the change in pressure losses due to solid composition in slurry.

An industrial test rig was built that allowed for conducting experimental runs on three concentrations for each of the sand populations. Different flow rates were achievable that represented a fairly adequate range to obtain adequate number of data points for the development of a correlation.

Experimental test runs were obtained, tabulated, discussed and correlations developed. The work included an introductory part that addressed the importance of characterizing the solids peculiarities in terms of shape effects on drag mechanism as compared with perfect spheres. Experimental measurements of terminal velocity were obtained for the specific purpose of defining a suitable coefficient of drag.

Experimental results were obtained under stable pumping conditions. The results were discussed. Summary of the conclusions are as follows.

1) The coefficient of drag for the sand particles departs from that of perfect spheres. Investigation of existing correlations for spheres revealed fair degree of accuracy and any of them would be applicable en par. Devising a mass ratio to equate the sand particle mass to that of an equivalent sphere worked well in developing a correlation that highlights the differences in the coefficient of drag due to shape departures from perfect spherical shape (particles having similar masses). However, terminal fall velocity, as a unique property of drag of a single particle, was needed in the development of coefficient of drag for sand (non uniform shape). Empirical correlation of terminal velocity for the actually used sand was developed through experimental measurement as a function of standard sphere correlation and fluidisation number. Thus:

$$\frac{U_t}{U_{ts}} = 0.7941[Ar]^{-0.0333} \qquad \text{ch. 6} \quad (6.8)$$

The accuracy of the correlation is within ±8%. The coefficient of drag correlation followed:

$$C_D = 3.4531(X)^{0.7862} \qquad \text{ch.6} \quad (6.11)$$

The independent variable is a correlation of coefficient of drag of a perfect spherical shape. The accuracy of the correlation is in the range of ±12% of which about ±8% is due to the terminal velocity correlation.

2) Graphical plots of pressure losses against velocity of flow range (0.2- 2 m/s) for the concentrations of 4%, 5.6% and 9% were plotted for Sand (A) and Sand (B) separately.

   a) Coarser sand results (Sand (A)) showed gradual rise of trend lines at velocities below approximately 1 m/s while rise increased at higher velocities. Trend lines for all concentrations approached the liquid carrier

curve at lower velocity end while they diverged significantly at higher velocities. The latter case is more pronounced for higher concentrations. It can be concluded that coarser sand behaviour suggests a change in the drag mechanism above 1 m/s flow velocity. Accelerated suspension takes place due to more effective drag mechanism. Supporting evidence to this conclusion is the lesser effect on lower concentration. A combination of increased turbulence and diffusion (due to inter-particle collisions) enhances suspension at higher concentrations and velocities of flow.

b) Finer Sand results (Sand (B) showed higher pressure drops for the same concentrations and velocities of flow compared with Sand (A). Although the concentrations were the same, finer particles produced significantly higher pressure losses. The conclusion is that pressure losses are not only affected by the concentration but also the composition of the solid particles. Lower particle sizes are more prone to suspension at lower velocities and tend to assume a more homogeneous flow pattern. Further evidence confirm that at higher flow rates the pressure loss increase is more due to increased particle collisions.

3) Paired comparisons of results for both sand populations at similar concentrations showed that at lower concentration the effect of particle size was dominant. Finer particles incurred more losses at lower velocities but a reversal is observed at higher velocities. Thus, marking significant accelerated suspension of coarse sand at higher flow velocities. At the higher concentrations the finer sand consistently produced higher pressure losses. This further suggests that finer particles are more affected by drag mechanism embracing turbulent diffusion due to confinement. Earlier suspension of finer sand is confirmed by the lesser rise of the curves compared of the sudden changes experienced in coarser sand, indicating no changes of drag mechanism similar to that of coarse sand.

4) Comparisons of the gradients in relative sense between Sand (A) and (B) as a pressure drop change with respect to flow velocity indicate that coarse sand changes behaviour at higher rate compared with finer sand. However, further

higher up on the scale reversal takes place (probably due to the inter particle collisions becoming significantly dominant favouring finer sand to incur more pressure losses)

5) Empirical correlations were developed for each sand population separately and for the collective case for both sands. The correlations were developed using the famous multiple linear regression. The goodness of fit was examined in detail and showed remarkably higher values of correlation (nearly linear in logarithmic coordinates. Thus:

for Sand (A):

$$\frac{i_m - i_w}{i_w} = 1.2523 \cdot C_A^{4.3623} \cdot Fr_A^{2.692} \cdot C_{DA}^{.15444} \qquad \text{ch.6, (6.12)}$$

for Sand(B):

$$\frac{i_m - i_w}{i_w} = 1.2789 \cdot C_B^{7.367} \cdot Fr_B^{6.6} \cdot C_{DB}^{.12594} \qquad \text{ch.6 (6.13)}$$

for all results:

$$\frac{i_m - i_w}{i_w} = 110.83 \cdot C^{5.398} \cdot Fr^{2.043} C_D^{6.514} \qquad \text{ch. 6 (6.14)}$$

6) It is worth concluding that in the context of this work drag mechanism is taken to embrace the various components of forces that may prevail in a given mix of solids and liquid carrier. Drag by the fluid stream is supported by turbulence and dispersion to produce a final effect that is greatly affected by the nature of the solids. It is clearly shown in this work that polyfractional slurries produce different pressure losses in accordance of a complex matrix of properties and flow mechanisms.

7.2. Recommendations for Further Work:

Although significant effort has been put in this work, the aims of the exercise met to an acceptable degree and the experimental data formed an adequate basis for the development of empirical correlations for polyfractional slurries, still in many aspects continuation is very much recommended. This is partly due to the time and cost limitations imposed on a single research programme and partly due to the great number of problem formulations that may accrue for a slurry flow problem.

Thus, recommendations for further work may be summarized as follows:

1) Although an industrial size test rig is very much desirable for serving the industry best but it incurs much burden on its operation, running and equipping. A reasonably lower size may allow much freedom of control for the researcher.

2) Flow velocities of wider range may reveal further enhancements of the results. This is desirable despite the fact that in industrial applications velocities do not normally exceed the investigated ranges.

3) An increased number of solids particles populations will certainly cast more light on the effects of solid populations structures on pressure losses associated with slurry flow. It could be beneficial to separate populations of closer particle size distributions and increasing the number of populations experimented on.

4) An ambitious experimental plan may allow for not only using different populations but also combinations thereof.

5) Different carrier fluids other than water may be of benefit to study the effects of viscosity on slurry flow.

6) Different pipeline geometries may be employed to extract more conclusions regarding the possible differences attributed to conveying boundary properties.

7) Solid materials used in experiments may be varied in properties and shapes to investigate possible differences due to different densities and shapes.

8) In all cases, enhancements are possible in the characterization of solids drag and drag measurement.

9) In the stage of the design of the experiments there are possibilities to set up a programme that studies certain mechanisms specifically (i.e. study of pressure losses in the neighbourhood of settling).

10) Numerical analyses may ultimately be developed for a given set of experimental results associated with a numerical algorithm that simplifies an analytical expression. This is much needed in the development of simulation applications on computers.

APPENDICES

Appendix (A): Calculation of the Coefficient of Drag for A Spherical Particle

Appendix (B): Calculation of the Annual Pumping Costs for a Slurry Pipeline (Illustrative Example)

Appendix (C): Mathematical Model Building, Regression Analysis and Statistical Testing of the Goodness of Fit of Correlations

Appendix (D): Instrumentation Description and Calibration

Appendix (A):

Calculation of the Coefficient of Drag for A Spherical Particle

A.1. Physical Discussion:

The motion of a free falling sphere under the influence of gravity in a stationary column of liquid is resisted by an inertial force, buoyancy force and viscous force. If the diameter of the sphere is small enough and the fall is free (velocity is not significantly high), then the wave making effects and compressibility effects can safely be ignored. Furthermore, after an initial acceleration, the velocity of the sphere assumes a constant value (the free fall or terminal velocity). At this equilibrium state, the sphere is under the influence of a gravitational force driving it downwards and a drag force constituting a buoyancy force and a complex combination of inertial and viscous forces counteracting its free downfall.

Shear stresses develop at the boundary of the sphere due to its motion producing a drag force, which can be correlated with the kinetic energy available per unit volume of the liquid.

The ratio between the drag force and the kinetic energy per unit volume of the liquid, thus, defines the coefficient of drag.

$$C_D = \frac{D}{\frac{1}{2}\rho_L U_t^2 A} \qquad \text{(A.1)}$$

Where C_D is the coefficient of drag,

D is the drag force (N)

ρ_l is the liquid density (Kg/m^3)

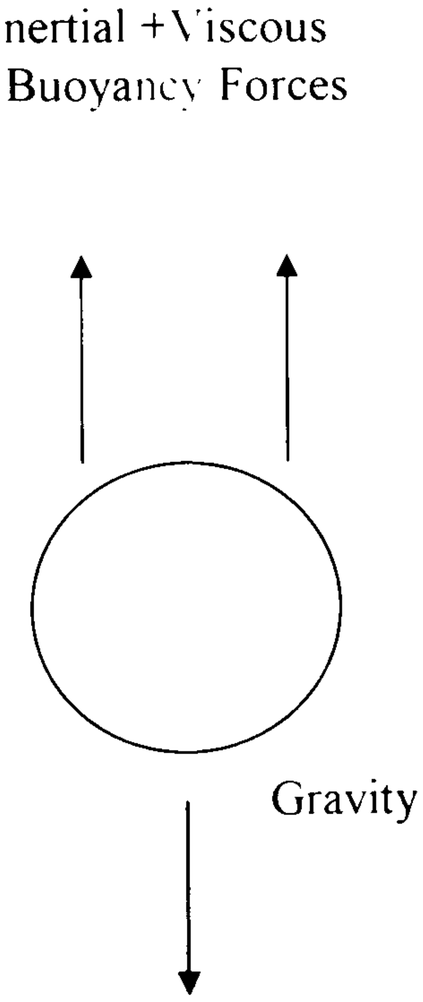

Fig. A- 1, Force Balance on a Free Falling Sphere

U_t is the free fall (terminal) velocity (m/s)

$A = \frac{\pi}{4} d^2$ is the sphere cross section (m^2)

The force balance becomes:

D = G - B

Drag Force = Gravity Force - Buoyancy Force

$$C_D \frac{1}{2} \rho_L U_t^2 A = \pi \frac{d^3}{6} \rho_S g - \pi \frac{d^3}{6} \rho_L g$$

Where d is the sphere diameter (m)

ρ_S is the density of the sphere (Kg/m^3)

g is the gravitational acceleration (m/s^2)

and equation (A- 1) becomes:

$$C_D = \frac{4}{3} dg \frac{(\rho_S - \rho_L)}{U_t^2 \rho_L} \qquad (A.2)$$

The calculation of the coefficient of drag is governed by the physical nature of the flow past the sphere. This, in turn, is dependent on the level of turbulence and can only be found experimentally through correlation of the coefficient of drag with Reynolds number defined for the sphere dimensions. Figure (A-2) [47] depicts three different regions, the first obeys Stokes law for creeping flow of which sphere Reynolds number is below unity, followed by a transition region up to Reynolds number less than 1000 and the last region extends for higher up Reynolds numbers. The last region is of the one of most interest in industrial applications since it coincides with the turbulent flow regime. Fortunately, in the higher region of Reynolds numbers (>1000) the coefficient of drag becomes a function of Reynolds

number only. However, due to the complexities associated with turbulence, the coefficient of drag is found experimentally. A formula that spans all flow regimes is reported [47] after Turton and Levenspiel:

$$C_D = \frac{24}{\mathrm{Re}_p}\left(1 + 0.173\,\mathrm{Re}_p^{\,0.657}\right) + \frac{0.413}{1 + 16300\,\mathrm{Re}_p^{-1.09}} \qquad \text{(A.3)}$$

Where Re_d is the Reynolds number defined for the sphere diameter, the free fall velocity and the liquid density and viscosity ($\mathrm{Re}_p = \rho_L U_t d / \mu_L$). Alternatively, another empirical formula can be used [48] which yields similar results:

$$C_D = 0.5\left\{16\left[\left(\frac{24}{\mathrm{Re}_p}\right)^{1.6} + \left(\frac{130}{\mathrm{Re}_p}\right)^{0.72}\right]^{2.5} + \left[\left(\frac{40000}{\mathrm{Re}_p}\right)^{2} + 1\right]^{-0.25}\right\}^{0.25} \qquad \text{(A.4)}$$

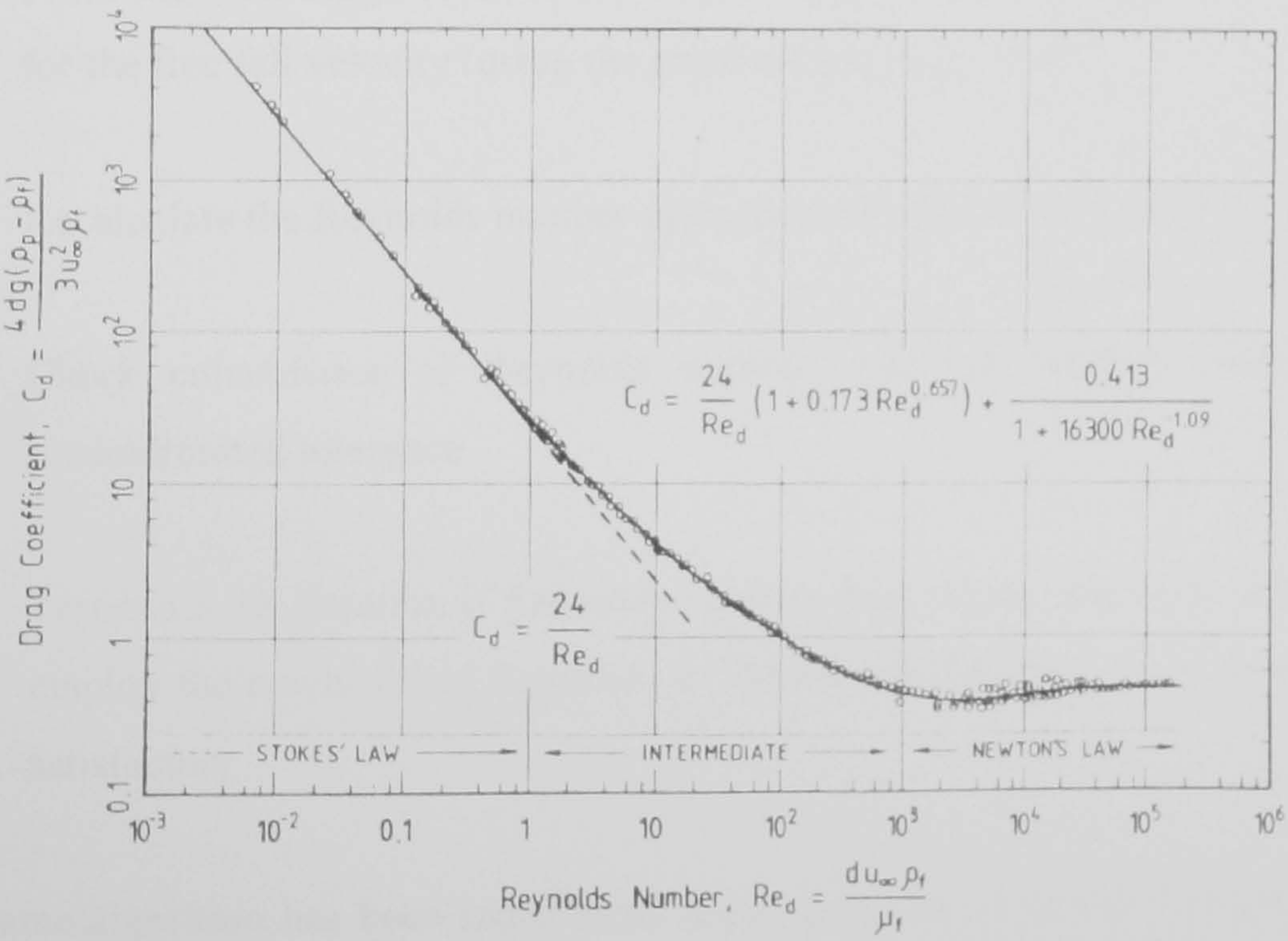

Fig. (A-2), Coefficient of Drag viz. Reynolds No. [47]

A.2. Calculation of the Coefficient of Drag:

Turton and Levenspiel [47] formula cannot readily be employed since the free fall velocity that is embedded in the definition of the Reynolds number is unknown. The free fall velocity appears in the physical law defining the drag coefficient (equation A.2). Thus, two equations with two unknowns can be solved (though by an iteration algorithm since the free fall velocity is implicit in the equations). The following steps are followed to find the coefficient of drag:

- Assign a starting value for the Reynolds number
- Use Turton and Levenspiel formula to find the coefficient of drag (Eqn. A.3)
- From the knowledge of the coefficient of drag, a starting value can be found for the free fall velocity (using the physical law, Eqn. A.2)
- Recalculate the Reynolds number using the free fall velocity starting value
- Check coincidence of Reynolds number with the starting value for a predetermined tolerance
- Terminate the iteration if Reynolds number falls within tolerance, other wise employ the newly found Reynolds in Turton and Levenspiel and repeat until satisfactory

The same algorithm has been reproduced using a second empirical formula for the coefficient of drag [48]. The results were the same for the fifth decimal place. The flow chart to execute the above steps is shown in fig. (A-3). The results of the flowchart are shown in the graph of fig. (A-4) and the listing of the data produced by the algorithm is shown in the calculation sheets Table (A-1) according to two correlations (first, is according to Turton & Levenspiel [47] and second is according to Swamee & Ojha [48]).

The iteration algorithm described above revealed a relative error in the prediction of the coefficient of drag in the range of ± 10% between the two correlations in the extreme cases and an average relative error of around ± 1% for the set of data iterated.

The data is generated for a single sphere of sand of density (2650 Kg/m^3), liquid is water at (20 C°) having density (998.2 Kg/m^3) and dynamic viscosity (1.002x10^{-3} Kg/ms).

It is worth mentioning, that each value of the coefficient of drag is a unique value for its corresponding sphere diameter and its terminal fall velocity for the same material of the sphere and the same fluid properties.

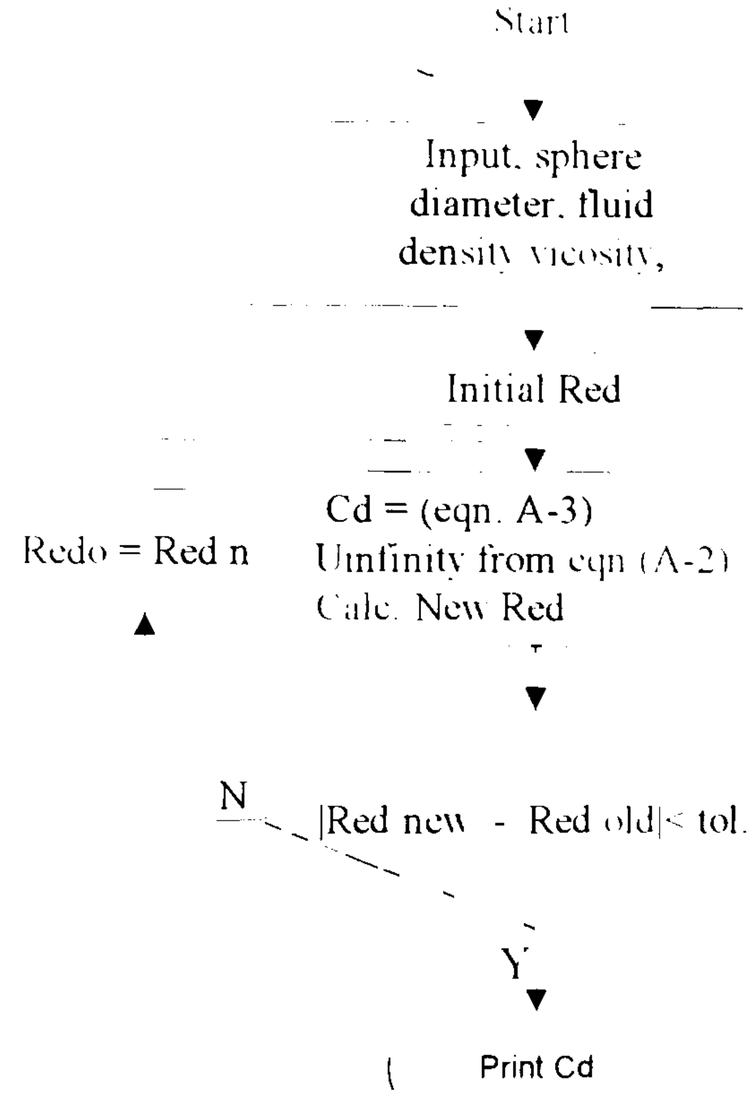

Fig. (A- 2), Flowchart fort the Coefficient of Drag Iterations

A.3. Calculation of the Terminal Velocity:

The terminal velocity for a free falling sphere can be obtained from the force balance on it at equilibrium state. Rewriting equation (A.2), terminal velocity can be correlated to the square root of the sphere diameter and the coefficient of drag for the same fluid and solid material as follows:

$$U_t = f\left(\sqrt{\frac{dg}{C_D}}\right) \qquad (A.5)$$

The importance of finding the terminal velocity lies in that it can be directly measured by timing the fall of a particle in a static liquid medium. Thus, it can be used to calibrate the coefficient of drag for a sphere and, furthermore, for finding the coefficient of drag for a non-spherical particles.

The results of flowchart (Table A- 1) tabulated the terminal velocity for two correlations. For further comparison, a third correlation reported by Wilson [49] was employed to check the consistency of these correlations. It is noted that the max relative error for the first two correlations is in the range of ± 5% while that for Wilson is around ± 8% from the average being more towards higher terminal velocity (higher sphere diameter). Figure (A- 5) correlates a velocity parameter (Y) with the terminal velocity for constant fluid and solid densities. The relation is linear with slight non-linearity in Wilson's correlation for presumably same physical conditions.

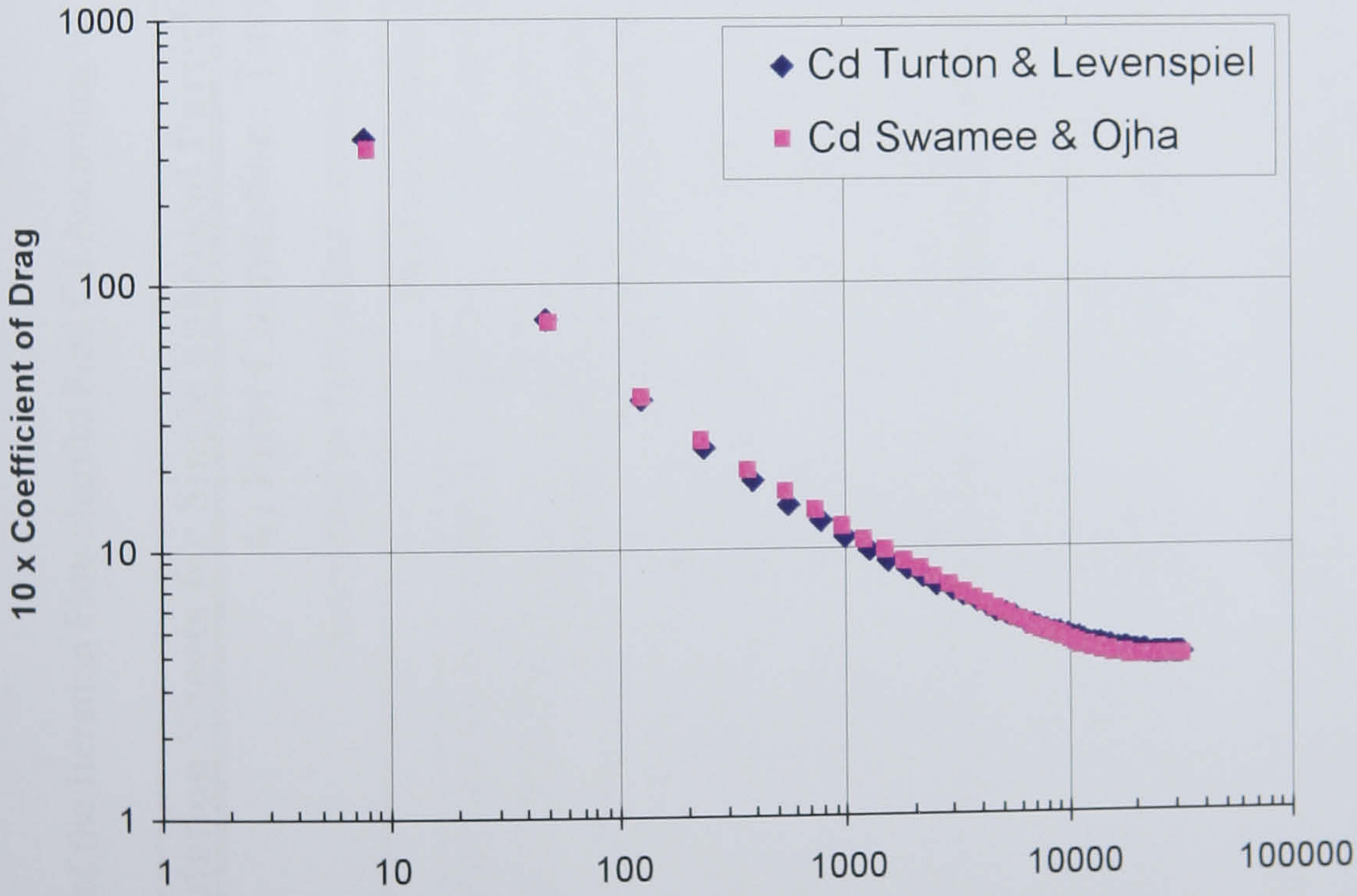

Fig. (A-4), Coefficient of Drag viz. Spherical Particle Reynolds No.

Table (A- 1). Listings of the Iteration Flowchart to Find Cd According to Two Different Correlations

Calculation Sheets for Single Spherical Particle Coefficient of Drag (Iteration Results)

A) First Correlation: Turton and Levenspiel

According to Turton and Levenspiel (as cited by: Brown, N. P.)[47]

Fluid and Particle Properties

	Fluid dynamic Viscosity (Kg/m.s)	0.0010	Fluid Density (Kg/Cu.m)	998
	Particle Density (Kg/Cu.m)	2650	Temperature (Deg.C)	20

1.2) Turton and Levenspiel Correlation Calculations (SHEET 1)

1.2.1) Starting Data for Cd Iterations

Particle Dia (m)	0.0001	0.0002	0.0003	0.0004	0.0005	0.0006	0.0007	0.0008	0.0009	0.0010	0.0011	0.0012
Star.Val. Red	0.7803	4.8181	12.6181	23.9280	38.4967	56.1320	76.6833	100.0261	126.0528	154.6663	185.7766	219.2983
Calculate Cd	35.2770	7.4025	3.6427	2.4011	1.8118	1.4726	1.2530	1.0992	0.9855	0.8980	0.8284	0.7718
Ut (m/s)	0.0078	0.0242	0.0422	0.0600	0.0773	0.0939	0.1100	0.1255	0.1406	0.1553	0.1695	0.1834

1.2.2) Iterations Algorithm Converging Results for Cd according to Turton and Levenspiel

Final Red (FRed)	0.7803	4.8181	12.6181	23.9280	38.4967	56.1320	76.6833	100.0261	126.0528	154.6663	185.7766	219.2983
Final Cd	35.2770	7.4025	3.6427	2.4011	1.8118	1.4726	1.2530	1.0992	0.9855	0.8980	0.8284	0.7718
Ut (m/s)	0.0078	0.0242	0.0422	0.0600	0.0773	0.0939	0.1100	0.1255	0.1406	0.1553	0.1695	0.1834
Check Final Red (CFRed)	0.7803	4.8181	12.6181	23.9280	38.4967	56.1320	76.6833	100.0261	126.0528	154.6663	185.7766	219.2983

1.2.3) Error Check on Red According to Iteration Algorithm (=FRed- CFRed)

Error	7.60E-12	-4.88E-12	-4.75E-08	-1.19E-11	-3.13E-12	-3.92E-09	-2.98E-11	-2.91E-10	-1.58E-08	-1.31E-12	-1.21E-08	-3.68E-10

../ Continued (Table A.1)

2.2) Turton and Levenspiel Correlation Calculations (SHEET 2)

2.2.1) Starting Data for Cd Iterations

Particle Dia (m)	0.0013	0.0014	0.0015	0.0016	0.0017	0.0018	0.0019	0.0020	0.0021	0.0022	0.0023	0.0024
Start. Val.Red	255.1489	293.2482	333.5175	375.8794	420.2573	466.5760	514.7615	564.7410	616.4431	669.7984	724.7391	781.1996
Calculate Cd	0.7249	0.6854	0.6518	0.6227	0.5975	0.5755	0.5560	0.5388	0.5235	0.5098	0.4976	0.4866
Ut (m/s)	0.1970	0.2103	0.2232	0.2358	0.2482	0.2602	0.2720	0.2834	0.2947	0.3056	0.3163	0.3267

2.2.2) Iterations Algorithm Converging Results for Cd according to Turton and Levenspiel

Final Red (FRed)	255.1489	293.2482	333.5175	375.8794	420.2573	466.5760	514.7615	564.7410	616.4431	669.7984	724.7391	781.1996
Final Cd	0.7249	0.6854	0.6518	0.6227	0.5975	0.5755	0.5560	0.5388	0.5235	0.5098	0.4976	0.4866
Ut (m/s)	0.1970	0.2103	0.2232	0.2358	0.2482	0.2602	0.2720	0.2834	0.2947	0.3056	0.3163	0.3267
Check Final Red (CFRed)	255.1489	293.2482	333.5175	375.8794	420.2573	466.5760	514.7615	564.7410	616.4431	669.7984	724.7391	781.1996

2.2.3) Error Check on Red According to Iteration Algorithm (=FRed- CFRed)

Error	-4.43E-08	-2.61E-11	-7.53E-09	-9.66E-13	-5.20E-11	-1.07E-09	-1.24E-08	0.00E+00	-3.08E-11	-6.19E-10	-7.22E-09	-5.74E-08

../ Continued (Table A.1)

3.2) Turton and Levenspiel Correlation Calculations (SHEET 3)

3.2.1) Starting Data for Cd Iterations

Particle Dia (m)	0.0025	0.0026	0.0027	0.0028	0.0029	0.0030	0.0031	0.0032	0.0033	0.0034	0.0035	0.0036
Start. Val Red	839.1165	898.4286	959.0774	1021.0066	1084.1628	1148.4948	1213.9543	1280.4954	1348.0748	1416.6515	1486.1871	1556.6453
Calculate Cd	0.4767	0.4677	0.4597	0.4523	0.4457	0.4397	0.4342	0.4293	0.4248	0.4207	0.4170	0.4136
Ut (m/s)	0.3369	0.3469	0.3566	0.3660	0.3753	0.3843	0.3931	0.4017	0.4101	0.4182	0.4262	0.4340

3.2.2) Iterations Algorithm Converging Results for Cd according to Turton and Levenspiel

Final Red (FRed)	839.1165	898.4286	959.0774	1021.0066	1084.1628	1148.4948	1213.9543	1280.4954	1348.0748	1416.6515	1486.1871	1556.6453
Final Cd	0.4767	0.4677	0.4597	0.4523	0.4457	0.4397	0.4342	0.4293	0.4248	0.4207	0.4170	0.4136
Ut (m/s)	0.3369	0.3469	0.3566	0.3660	0.3753	0.3843	0.3931	0.4017	0.4101	0.4182	0.4262	0.4340
Check Final Red (CFRed)	839.1165	898.4286	959.0774	1021.0066	1084.1628	1148.4948	1213.9543	1280.4954	1348.0748	1416.6515	1486.1871	1556.6453

3.2.3) Error Check on Red According to Iteration Algorithm (= FRed-CFRed)

Error	-1.48E-12	-2.01E-11	-1.86E-10	-1.40E-09	-8.65E-09	-4.55E-08	0.00E+00	-1.23E-11	-1.33E-10	-1.17E-09	-8.23E-09	-4.88E-08

../ Continued (Table A.1)

2.2) Turton and Levenspiel Correlation Calculations (SHEET 4)

2.2.1) Starting Data for Cd Iterations

Particle Dia (m)	0.0037	0.0038	0.0039	0.0040	0.0041	0.0042	0.0043	0.0044	0.0045	0.0046	0.0047	0.0048
Start. Val.Red	1627.9922	1700.1958	1773.2264	1847.0561	1921.6586	1997.0096	2073.0864	2149.8677	2227.3336	2305.4658	2384.2469	2463.6610
Calculate Cd	0.4105	0.4078	0.4052	0.4030	0.4009	0.3991	0.3974	0.3959	0.3946	0.3934	0.3923	0.3914
Ut (m/s)	0.4417	0.4491	0.4564	0.4635	0.4705	0.4773	0.4839	0.4905	0.4968	0.5031	0.5092	0.5152

2.2.2) Iterations Algorithm Converging Results for Cd according to Turton and Levenspiel

Final Red (FRed)	1627.9922	1700.1958	1773.2264	1847.0561	1921.6586	1997.0096	2073.0864	2149.8677	2227.3336	2305.4658	2384.2469	2463.6610
Final Cd	0.4105	0.4078	0.4052	0.4030	0.4009	0.3991	0.3974	0.3959	0.3946	0.3934	0.3923	0.3914
Ut (m/s)	0.4417	0.4491	0.4564	0.4635	0.4705	0.4773	0.4839	0.4905	0.4968	0.5031	0.5092	0.5152
Check Final Red (CFRed)	1627.9922	1700.1958	1773.2264	1847.0561	1921.6586	1997.0096	2073.0864	2149.8677	2227.3336	2305.4658	2384.2469	2463.6610

2.2.3) Error Check on Red According to Iteration Algorithm (=FRed- CFRed)

Error	0.00E+00	-1.27E-11	-1.27E-10	-1.05E-09	-7.44E-09	-4.61E-08	0.00E+00	-2.27E-11	-2.55E-10	-2.64E-09	-2.37E-08	0.00E+00

../ Continued (Table A.1)

3.2) Turton and Levenspiel Correlation Calculations (SHEET 5)

3.2.1) Starting Data for Cd Iterations

Particle Dia (m)	0.0049	0.0050	0.0051	0.0052	0.0053	0.0054	0.0055	0.0056
Start. Val.Red	2543.6930	2624.3290	2705.5561	2787.3621	2869.7357	2952.6664	3036.1444	3120.1605
Calculate Cd	0.3906	0.3899	0.3893	0.3888	0.3883	0.3880	0.3877	0.3875
Ut (m/s)	0.5211	0.5269	0.5325	0.5381	0.5435	0.5489	0.5541	0.5593

3.2.2) Iterations Algorithm Converging Results for Cd according to Turton and Levenspiel

Final Red (FRed)	2543.6930	2624.3290	2705.5561	2787.3621	2869.7357	2952.6664	3036.1444	3120.1605
Final Cd	0.3906	0.3899	0.3893	0.3888	0.3883	0.3880	0.3877	0.3875
Ut (m/s)	0.5211	0.5269	0.5325	0.5381	0.5435	0.5489	0.5541	0.5593
Check Final Red (CFRed)	2543.6930	2624.3290	2705.5561	2787.3621	2869.7357	2952.6664	3036.1444	3120.1605

3.2.3) Error Check on Red According to Iteration Algorithm (= FRed-CFRed)

Error	-3.456E-11	-7.594E-10	-1.390E-08	-3.638E-12	-2.160E-10	-1.329E-08	-2.774E-11	-1.420E-08

../ Continued (Table A.1)

Calculation Sheets for Single Spherical Particle Coefficient of Drag (Iteration Results)

B) Second Correlation: Swamee & Ojha

According to Swamee PK and Ojha CSP [48]

Fluid and Particle Properties

Fluid dynamic Viscosity (Kg/m.s)	0.0010	Fluid Density (Kg/Cu.m)	998	
Particle Density (Kg/Cu.m)	2650	Temperature (Deg.C)	20	

1.2) Swamee & Ojha Correlation Calculations (SHEET 1)

1.2.1) Starting Data for Cd Iterations

Particle Dia (m)	0.0001	0.0002	0.0003	0.0004	0.0005	0.0006	0.0007	0.0008	0.0009	0.0010	0.0011	0.0012
Star.Val. Red	0.8108	4.9012	12.4408	23.1299	36.8203	53.4312	72.9088	95.2114	120.3027	148.1480	178.7115	211.9542
Calculate Cd	32.6720	7.1538	3.7473	2.5697	1.9805	1.6252	1.3861	1.2132	1.0820	0.9787	0.8952	0.8262
Ut (m/s)	0.0081	0.0246	0.0416	0.0580	0.0739	0.0894	0.1046	0.1195	0.1342	0.1487	0.1631	0.1773

1.2.2) Iterations Algorithm Converging Results for Cd according to Swamee & Ojha

Final Red (FRed)	0.8108	4.9012	12.4408	23.1299	36.8203	53.4312	72.9088	95.2114	120.3027	148.1480	178.7115	211.9542
Final Cd	32.6720	7.1538	3.7473	2.5697	1.9805	1.6252	1.3861	1.2132	1.0820	0.9787	0.8952	0.8262
Ut (m/s)	0.0081	0.0246	0.0416	0.0580	0.0739	0.0894	0.1046	0.1195	0.1342	0.1487	0.1631	0.1773
Check Final Red (CFRed)	0.8108	4.9012	12.4408	23.1299	36.8203	53.4312	72.9088	95.2114	120.3027	148.1480	178.7115	211.9542

1.2.3) Error Check on Red According to Iteration Algorithm (=FRed- CFRed)

Error	8.11E-01	4.90E+00	1.24E+01	2.31E+01	3.68E+01	5.34E+01	7.29E+01	9.52E+01	1.20E+02	1.48E+02	1.79E+02	2.12E+02

../ Continued (Table A.1)

2.2) Swamee & Ojha Correlation Calculations (SHEET 2)

2.2.1) Starting Data for Cd Iterations

Particle Dia (m)	0.0013	0.0014	0.0015	0.0016	0.0017	0.0018	0.0019	0.0020	0.0021	0.0022	0.0023	0.0024
Start Val Red	247.8320	286.2943	327.2823	370.7278	416.5528	464.6691	514.9786	567.3742	621.7417	677.9614	735.9111	795.4679
Calculate Cd	0.7684	0.7191	0.6768	0.6402	0.6082	0.5802	0.5556	0.5338	0.5146	0.4976	0.4826	0.4693
Ut (m/s)	0.1914	0.2053	0.2190	0.2326	0.2460	0.2591	0.2721	0.2848	0.2972	0.3093	0.3212	0.3327

2.2.2) Iterations Algorithm Converging Results for Cd according to Swamee & Ojha

Final Red (FRed)	247.8320	286.2943	327.2823	370.7278	416.5528	464.6691	514.9786	567.3742	621.7417	677.9614	735.9111	795.4679
Final Cd	0.7684	0.7191	0.6768	0.6402	0.6082	0.5802	0.5556	0.5338	0.5146	0.4976	0.4826	0.4693
Ut (m/s)	0.1914	0.2053	0.2190	0.2326	0.2460	0.2591	0.2721	0.2848	0.2972	0.3093	0.3212	0.3327
Check Final Red (CFRed)	247.8320	286.2943	327.2823	370.7278	416.5528	464.6691	514.9786	567.3742	621.7417	677.9614	735.9111	795.4679

2.2.3) Error Check on Red According to Iteration Algorithm (=FRed- CFRed)

Error	-1.16E-08	-1.46E-11	-2.94E-09	-7.39E-13	-8.12E-08	-1.11E-08	-2.35E-11	-2.56E-09	-1.82E-12	-7.78E-10	-3.57E-08	-3.52E-09

../ Continued (Table A.1)

3.2) Swamee & Ojha Correlation Calculations (SHEET 3)												
3.2.1) Starting Data for Cd Iterations												
Particle Dia (m)	0.0025	0.0026	0.0027	0.0028	0.0029	0.0030	0.0031	0.0032	0.0033	0.0034	0.0035	0.0036
Start Val Red	856.5117	918.9269	982.6046	1047.4440	1113.3536	1180.2513	1248.0648	1316.7310	1386.1955	1456.4121	1527.3416	1598.9513
Calculate Cd	0.4575	0.4471	0.4379	0.4298	0.4226	0.4164	0.4108	0.4060	0.4017	0.3980	0.3948	0.3920
Ut (m/s)	0.3439	0.3548	0.3653	0.3755	0.3854	0.3949	0.4041	0.4130	0.4217	0.4300	0.4380	0.4458
3.2.2) Iterations Algorithm Converging Results for Cd according to Swamee & Ojha												
Final Red (FRed)	856.5117	918.9269	982.6046	1047.4440	1113.3536	1180.2513	1248.0648	1316.7310	1386.1955	1456.4121	1527.3416	1598.9513
Final Cd	0.4575	0.4471	0.4379	0.4298	0.4226	0.4164	0.4108	0.4060	0.4017	0.3980	0.3948	0.3920
Ut (m/s)	0.3439	0.3548	0.3653	0.3755	0.3854	0.3949	0.4041	0.4130	0.4217	0.4300	0.4380	0.4458
Check Final Red (CFRed)	856.5117	918.9269	982.6046	1047.4440	1113.3536	1180.2513	1248.0648	1316.7310	1386.1955	1456.4121	1527.3416	1598.9513
3.2.3) Error Check on Red According to Iteration Algorithm (= FRed-CFRed)												
Error	-5.61E-09	-2.42E-11	-4.19E-09	-1.86E-11	-5.27E-09	0.00E+00	-7.89E-11	-2.85E-09	-5.47E-08	-6.14E-12	-4.97E-10	-1.84E-08

../ Continued (Table A.1)

2.2) Swamee & Ojha Correlation Calculations (SHEET 4)

2.2.1) Starting Data for Cd Iterations

Particle Dia (m)	0.0037	0.0038	0.0039	0.0040	0.0041	0.0042	0.0043	0.0044	0.0045	0.0046	0.0047	0.00
Start. Val.Red	1671.2137	1744.1061	1817.6100	1891.7098	1966.3928	2041.6488	2117.4689	2193.8462	2270.7747	2348.2495	2426.2662	2504.82
Calculate Cd	0.3896	0.3875	0.3857	0.3842	0.3829	0.3818	0.3809	0.3802	0.3796	0.3792	0.3788	0.37
Ut (m/s)	0.4534	0.4607	0.4678	0.4747	0.4814	0.4880	0.4943	0.5005	0.5065	0.5124	0.5182	0.52

2.2.2) Iterations Algorithm Converging Results for Cd according to Swamee & Ojha

Final Red (FRed)	1671.2137	1744.1061	1817.6100	1891.7098	1966.3928	2041.6488	2117.4689	2193.8462	2270.7747	2348.2495	2426.2662	2504.8213
Final Cd	0.3896	0.3875	0.3857	0.3842	0.3829	0.3818	0.3809	0.3802	0.3796	0.3792	0.3788	0.3786
Ut (m/s)	0.4534	0.4607	0.4678	0.4747	0.4814	0.4880	0.4943	0.5005	0.5065	0.5124	0.5182	0.5238
Check Final Red (CFRed)	1671.2137	1744.1061	1817.6100	1891.7098	1966.3928	2041.6488	2117.4689	2193.8462	2270.7747	2348.2495	2426.2662	2504.8213

2.2.3) Error Check on Red According to Iteration Algorithm (=FRed- CFRed)

Error	-2.73E-12	-1.57E-10	-1.58E-08	-4.56E-10	0.00E+00	-3.83E-09	-2.14E-11	-6.72E-08	-1.53E-08	-7.77E-10	-4.59E-11	-9.27E-10

../ Continued (Table A.1)

3.2) Swamee & Ojha Correlation Calculations (SHEET 5)

3.2.1) Starting Data for Cd Iterations

Particle Dia (m)	0.0049	0.0050	0.0051	0.0052	0.0053	0.0054	0.0055	0.0056
Start. Val.Red	2583.9115	2652.7114	2576.3524	2505.6610	2440.0311	2378.9383	2321.9267	2268.5986
Calculate Cd	0.3785	0.3785	0.3785	0.3786	0.3788	0.3790	0.3793	0.3796
Ut (m/s)	0.5293	0.5347	0.5400	0.5452	0.5503	0.5553	0.5602	0.5651

3.2.2) Iterations Algorithm Converging Results for Cd according to Swamee & Ojha

Final Red (FRed)	2583.9115	2663.5340	2743.6862	2824.3656	2905.5700	2987.2973	3069.5452	3152.3117
Final Cd	0.3785	0.3785	0.3785	0.3786	0.3788	0.3790	0.3793	0.3796
Ut (m/s)	0.5293	0.5347	0.5400	0.5452	0.5503	0.5553	0.5602	0.5651
Check Final Red (CFRed)	2583.9115	2663.5340	2743.6862	2824.3656	2905.5700	2987.2973	3069.5452	3152.3117

3.2.3) Error Check on Red According to Iteration Algorithm (= FRed-CFRed)

Error	-1.00E-11	-1.99E-08	-2.91E-10	-1.22E-09	-8.30E-10	0.00E+00	6.04E-08	1.34E-09

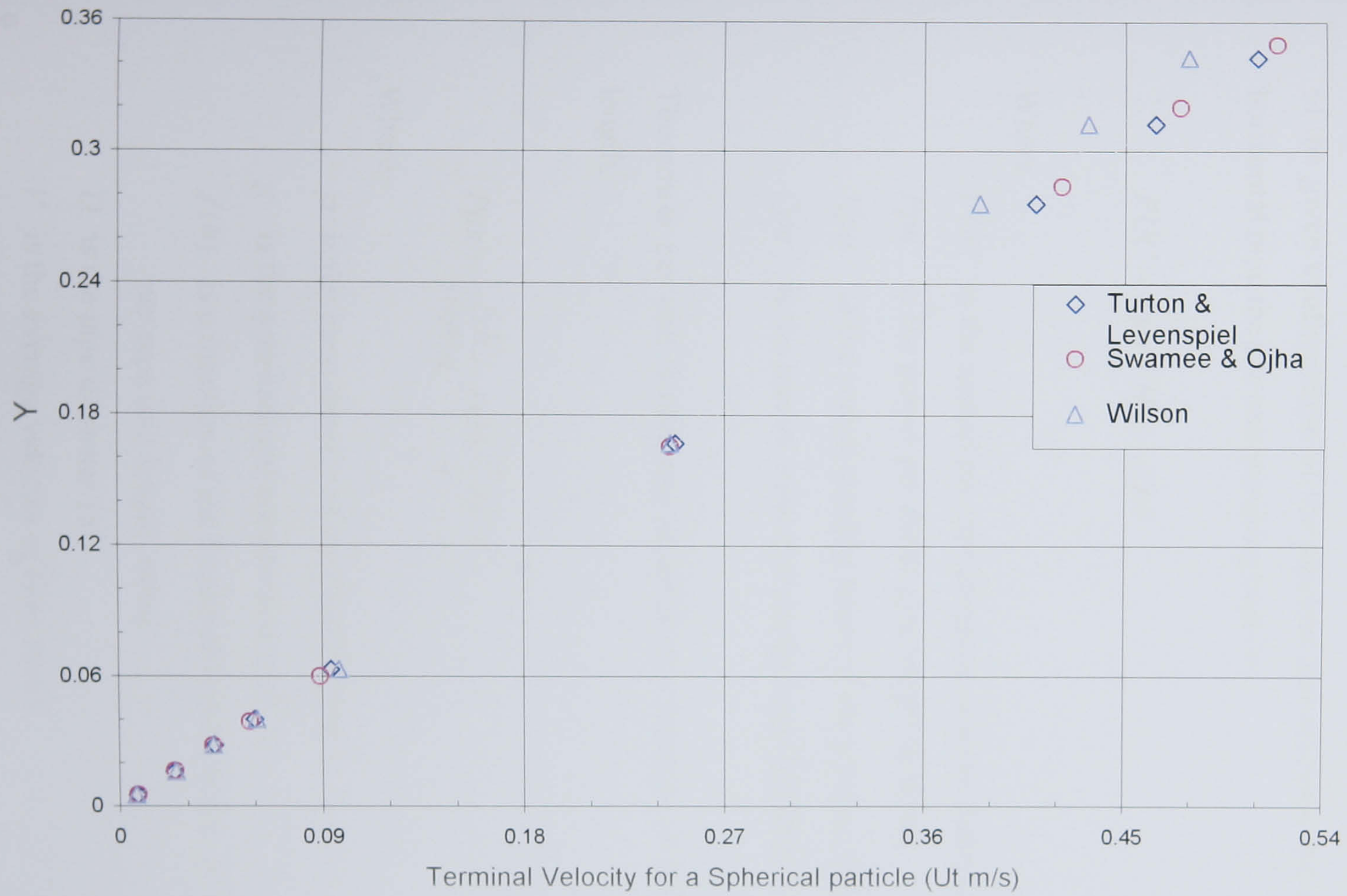

Fig. (A- 5), The velocity Parameter $Y = \sqrt{\frac{d.g}{C_D}}$ viz. Terminal Velocity for Spherical Particle (Uts)

Appendix (B):

Calculation of the Annual Pumping Costs for a Slurry Pipeline (Illustrative Example)

B.1. Annual Pumping Cost

The annual pumping costs of a unit pipe length of a given diameter are those associated with the energy cost to overcome the pressure drop (loss) per unit length of the given configuration of the pipeline and maintain the desired flow rate. For a horizontal pipe the per unit pumping cost is;

$$PUC = Ppu \times Hpa \times Cpu \qquad \text{(B.1)}$$

Where

PUC is the annual per unit pumping cost per meter of pipe length ($/m)

Ppu is the power per meter pipe length (KW/m)

Hpa is the annual running hours of the pipeline (Hours)

Cpu is the money value per energy unit ($/KWH)

The power per unit is obtained in terms of a function of friction head loss per unit length:

$$Ppu = \frac{\rho . g}{1000 . \eta} . f(h) . \frac{\pi}{4} D^2 . V \qquad \text{(B.2)}$$

Where

ρ is the mass density of the liquid (Kg/m^3)

g is the gravitational acceleration (m/s^2)

$f(h)$ is a function of the frictional loss in meters of liquid per pipe unit length (m/m)

D is the pipe diameter (m)

V is the average velocity of flow (m/s)

η is the overall efficiency of the pump and the prime mover

Thus, the per unit pumping cost (PUC) becomes:

$$PUC = \frac{\rho.g}{1000.\eta} . f(h) . \frac{\pi}{4} D^2 . V . Hpa \times Cpu \qquad \text{(B.3)}$$

B.2. Worked Example:

B.2.1. Clear Water Flow

Take a 6" pipe diameter running full of water, in the turbulent regime at 20 Deg. C, the pipe material is steel, the water mass density is 998.2 Kg/m^3, the dynamic viscosity is $1.002*10^{-3}$ Kg/ms and the average velocity of flow is in the range of 1.9 to 2.1875 m/s as per normal industrial practice. The energy cost for industrial applications is 0.06 $/KWH (in Jordan). It is required to find the per annum pumping cost per unit pipe length.

As a first approximation of the friction factor (Fanning friction factor) for steel pipes in the turbulent flow regime, the friction factor is [7]:

$$f = \frac{0.04}{\mathrm{Re}^{0.16}} \qquad \text{(B.4)}$$

The friction loss function per unit pipe length in meters of water per meter of pipe length is:

$$f(h) = \frac{4f}{D} \frac{V^2}{2g} \qquad \text{(B.5)}$$

Assuming a pump overall efficiency of 70% and normal running hours per annum of 7500 hours (as standard design figures in industrial practice)

The per unit pumping cost (PUC) for clear water becomes (from equations B.3 and B.5);

$$PUC = \frac{11}{7 \times 1000.\eta} . \rho . f . V^3 . D \cdot Hpa \cdot Cpu \qquad \text{(B.6)}$$

Table (B.1) summarizes the output of equation (B.6) for the normal range of average flow velocities encountered in discharge pipelines.

B.2.2. Example Repeated with Slurry Flow:

Take the same pipe diameter filled with slurry of volumetric concentration (C) of 10% of sand having a spherical shape of 5 mm diameter and having the same average flow velocity range as in table (B.1). Using six correlations for pressure drop in slurries that gained relatively wide use in pipeline design, table (B.2) summarizes the results for the annual per unit cost for one-meter pipe length.

These correlations are originally expressed in different forms and need to be normalized in a standard form so that they can be compared. The standard form used here is expressing the correlations in the form of a friction factor similar to that used for clear water. Thus, the friction losses can be directly expressed in a Darcy like formula.

Before normalization, the slurry density must be found. This is derived from the simple mass balance for a given mass of slurry mixture as follows:

$$m_m = m_s + m_L \qquad \text{(B.7)}$$

Where m_m is the mass of slurry (Kg)

m_s is the mass of solids contained in the given mass of the slurry (Kg)

m_L is the mass of liquid contained in the given mass of the slurry (Kg)

and

$$V_m \rho_m = V_s \rho_s + V_L \rho_L \quad , \quad V_s = C.V_m \quad \text{and} \quad V_L = (1-C).V_m$$

Thus, the slurry density becomes:

$$\rho_m = C.\rho_s + (1-C).\rho_L \tag{B.8}$$

The normalized forms of the slurry friction factor are as follows:

Durand Formula: [2]

$$f_{mDurand} = f_w \left(\frac{\rho_w}{\rho_m} \right) . \left\{ 176.C \left[\frac{V^2.C_D^{0.5}}{g.D.(S-1)} \right]^{-1.5} + 1 \right\} \tag{B.9}$$

Zandi and Govatos Formula: [1]

$$f_{mZ\&G} = f_w \left(\frac{\rho_w}{\rho_m} \right) \left\{ 280.C \left[\frac{V^2.C_D^{0.5}}{g.D.(S-1)} \right]^{-1.93} + 1 \right\} \tag{B.10}$$

Chhabra and Richardson Formula: [4]

$$f_{mCh\&Rich} = f_w \left(\frac{\rho_w}{\rho_m} \right) \left\{ 0.55. \frac{C}{f_w} \left[\frac{V^2}{g.D.(S-1)} \right]^{-1.25} + 1 \right\} \tag{B.11}$$

Fangary et al Formula: [3]

$$f_{mFangary} = f_w \left(\frac{\rho_w}{\rho_m} \right) \left\{ 131.C \left[\frac{V^2}{g.D.(S-1)} \right]^{-1.2} + 1 \right\} \tag{B.12}$$

Turian et al Formula: [5]

$$f_{mTurian} = C^{0.8687}.30.115.f_w^{1.2}.C_D^{-0.1677} . \left[\frac{V^2}{g.D.(S-1)} \right]^{-0.6938} + .f_w \tag{B.13}$$

Swamee Formula: [6]

$$f_{mSwam} = \left\{ \left(\frac{64}{\mathrm{Re}} \right)^{8} + 9.5 \left[\ln\left(\frac{\varepsilon}{3.7D} + \frac{5.74}{\mathrm{Re}^{0.9}} \right) - \left(\frac{2500}{\mathrm{Re}} \right)^{6} \right]^{-16} \right\}^{0.125} \qquad \text{(B.14)}$$

Figure (B.1) illustrates the friction factors for the different normalized slurry correlations as ratios of the clear water friction factor viz Reynolds number for the range of velocities applied earlier to the clear water example. Figure (B.2) illustrates the yearly pumping cost money value ($/m) per one meter of pipe length.

B.3. Concluding Remarks:

Friction factors for the assumed slurry are widely varying depending on the correlation applied. The highest is that of Durand that gives a friction factor that is approximately 28 folds the friction factor of clear water. The second highest is that of Zandi & Govatos giving around 18 folds while the other correlations form two bands that are much lower. Fangary et al and Chhabra and Richardson give a band that is 8 to 6 folds while Turian et al and Swamee give much lower value of around 2 to 3 folds.

The variation of the friction factors with Reynolds number is relatively more significant for the upper edge correlations while it is minimal for the lower edge ones.

The same conclusions can be drawn for the yearly pumping cost per unit pipe length. Figure (B.2) summarizes the results. The yearly per unit pumping cost could be any value between 10 $/m a year to around 160 $/m a year.

Finally, there are no apparent significant differences in the range of application, reported in the literature, for any of the correlations under investigation. They all are reported to hold universally good. Thus, a pipeline designer will be left with a hard

decision to make and normally he will go for the highest friction factor reported so as to stay in the safe side.

Table (B.1.), Clear Water Annual Pumping Cost per Unit Pipe Length

Pipe Diameter = 0.154 m (6¨). Medium: Water. Temperature: 20 °C. Density: 998.2 Kg/m^3
Dynamic Viscosity: 1.002 *10^{-3} Kg/ms, Pump efficiency (η): 70%
Yearly Running Hrs. (*Hpa*): 7500 Cost of KWH (*Cpu*): 0.06 $/KWH

Flow Velocity (V) m/s	Reynolds Number (*Re*)	Friction Factor (f_w)	Yearly Per Unit Cost (*PUC*) $/m
1.9	288461.9	0.005351	5.640509
1.9125	290359.6	0.005346	5.746537
1.925	292257.4	0.00534	5.853847
1.9375	294155.2	0.005334	5.962447
1.95	296053	0.005329	6.072344
1.9625	297950.7	0.005323	6.183545
1.975	299848.5	0.005318	6.296057
1.9875	301746.3	0.005313	6.409887
2	303644.1	0.005307	6.525041
2.0125	305541.8	0.005302	6.641528
2.025	307439.6	0.005297	6.759353
2.0375	309337.4	0.005292	6.878525
2.05	311235.2	0.005286	6.999049
2.0625	313132.9	0.005281	7.120933
2.075	315030.7	0.005276	7.244184
2.0875	316928.5	0.005271	7.368809
2.1	318826.3	0.005266	7.494814
2.1125	320724.1	0.005261	7.622207
2.125	322621.8	0.005256	7.750995
2.1375	324519.6	0.005251	7.881184
2.15	326417.4	0.005246	8.012781
2.1625	328315.2	0.005241	8.145794
2.175	330212.9	0.005237	8.28023
2.1875	332110.7	0.005232	8.416094

Table (B.2): Summary of Friction Factors and PUC for the Different Correlations

	Slurry Friction Factor (f_m)							Yearly Pumping per Unit Cost (PUC) $/m						
/ m/s	Water	[2]	[1]	[4]	[3]	[5]	[6]	Water	[2]	[1]	[4]	[3]	[5]	[6]
.9	0.005351	0.092607	0.148089	0.034016	0.04281	0.01217	0.016083	5.640509	97.61535	156.0972	35.85592	45.12523	12.83	16.95226
.9125	0.005346	0.090798	0.144351	0.033533	0.042169	0.012094	0.01607	5.746537	97.60904	155.1798	36.04875	45.3326	13	17.27531
.925	0.00534	0.089036	0.140733	0.033061	0.041543	0.012019	0.016057	5.853847	97.60456	154.2768	36.24235	45.54066	13.18	17.60239
.9375	0.005334	0.087322	0.137232	0.032599	0.040931	0.011946	0.016045	5.962447	97.60191	153.3879	36.43673	45.74939	13.35	17.93352
1.95	0.005329	0.085652	0.133841	0.032147	0.040332	0.011873	0.016032	6.072344	97.60109	152.5128	36.6319	45.95882	13.53	18.26874
1.9625	0.005323	0.084027	0.130559	0.031706	0.039747	0.011802	0.01602	6.183545	97.6021	151.6512	36.82786	46.16896	13.71	18.60805
1.975	0.005318	0.082444	0.127379	0.031274	0.039176	0.011732	0.016008	6.296057	97.60492	150.8031	37.02462	46.37982	13.89	18.95149
1.9875	0.005313	0.080902	0.124298	0.030851	0.038616	0.011663	0.015996	6.409887	97.60956	149.968	37.22221	46.5914	14.07	19.29908
2	0.005307	0.0794	0.121314	0.030438	0.03807	0.011595	0.015984	6.525041	97.61601	149.1459	37.42061	46.80372	14.26	19.65084
2.0125	0.005302	0.077936	0.118421	0.030033	0.037535	0.011528	0.015972	6.641528	97.62427	148.3365	37.61985	47.01678	14.44	20.0068
2.025	0.005297	0.07651	0.115617	0.029637	0.037012	0.011463	0.01596	6.759353	97.63434	147.5396	37.81992	47.2306	14.63	20.36699
2.0375	0.005292	0.075119	0.112898	0.029249	0.0365	0.011398	0.015949	6.878525	97.64621	146.7549	38.02085	47.44519	14.82	20.73142
2.05	0.005286	0.073764	0.110262	0.02887	0.035999	0.011334	0.015937	6.999049	97.65989	145.9823	38.22264	47.66055	15.01	21.10012
2.0625	0.005281	0.072442	0.107705	0.028499	0.035508	0.011271	0.015926	7.120933	97.67536	145.2217	38.42529	47.87669	15.2	21.47312
2.075	0.005276	0.071153	0.105225	0.028135	0.035029	0.011209	0.015915	7.244184	97.69264	144.4727	38.62882	48.09364	15.39	21.85044
2.0875	0.005271	0.069897	0.102819	0.027779	0.034559	0.011148	0.015903	7.368809	97.7117	143.7352	38.83323	48.31138	15.58	22.2321
2.1	0.005266	0.06867	0.100483	0.02743	0.034099	0.011088	0.015892	7.494814	97.73256	143.0091	39.03854	48.52994	15.78	22.61813
2.1125	0.005261	0.067474	0.098217	0.027088	0.033649	0.011028	0.015881	7.622207	97.75521	142.2941	39.24475	48.74932	15.98	23.00856
2.125	0.005256	0.066307	0.096016	0.026753	0.033208	0.01097	0.01587	7.750995	97.77965	141.5901	39.45187	48.96954	16.18	23.4034
2.1375	0.005251	0.065168	0.09388	0.026425	0.032776	0.010912	0.01586	7.881184	97.80588	140.897	39.6599	49.19059	16.38	23.80268
2.15	0.005246	0.064056	0.091805	0.026104	0.032353	0.010855	0.015849	8.012781	97.83389	140.2145	39.86887	49.4125	16.58	24.20643
2.1625	0.005241	0.062971	0.08979	0.025789	0.031938	0.010799	0.015838	8.145794	97.86369	139.5425	40.07877	49.63527	16.78	24.61466
2.175	0.005237	0.061912	0.087832	0.02548	0.031532	0.010744	0.015828	8.28023	97.89527	138.8809	40.28961	49.8589	16.99	25.02741
2.1875	0.005232	0.060877	0.08593	0.025178	0.031134	0.01069	0.015818	8.416094	97.92864	138.2294	40.50141	50.08342	17.2	25.4447

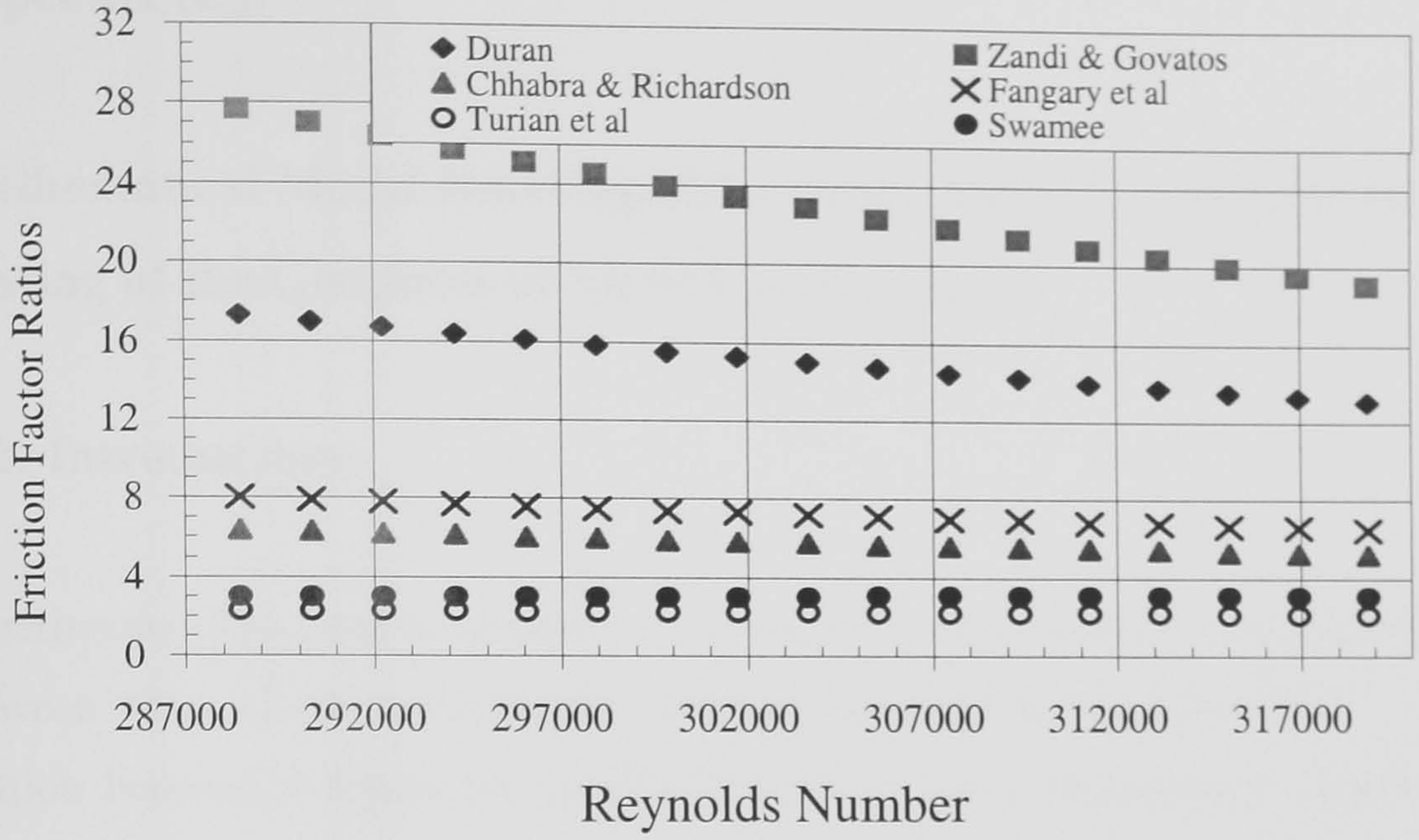

Fig. (B.1), Friction Factor Ratios (Slurry/Water) for Different Correlations

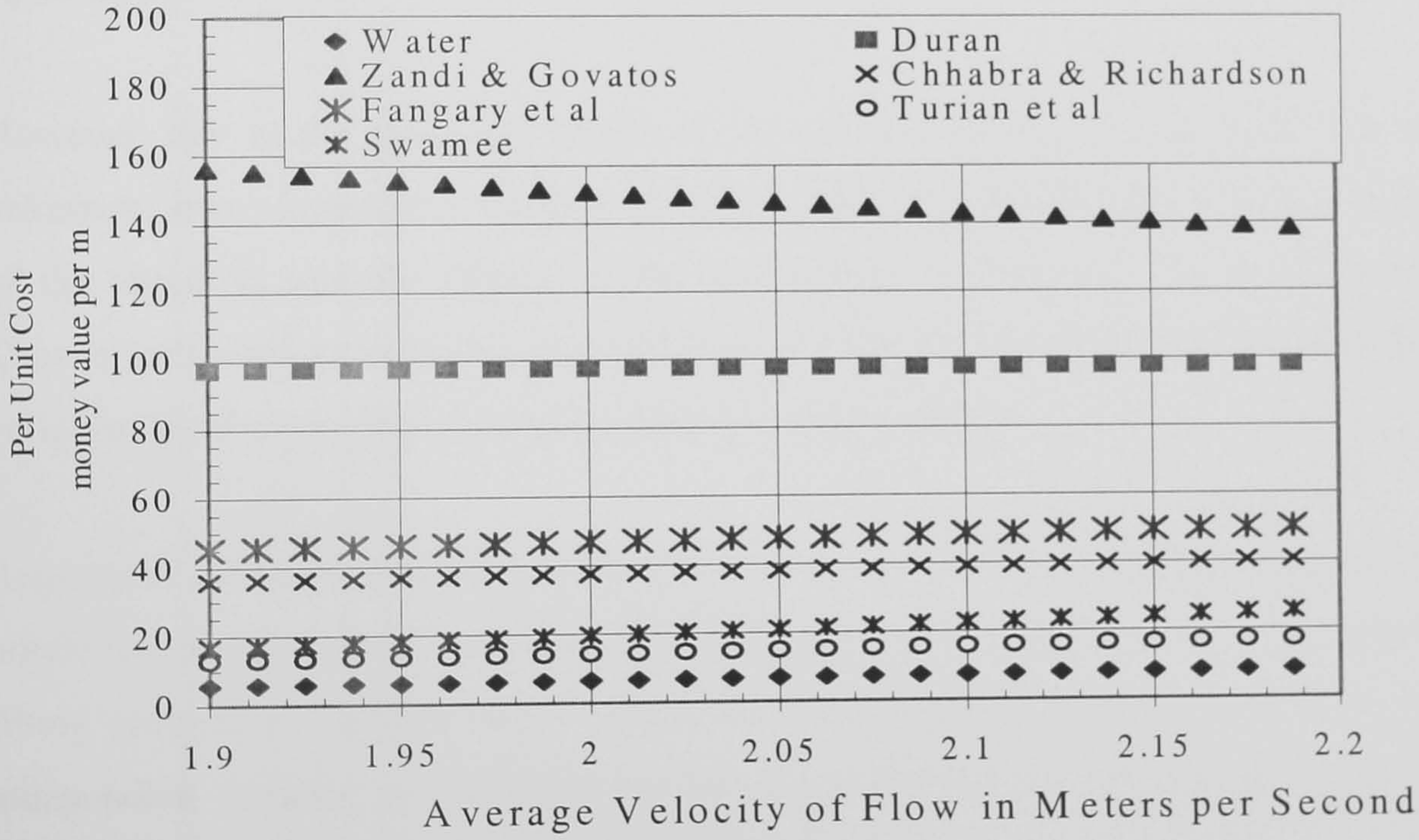

Fig. (B.2), PUC Comparison for Different Correlations

Appendix (C):

Mathematical Model Building, Regression Analysis and Statistical Testing of the Goodness of Fit of Correlations:

C.1. Introduction:

Experimental data need to be put in a reduced form that manifests the interrelations between them. Every observation obtained experimentally represents a certain relation between a dependent variable and one or more independent variables. In research, variables are reduced into non-dimensional groups. Next logical step would be finding an algebraic form that transform experimental data (observations) into an equation (correlation).

However, due to the empirical nature of the correlations (the true physical law is unknown) many inaccuracies due to the measurement methods, human error, nature of the variables and the effects of the surrounding environment are unavoidable. Thus, a methodology is necessary to estimate the functional relationship between the variables (or the non-dimensional groups) with fair accuracy.

Regression analysis, in conjunction with statistical means, is employed to give a prediction of the required correlation with the minimum possible error in the curve fitting procedure. Multiple linear regression is normally used when more than one independent variable is involved. Further on, consistent set of statistical tests is applied to examine the goodness of fit of the regression.

C.2. Multiple Linear Regression:

The main justification for using this method is that it estimates the path of a straight line that best fits the association between the variables with the least value of error. The method is built on the estimation of the normal least squares of errors in observations. According to the theory of Gauss-Markov [50] " the estimates of the normal least squares are the best unbiased linear estimates". The basic underlying

assumption in the method of least squares is that the independent variables are error free (or subject to negligible error) while the dependent variable is subject to errors that have to be eliminated [51].

C.3. Application of the Multiple Linear Regression:

The first step in the application is to linearize the candidate mathematical model (equation (C.1)) for which the multiple linear regression is to be applied. In this work, the dependent variable is the pressure loss coefficient non-dimensional group $\frac{i_m - i_w}{i_w}$ while the independent variables are the volumetric concentration C, the non-dimensional group Froude's number Fr and the non-dimensional group coefficient of drag C_D. Thus:

$$\frac{i_m - i_w}{i_w} = K.C^a.Fr^b C_D^c \qquad (C.1)$$

where K, a, b, and c are the curve fitting coefficients

The above equation is made linear by taking the natural logarithm for both sides of the equation:

$$\ln\left(\frac{i_m - i_w}{i_w}\right) = \ln K + a\ln C + b\ln Fr + c\ln C_D \qquad (C.2)$$

The estimation equation takes the observations (experimental results) in the following matrix form:

$$\mathbf{Y} = \mathbf{X}\beta + \mathbf{u} \qquad (C.3)$$

Where $\mathbf{Y}$ is the array of the dependent variable of the degree $n \times 1$ containing n observations of variable $\mathbf{Y}$, $\mathbf{X}$ is the matrix of the independent variables of the degree $n \times k$ containing n observations for k independent variables with the first column

assuming the value of 1, β is the array of the degree $k \cdot 1$ containing the unknown coefficients and **u** is the array of the degree $n \times 1$ representing the unknown random variable of marginal error.

The method of least squares is used to estimate the values of the unknowns under the following assumptions [50]:

i) The expected mean value of the marginal random error variable array is zero for all the observations:

$$E(\mathbf{u}) = 0$$

ii) The variance of the random variable between the observations is the same and the non-existence of autocorrelation:

$$V(u_i) = E(u_i^2) = \sigma^2$$
$$\text{cov}(u_i u_j) = E(u_i u_j) = 0, \quad i \neq j$$

iii) The matrix of observations **X** is not random

iv) The number of observations exceeds the number of variables.

v) The random variable array has normal distribution:

$$\mathbf{u} \approx N(0, \sigma^2)$$

Under the above assumptions the multiple regression is carried out through the estimation of errors according to the method of least squares. The calculation procedure is lengthy and software is used to obtain the output result. In this work, SPSS for Windows®[52] was used. The level of confidence under which calculations were carried out is 95% (i.e. no more than one observation out of twenty observations may occur due to chance).

C.4. Statistical Tests for the Goodness of Fit:

It is important to have an idea about how far does the linear curve obtained through regression analysis predict the actual physical relationship between the curve fitted variables. For this purpose three tests are normally sufficient to decide whether a correlation is truly representative or not:

C.4.1. Coefficient of Determination Test Statistic:

It measures the strength of association between the dependent variable and the independent variables. The percentage output of the coefficient of determination (denoted R^2) explains how much of the observations of the independent variables explain the dependent variable. The remaining percentage is unexplained by the regression. Statistically speaking [51], R^2 is that fraction of the total variance of y, which is contributed by its regression upon the variables $x_1, x_2 \ldots x_k$ Thus:

$$R^2 = \frac{sum\ of\ squares\ of\ deviations\ in\ y\ accounted\ for\ by\ regression}{total\ sum\ of\ squares\ of\ in\ y\ from\ actual} \qquad (C\ 4)$$

C.4.2. Significance Test Statistic:

In addition to the extent by which the assumed regression equation is capable to explain the dependent variable by the associated independent variables, measured by R^2, it is required to ascertain if the differences between the different values of y as predicted by the different settings of the independent variables are not due to chance. The hypothesis that all the coefficients of the independent variables are equal to zero is rejected to prove that the prediction equation gives significant values. Statistic F is employed to calculate the ratio of the mean sum of squares of deviations between the predicted values and the actual values of the regression to the mean sum of squares of errors in the regression. F distribution tabulation shows the critical values below

which the regression is in error and the values predicted by the assumed model are insignificant. Thus:

$$F = \frac{MSR}{MSE} \qquad (C.5)$$

Where MSR is the mean sum of squares of deviations in the regression and MSE is the mean sum of squares of errors.

C.4.3. Durbin Watson Statistic:

The Durbin Watson Statistic is used to test for the presence of first order autocorrelation in the residuals of a regression equation [5.3]. It is a measure of the sequential propagation of error amongst the successive settings of the predicted values. Thus:

$$d = \frac{\sum_{t=2}^{n} (e_t - e_{t-1})^2}{\sum_{t=1}^{n} e_t^2} \qquad (C.6)$$

Where d = Durbin Watson statistic, e = residual (Yi-Yc), and t = the interval.

A regression is autocorrelation free if the d statistic rates above a given tabulated critical value at confidence of 95%.

C.4.4. Case wise Residual Analysis:

It is of interest to try to find how close the prediction of the measured value to the predicted one for each data point. Statistically, residual analysis serves this purpose. Standardized residual is defined as a ratio of the residual to the estimated standard deviation for each case (experimental observation viz. predicted value). Thus:

$$e_{si} = \frac{e_i}{\sqrt{\hat{\sigma}^2}} \qquad (C.7)$$

Where e_{si} is the standardized residual, $e_i = Y_i - \hat{Y}_i$ is the deviation of the measured value Y_i from the predicted value $\hat{Y}_i$ and σ is the estimated standard deviation.

If the errors are normally distributed [54], then approximately 95% of the standardized residuals fall in the interval (-2, +2). Residuals that are outside this interval may indicate the presence of an outlier [54]; that is, an observation that is not typical of the rest of the data. However, criteria on discarding an outlier are varying and no agreement on general rules is available. Sometimes, an outlier may indicate a physical significance that is a property of the observation. In this work, although case wise residual analysis was conducted, the results do not suggest serious lack of fit that may necessitates a need to pursue adoption an outlier criterion.

Tables (C.1, C.2 and C.3) summarise the output of the case wise analysis obtained through using SPSS® for the empirical correlations of Sand (A), Sand (B) and the global correlation for all the experimental results for both Sands (A&B). In table (C.1), results of Sand (A), only one case (number 19) out of 24 cases exceeded the limit of the standardised residual while the rest of the cases distributed fairly between negative and positive values. In table (C.2), results of Sand (B), only two cases (number 25 and number 29) exceeded the limits out of 32 cases while the other cases distributed fairly around zero. In table (C.3) only 5 cases out of 56 exceeded limits. The number of exceeding cases is fairly low as compared with total number of observations studied. Thus, it is not believed to affect the predictions of the

correlations significantly. Considering the random nature of the fluid flow problems in general and the slurry flow problems in particular, the case wise analysis may safely be assumed adequate.

Table (C.1), Case wise Diagnostics of Pressure Loss Coefficient for Sand A Correlation in Logarithmic Form

Case Number	Std. Residual	Measured Value	Predicted Value	Residual
1	1.2703308	0.9913653	0.66548581	0.3258795
2	-0.884035	0.9027177	1.129500351	-0.226783
3	-0.066936	1.0353552	1.052526538	-0.017171
4	-0.170087	1.6355494	1.679181992	-0.043633
5	-0.350839	0.3893308	0.479332026	-0.090001
6	-0.631923	0.733472	0.895579978	-0.162108
7	-0.487582	1.4294672	1.554547342	-0.12508
8	-0.553132	0.2184637	0.360359444	-0.141896
9	0.1223087	1.5760062	1.544630176	0.031376
10	-0.702148	1.3053559	1.48547887	-0.180123
11	0.6650936	0.3985965	0.227979182	0.1706173
12	1.352689	1.0268566	0.679849566	0.347007
13	0.6224349	0.815495	0.655821017	0.159674
14	-0.702704	1.1683675	1.348632949	-0.180265
15	1.1662233	0.3480135	0.048840762	0.2991727
16	0.8237909	0.7481554	0.536827321	0.2113281
17	-0.051647	1.2123423	1.225591371	-0.013249
18	0.9219024	1.4464003	1.209903538	0.2364968
19	-2.416774	-0.589092	0.030885717	-0.619978
20	-0.302989	1.1488093	1.226535522	-0.077726
21	1.029132	0.7918462	0.527841645	0.2640045
22	-1.363324	0.5356347	0.885369828	-0.349735
23	1.0070565	2.7479495	2.489608041	0.2583415
24	-0.296842	1.3571333	1.433282546	-0.076149

Table (C.2), Case wise Diagnostics of Pressure Loss Coefficient for Sand B Correlation in Logarithmic Form

Case Number	Std. Residual	Measured Value	Predicted Value	Residual
1	0.6047342	0.7866805	0.6531739	0.1335066
2	-0.551471	1.2006165	1.3223643	-0.121748
3	-0.793106	0.4476972	0.6227906	-0.175093
4	0.4535502	0.7185665	0.6184366	0.1001299
5	1.2414651	0.8743297	0.6002526	0.2740772
6	-1.438469	0.9505033	1.2680728	-0.31757
7	0.7221963	0.7520481	0.5926094	0.1594386
8	0.6278757	1.4021988	1.2635832	0.1386156
9	-0.020323	2.2028955	2.2073823	-0.004487
10	-0.690572	1.1065005	1.2589574	-0.152457
11	0.4042467	1.3479107	1.2586655	0.0892452
12	-0.063303	2.1952188	2.2091942	-0.013975
13	-0.455544	2.1132385	2.2138085	-0.10057
14	-0.810136	2.0399126	2.2187656	-0.178853
15	0.0402887	1.2889359	1.2800414	0.0088945
16	-0.334045	2.1725267	2.2462736	-0.073747
17	-0.468634	2.150687	2.2541469	-0.10346
18	-0.166582	2.2261642	2.2629403	-0.036776
19	0.4816776	1.4264891	1.3201496	0.1063395
20	-1.061071	0.4242213	0.658473	-0.234252
21	0.534497	0.7820319	0.6640315	0.1180004
22	0.47442	0.7939749	0.6892377	0.1047373
23	0.7571211	2.4904767	2.3233278	0.167149
24	0.6594443	2.5430764	2.3974914	0.1455849
25	2.292603	1.9674594	1.4613235	0.5061359
26	-0.392264	0.7540786	0.8406784	-0.0866
27	-0.585724	2.4292182	2.558528	-0.12931
28	-0.179591	0.8993486	0.9389968	-0.039648
29	-3.193762	0.3677703	1.0728542	-0.705084
30	0.5505922	1.2801042	1.1585504	0.1215538
31	0.751365	3.0467805	2.8809023	0.1658782
32	0.6085204	2.1066372	1.9722947	0.1343425

Table (C.3), Casewise Diagnostics of Pressure Loss Coefficient for Both Sand A and B Correlation in Logarithmic Form

Case Number	Std. Residual	Measured value	Predicted Value	Residual
1	-2.581031	-0.589092	0.233344125	-0.822436
2	-0.051921	0.2184637	0.235008137	-0.016544
3	0.4380817	0.3480135	0.208420336	0.1395931
4	-2.780414	0.3677703	1.253739138	-0.885969
5	0.438756	0.3893308	0.249522843	0.139808
6	0.5591945	0.3985965	0.220411167	0.1781853
7	-1.383659	0.4242213	0.865119275	-0.440898
8	-0.369717	0.4476972	0.565506064	-0.117809
9	-1.171347	0.5356347	0.908880058	-0.373245
10	0.4610132	0.7185665	0.571666262	0.1469002
11	-0.230741	0.733472	0.806996922	-0.073525
12	-0.086927	0.7481554	0.775854349	-0.027699
13	0.3915859	0.7520481	0.627270631	0.1247774
14	-0.979802	0.7540786	1.066288905	-0.31221
15	-0.285906	0.7820319	0.873134981	-0.091103
16	0.8004109	0.7866805	0.531632467	0.255048
17	-0.033355	0.7918462	0.802474599	-0.010628
18	-0.354547	0.7939749	0.90694996	-0.112975
19	0.1071251	0.815495	0.781359971	0.034135
20	0.8452243	0.8743297	0.605002035	0.2693277
21	-0.788904	0.8993486	1.150730165	-0.251382
22	0.2070417	0.9027177	0.836744616	0.0659731
23	-0.730132	0.9505033	1.183157072	-0.232654
24	2.2523491	0.9913653	0.273662428	0.7177029
25	0.7638273	1.0268566	0.783465746	0.2433908
26	0.6548612	1.0353552	0.826686077	0.2086692
27	-0.379115	1.1065005	1.22730404	-0.120804
28	-1.423345	1.1488093	1.60235292	-0.453544
29	-1.294171	1.1683675	1.580750482	-0.412383
30	0.3109969	1.2006165	1.101518463	0.099098
31	-1.142187	1.2123423	1.576296193	-0.363954
32	-0.108642	1.2801042	1.314722621	-0.034618
33	-0.164395	1.2889359	1.341319623	-0.052384
34	-0.90662	1.3053559	1.594247017	-0.288891
35	0.3647735	1.3479107	1.231676918	0.1162338
36	2.3917117	1.3571333	0.595023025	0.7621103
37	0.6395224	1.4021988	1.198417284	0.2037815

../ Continued Table (C.3)

Case Number	Std. Residual	Measured value	Predicted Value	Residual
38	0.0303314	1.4264891	1.416824151	0.009665
39	-0.541887	1.4294672	1.602137636	-0.17267
40	-0.457429	1.4464003	1.592158266	-0.145758
41	-0.07836	1.5760062	1.600975462	-0.024969
42	0.0570681	1.6355494	1.617364911	0.0181845
43	1.2005029	1.9674594	1.584923512	0.3825359
44	-0.24282	2.0399126	2.117286317	-0.077374
45	0.4077415	2.1066372	1.97671186	0.1299254
46	0.0402955	2.1132385	2.100398456	0.01284
47	-0.137557	2.150687	2.194519099	-0.043832
48	-0.024813	2.1725267	2.18043333	-0.007907
49	0.3642586	2.1952188	2.079149104	0.1160697
50	0.5782829	2.2028955	2.018627787	0.1842678
51	0.0533595	2.2261642	2.209161406	0.0170028
52	-0.278181	2.4292182	2.517859665	-0.088641
53	0.6224685	2.4904767	2.292129352	0.1983474
54	0.5323455	2.5430764	2.373446421	0.16963
55	2.5672546	2.7479495	1.929903063	0.8180464
56	0.9275401	3.0467805	2.751223186	0.2955573

C.5. Concluding Remarks:

A regression is statistically sound if it fulfils the above three statistics. Namely, it is powerful in explaining the functional relation, significant in predicting different values at different settings and free form sequential errors. Furthermore, case wise analysis did not show many observations that fall totally out of the statistically acceptable ranges.

Computer listings of the main test statistics are reported at the end of this appendix. They show reasonably powerful capability of the correlations in explaining the pressure loss coefficient by the volumetric concentration, the non-dimensional parameter (Fr) and the non-dimensional group (C_D). Table (C.4) summarises the results of the test statistics for four variables (4 degrees of freedom of variables including the dependent variable) and different number of observations (observations degrees of freedom (df)). The values of the coefficient of determination (R^2) are 0.857, 0.921 and 0.823 for the results of Sand (A), Sand (B) and the global results for both respectively. It is obvious that the correlation is less powerful in the latter case where all the results are considered. This may be physically explained by the differences in the nature of the slurry compositions. Test for significance proves the existence of a strong relationship between the dependent variable and the associated independent ones. Calculated F- statistic is good if it exceeds the tabulated value [51]. Comparing F values for different correlations, it is apparent that they exceed sufficiently the tabulated values. Values of Durbin Watson statistic fall in the range of – 4 to + 4. Commonly, values exceeding + 2 indicate absence of error propagation between successive observations [53].

Table (C.4), Summary of Test Statistics

Correlation	(df)	Test Statistic			
		(R^2)	F Statistic Values		Durbin- Watson
			Tabulated	Calculated	
Sand (A)	23	0.857	2.8	39.981	2.3489
Sand (B)	31	0.921	2.68	108.089	2.059
Sands (A&B)	55	0.823	2.57	80.696	1.68

However, statistical testing cannot alone judge the adequacy of a certain regression It is always the task of the researcher to ensure that there exists a physical meaning of the behaviour predicted by the regression equation.

C.6. SPSS ® Statistical Analysis Program Output:

The summary of the statistical program SPSS output is outlined below (all values are in linear units due to logarithmic modelling of the variables):

C.6.1. SPSS ® Regression Output for Sand A:

Variables Entered[b]

Model	Variables Entered
1	- Coefficient of Drag for Sand A (CDA), - Volumetric Solids Concentration (CA), - Froude No. squared (FRSQ)[a]

a. All requested variables entered.

b. Dependent Variable: Pressure Loss Coefficient (YA)

Model Summary

Model	R	R Square	Durbin-Watson
1	.926	.857	2.349

ANOVA

Model		Sum of Squares	df	F Statistic
1	Regression	7.893	3	39.981
	Residual	1.316	20	
	Total	9.209	23	

Model		Coefficients
1	(Constant)	.225
	CA	1.473
	FRSQ	.297
	CDA	9.645

C.6.2. SPSS ®Regression Output for Sand B:

Variables Entered[b]

Model	Variables Entered
1	CDB, CB, FRSQ[a]

a. All requested variables entered.

b. Dependent Variable: YB

Model Summary[b]

Model	R	R Square	Durbin-Watson
1	.959[a]	.921	2.059

a. Predictors: (Constant), CDB, CB, FRSQ

b. Dependent Variable: YB

ANOVA[b]

Model		Sum of Squares	df	F Statistic
1	Regression	15.804	3	108.089
	Residual	1.365	28	
	Total	17.169	31	

b. Dependent Variable: YB

Coefficients[a]

Model		Coefficients
1	(Constant)	.246
	CB	1.997
	FRSQ	1.195
	CDB	9.441

a. Dependent Variable: YB

C.6.3. Regression SPSS ® Output for Both Sands (A&B):

Variables Entered[b]

Model	Variables Entered
1	CDGLOBAL, CGLOBAL, FRSQGLOB[a]

a. All requested variables entered.

b. Dependent Variable: YGLOBAL

Model Summary[b]

Model	R	R Square	Durbin-Watson
1	.907[a]	.823	1.680

a. Predictors: (Constant), CDGLOBAL, CGLOBAL, FRSQGLOB

b. Dependent Variable: YGLOBAL

ANOVA[b]

Model		Sum of Squares	df	F Statistic
1	Regression	24.580	3	80.696
	Residual	5.280	52	
	Total	29.860	55	

b. Dependent Variable: YGLOBAL

Coefficients[a]

Model		Coefficients
1	(Constant)	4.708
	CGLOBAL	1.686
	FRSQGLOB	2.125E-02
	CDGLOBAL	1.874

a. Dependent Variable: YGLOBAL

Appendix (D):

Instrumentation Description and Calibration:

D.1. Differential Pressure Transmitter:

D.1.1. Description:

The differential pressure transducer used in experiments is Alphaline®, Model 1151DR, made by Rosemount Inc. designed to measure extremely low-pressure differentials [55]. Figure (D.1) shows an isometric cross-section of the measuring cell (δ-cell™). The measuring cell is housed in a robust casing to which the tube leads of the pressure measurement taps are connected. The electronic circuitry is directly connected to the signal lead wires in a metallic housing protecting it from shocks, vibrations, stray signals and noise.

The physical principle (excerpted from PDS 4294)[55] employed in measuring pressure differentials is a changing capacitance proportional to the measured pressure changes. The isolating diaphragms detect and transmit the process pressure to the silicone oil fill fluid. The fluid in turn transmits the pressure to the sensing diaphragm in the centre of the cell. The sensing diaphragm functions as a spring element that deflects in response to differential pressure across it. The displacement of the sensing diaphragm, a maximum motion of 0.1 mm, is proportional to the differential pressure. Capacitor plates on both sides of the sensing diaphragm detect the position of the sensing diaphragm. The differential capacitance between the sensing diaphragm and the capacitor plates is converted electronically to a two-wire, linear, 4-20 mA dc signal.

The transmitter operates on a 24 V dc power supply and outputs signals in the range of 4-20 mA, the temperature limits are –29 to 93 °C, The differential pressure span is 0 to 3500 mmH2O and upper range limit (URL) is 3810 mm H2O. The transmitter can withstand overpressure of 138 bars without damage.

Reported accuracy is:

Accuracy = ± [0.02(URL / Span) – 0.1] % of calibrated flow span

= ± [0.02(3810/3500) – 0.1] % = ± 0.078%

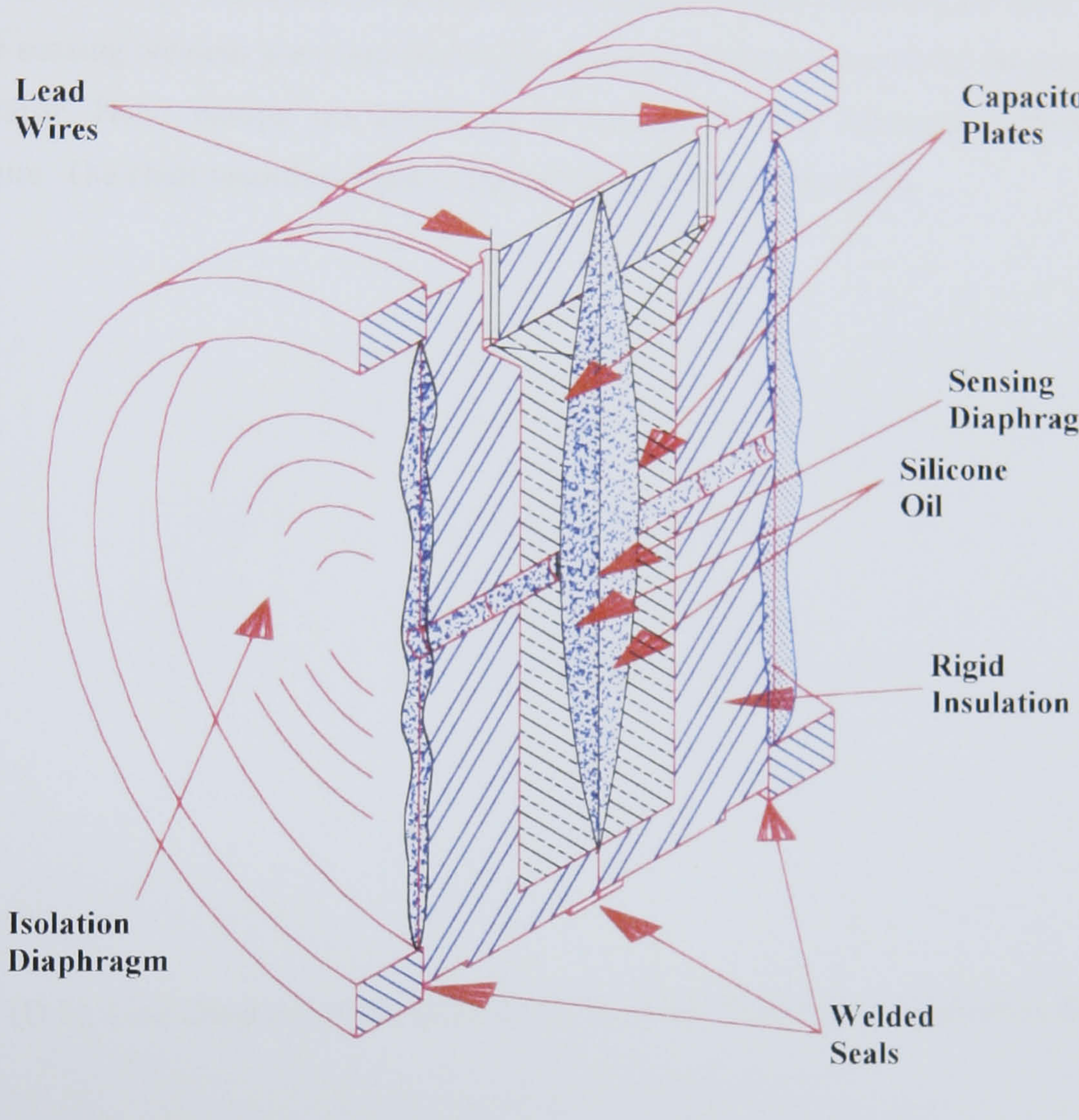

Fig. (D.1), Isometric Cross Section of the δ-cell™

D.1.2. Calibration:

The calibration of the differential pressure transducer as a separate unit does not help much in the evaluation of its performance in a measurement set-up that includes a train other instruments. Errors cannot be readily evaluated except if the whole train is calibrated in the same set-up that will be used in the actual test rig. Errors due to different sources (i.e. wiring, pressure transmitter, chart recorder) can be summed up

in one global relative error if the whole measuring train is calibrated as one unit. The worker preferred this approach as it reduces experimental effort and simulates the real measuring environment on the test rig.

Figure (D.2) shows the line diagram and fig. (D.3) shows a pictorial view of the calibration set-up. The differential pressure transmitter input chambers on both sides of the sensing element are connected to the reference pressure signals of the pressure calibrator. Hand pumps are employed to set the desired reference differential pressure. The chart recorder displays the actually measured pressures.

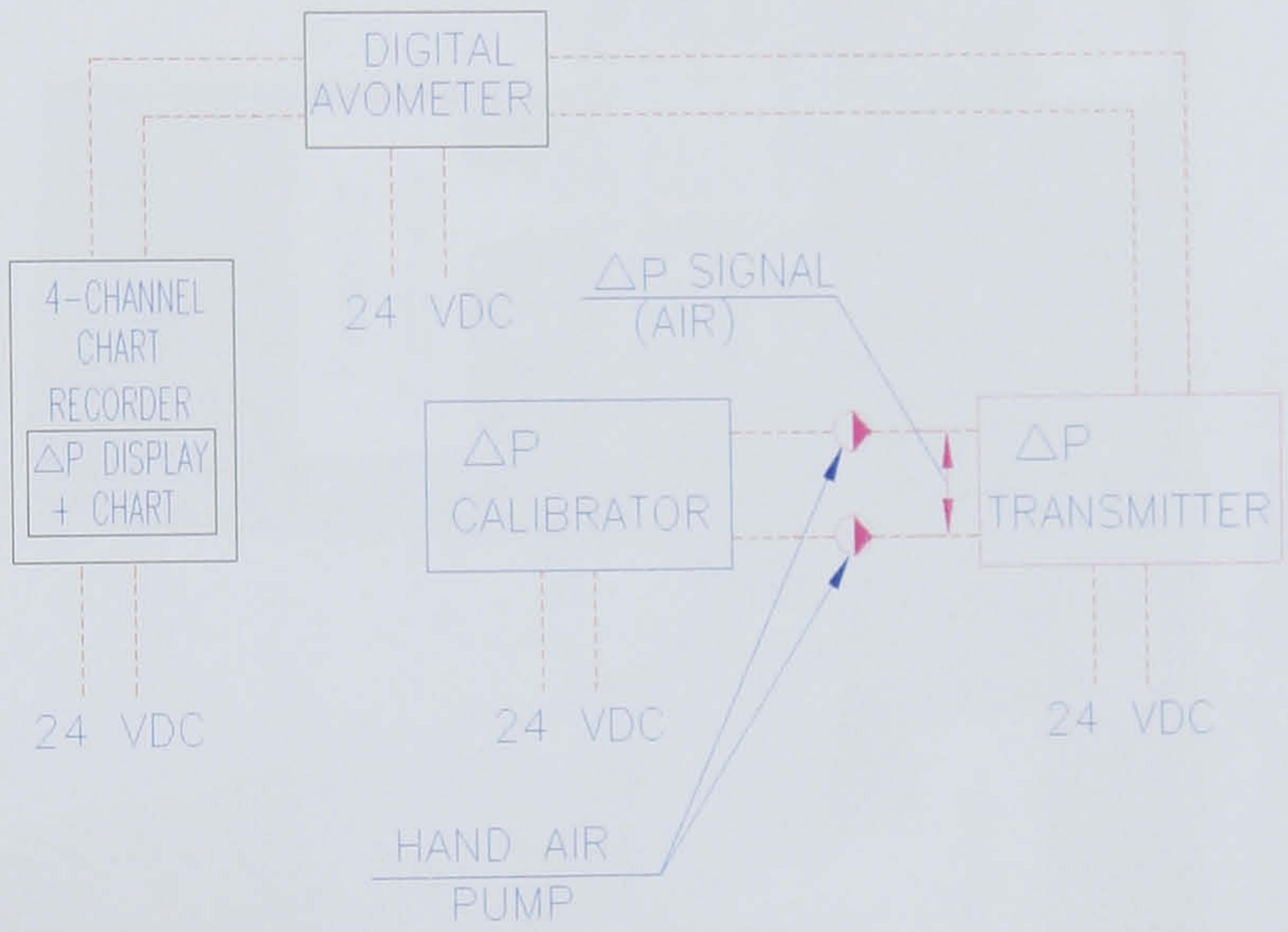

Fig. (D.2), Line Diagram of the Differential Pressure Transmitter Calibration Setup

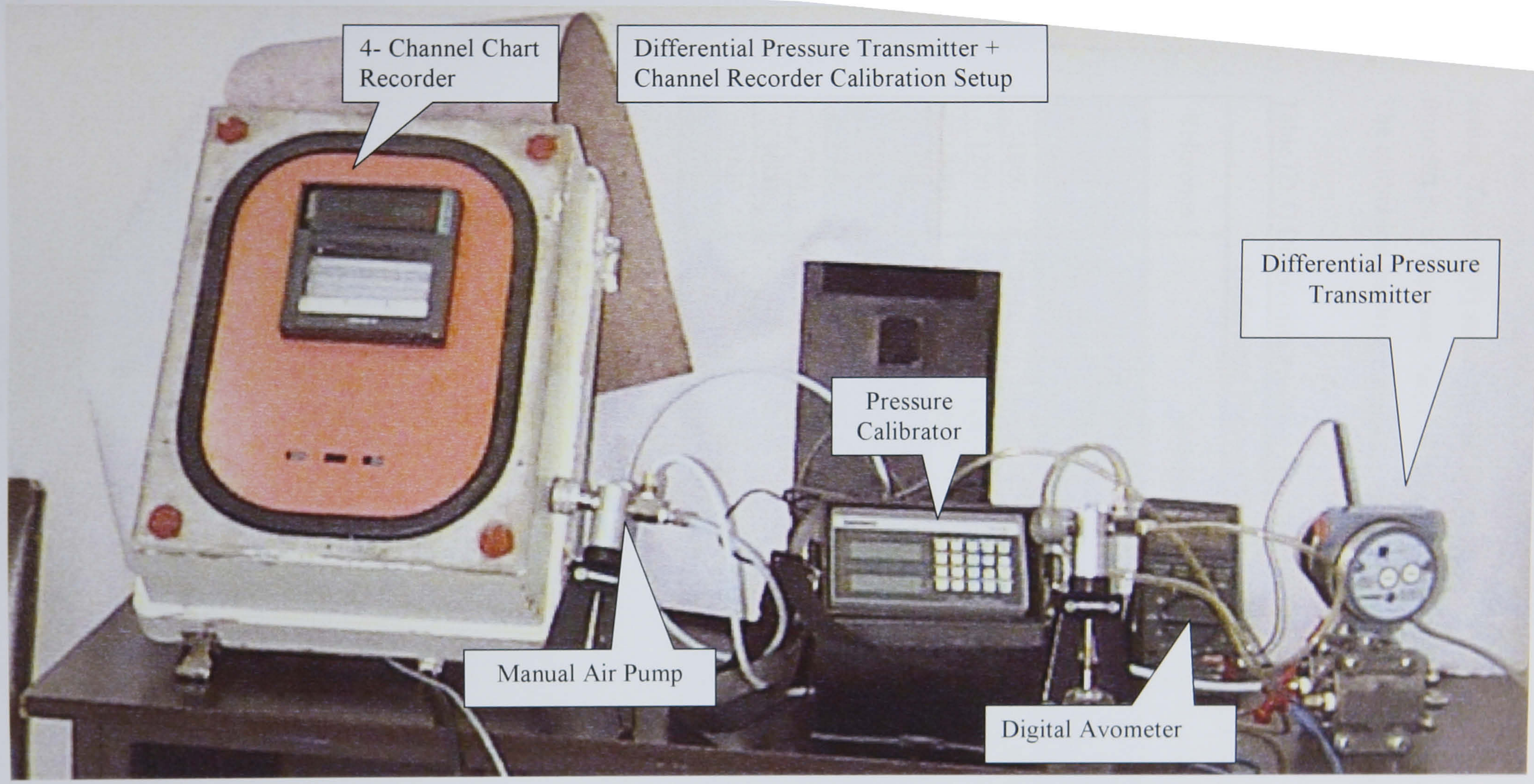

Fig. (D.3), Pictorial view of the Differential Pressure Transmitter Calibration Setup

Four test runs were made and relative error was calculated for the average of each setting. Table (D.1) shows the test results of the calibration. The relative error ranges from 3.1 % at the lower range of measurements down to 0.22% at the higher range. The calibration results are plotted in fig. (D.4) showing a fairly good linear relation.

Table (D.1) Differential Pressure Transducer Calibration

Differential Pressure Measurements in mm H2O						
Reference	Measured				Average	Relative Error
500	513	519	516	517	516.00	3.10%
700	715	712	712		713.00	1.82%
900	915	914	915	916	914.67	1.60%
1000	1010	1012	1012	1011	1011.33	1.12%
1200	1217	1213	1214	1213	1214.67	1.21%
1400	1409	1409	1408		1408.67	0.62%
1500	1516	1512	1512	1516	1513.33	0.88%
2000	2008	2012	2009	2006	2009.67	0.48%
2400	2411	2412	2414	2414	2412.33	0.51%
2700	2713	2715	2713	2713	2713.67	0.50%
3000	3013	3014	3012	3013	3013.00	0.43%
3300	3312	3312	3312	3316	3312.00	0.36%
3500	3508	3510	3505	3508	3507.67	0.22%

Figure (D.4) Calibration Curve for the Diff. Press. Transducer in mm H2O

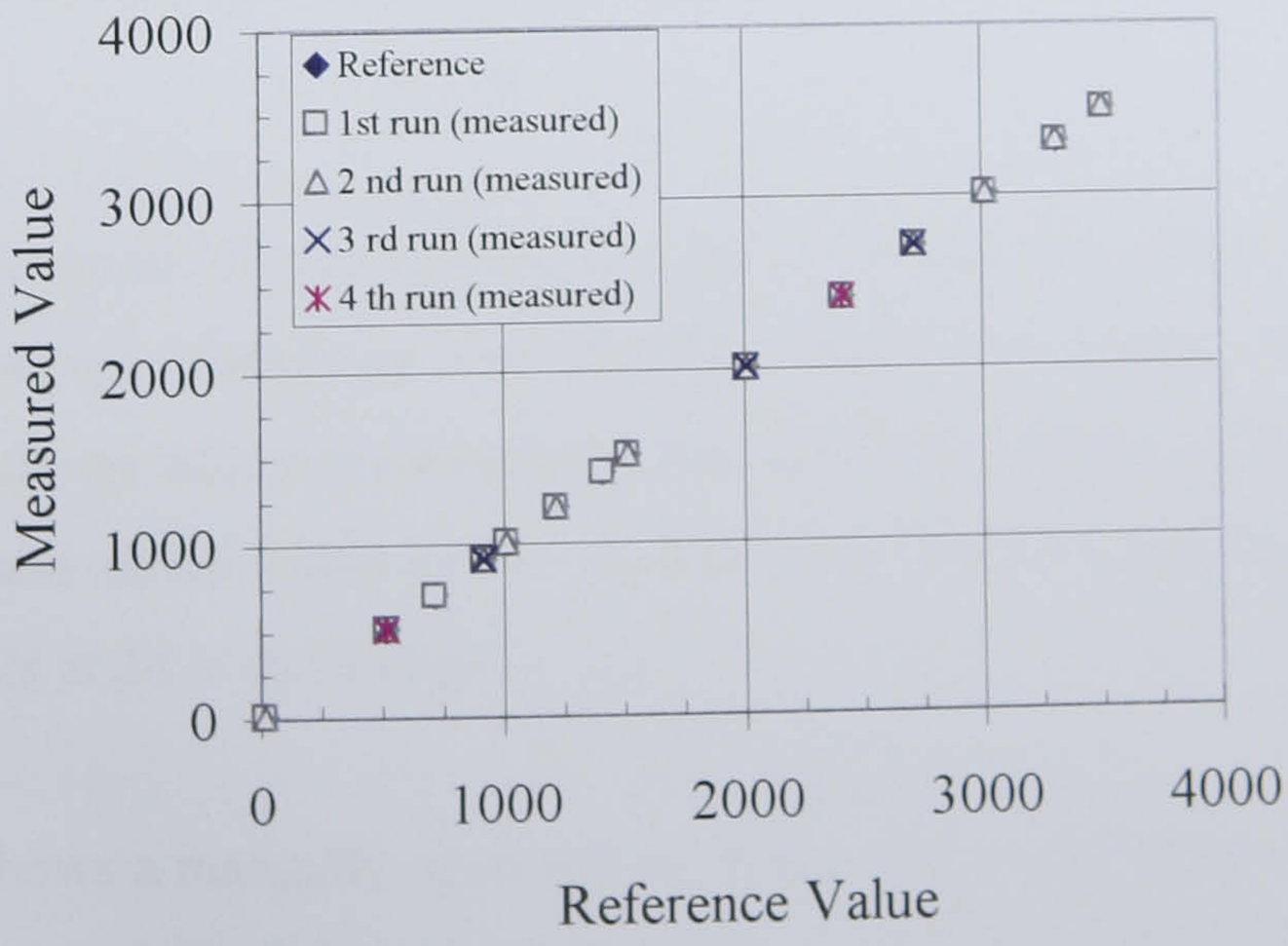

D.1.3. Description of the Calibration Instruments:

The pressure calibrator used in the calibration is PC106 made by OY Beamex AB [56]. Certified laboratories in Jordan regularly calibrate the Calibrator. Figure (D.5) shows the main functional parts of the calibrator. Analogue pressure signals are applied to one or more of the pressure module connections. The analogue to digital converters and amplification units make these signals ready at the micro controller input in a digital form. The user interface unit facilitates the configuration, range selection, units of measurement and user control of the calibrator. Display can be read out from two LCD panels and in various units as desired. In this exercise, it was possible to set the pressure reference signals down to few millimetres H2O.

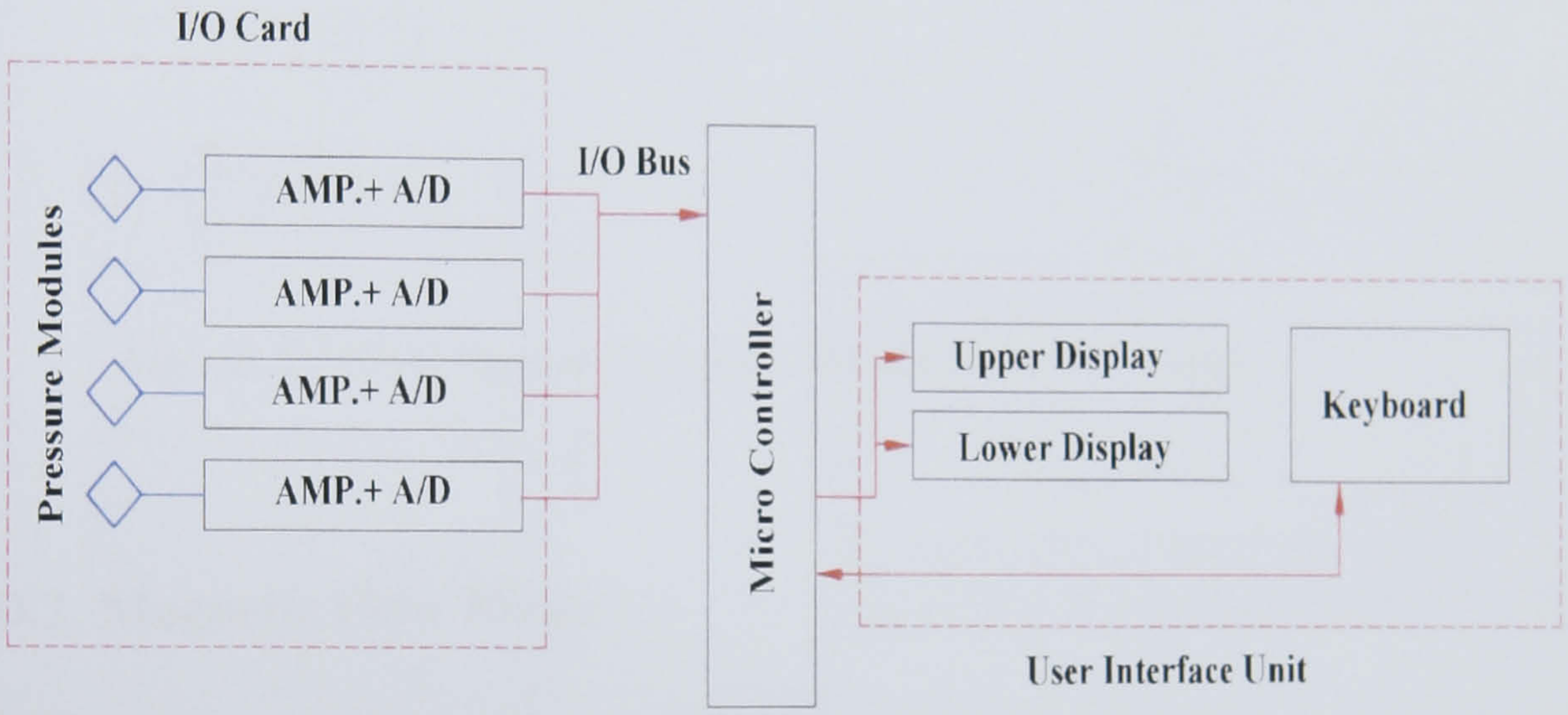

Fig. (D.5), Pressure Calibrator Block Diagram

Standard four-channel chart recorder is used to obtain the output signals of the differential pressure transducer and the flow rate. The range, chart speed and sampling rate can be adjusted through a menu driven procedure. LCD display shows channel state and signal value in the chosen units. The recorder accepts electrical analogue signals at 24 V dc voltage.

Figure (D.6) shows a manually operated air pump, (PGV 300) Beamex made, which can be finely tuned to deliver extremely low volumetric flow rate through the

adjustment of the side knob. The same knob is used to lock the pressure in the discharge line for reasonably long periods. A vent valve is placed at the top of the pump to relieve the line pressure.

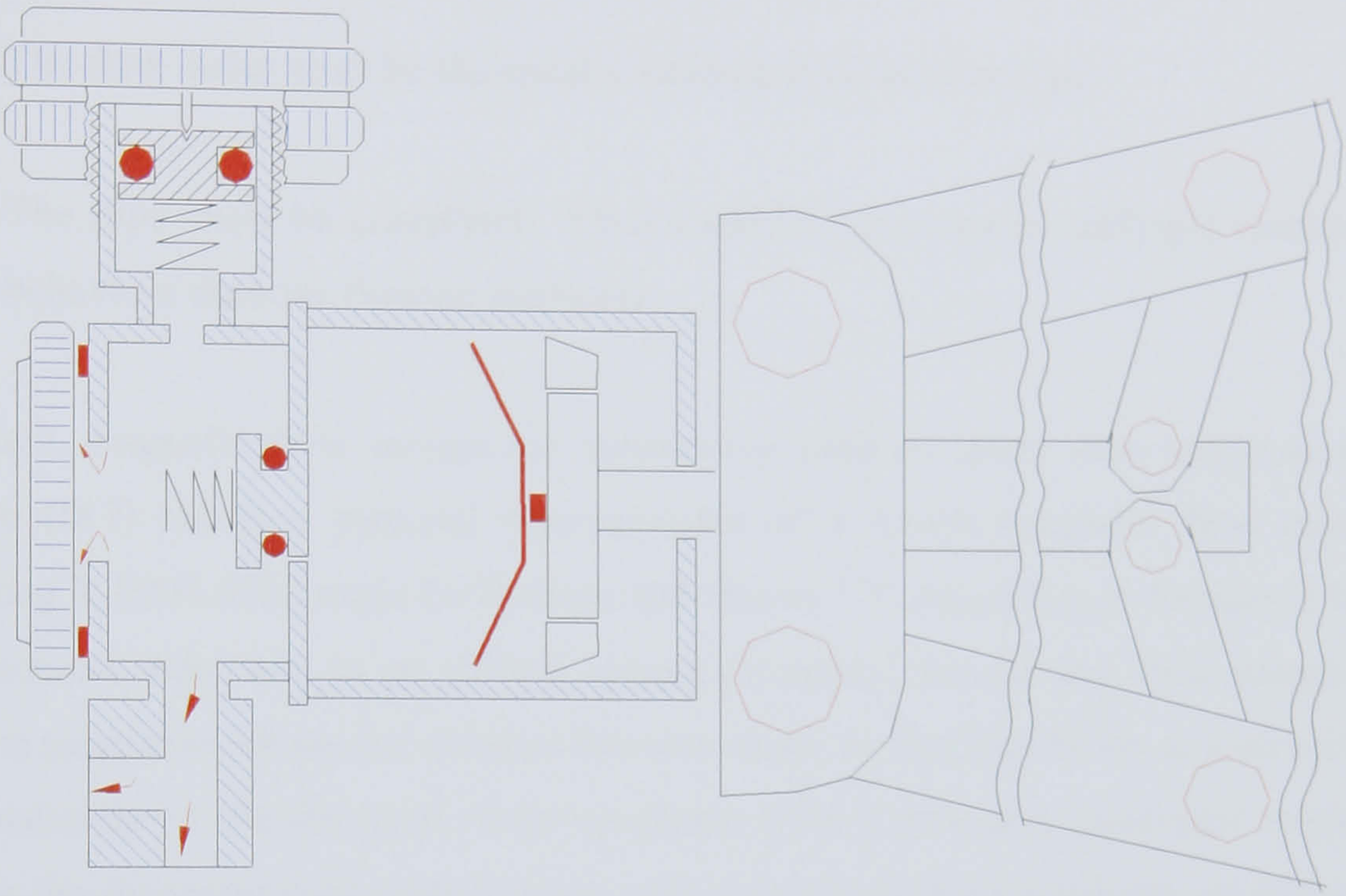

Fig. (D.6), Cross Section Through the Calibration Air Pump

D.2. Magnetic Flow Meter:

D.2.1. Description:

Magnetic flow meters are non-intrusive flow measurement instruments. Thus, they do not interact with the flow pattern. The result is much accuracy and fewer complications in the interpretation of the measured signals with minimal correction factors. The only limitations on the use of these flow meters are:

- Must be installed in a vertical pipe run direction to allow for averaging of the flow properties on the cross section of measurement.

- The fluid must contain electrically conductive material.

- Minimum distance of any direction and / or direction change must be not less than three pipe diameters. (for test rig applications this is raised to 10 pipe diameters).

- The flow meter must be electrically isolated from the line pipe.

- The pipe must be completely filled (bubbles give rise to different electrical behaviour than the flowing medium)

As such, magnetic flow meters are extensively used in slurry flow applications. Figure (D.7) shows a pictorial representation of a 4-inch magnetic flow meter. Pulsmag V DMI 6532 made by Endress and Hauser [57]. According to Faraday's law of electrical induction, as an electric current (I) passes through the coils, magnetic field is generated across the distance between them, as the fluid flows in a direction perpendicular to the direction of the magnetic field it acts as a conductor moving across the magnetic field with a given velocity (V) and thus generates an induced electromotive force (Ue) that is perpendicular to the direction of both the magnetic field and the moving conductor (in this case the flowing slurry). The induced voltage is directly proportional to the flow rate.

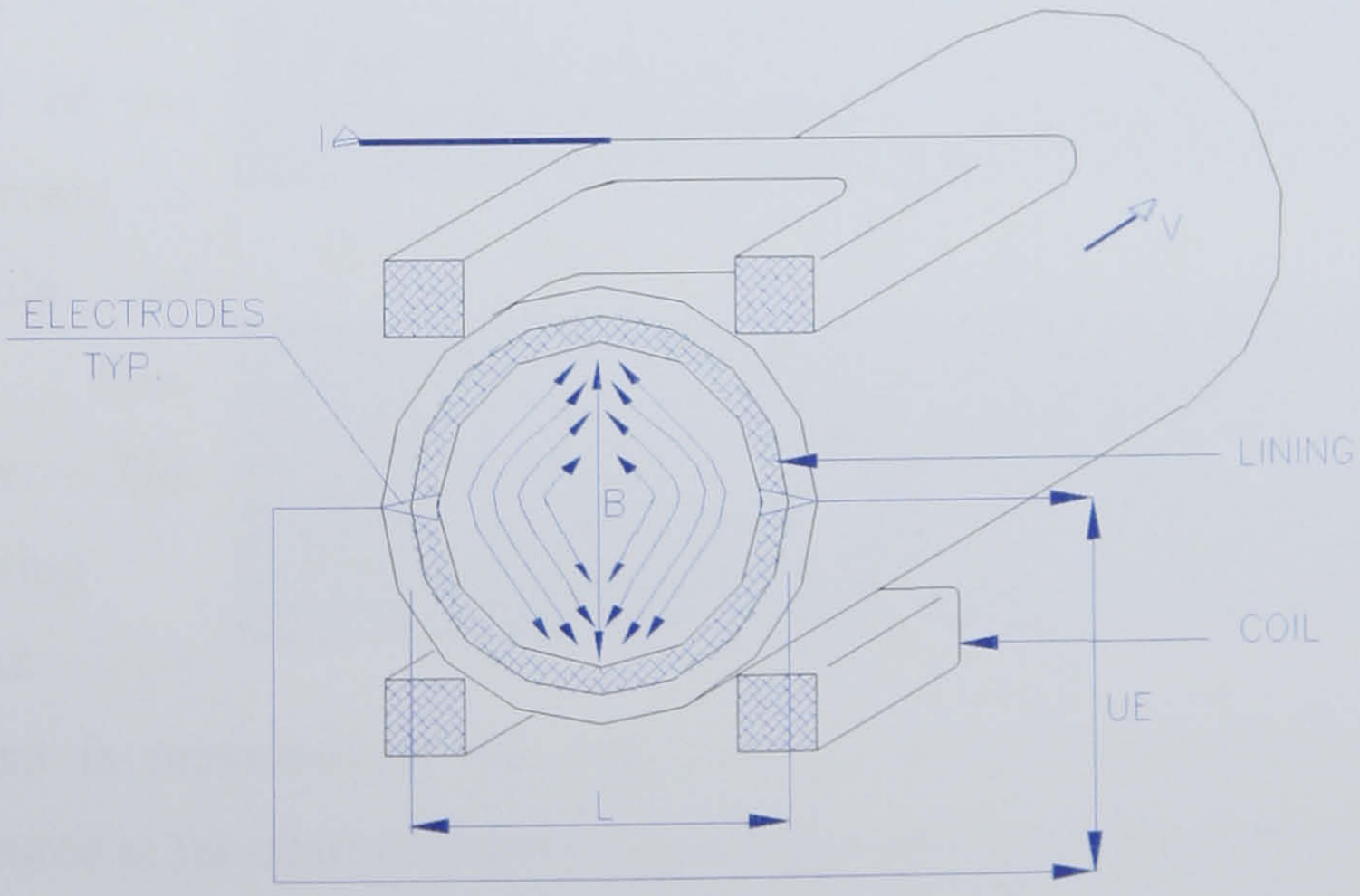

Fig. (D.7), Magnetic Flow Meter Pictorial view

n

electrically insulating liner is arranged with the same pipe diameter, two coils are

situated across the pipe and perpendicular to them two electrodes are arranged to measure the induced electromotive force. The flow meter is microprocessor controlled and can be programmed for any suitable unit of measurement. The range of flow rate in this exercise is from 0 to 198 cubic meters per hour.

D.2.2. Calibration:

Simulated calibration was carried out using standard electronic calibrator that is factory configured. This method of calibration was considered adequate due to the extensive experience with these flow meters at the site were this exercise was conducted and the decision of the repeated calibrations that were conducted and formed a proven record of accuracy of this method of calibration. Apparently, in cases were unknown behaviour of a flow meter it is necessary either to calibrate it using a standard volumetric and/ or gravimetric procedure. This was considered unnecessary under the circumstances.

Table D.2, Calibration of the Magnetic Flow Meter

Flow Rate (%)		Current (mA)		Relative Error	
Ref.	Measured	Impressed	Measured	Q %	Current
0	0	4	4.03	0	0.07%
25	24.5	8	8.02	0.02%	0.025%
50	49.9	12	12.05	0.02%	0.04%
75	74.8	16	16.05	0.027 %	0.03%
100	99.8	20	20.05	0.02%	0.025%

The calibrating set impresses current at the input test leads of the electronic module of the flow meter. The resulting output current is measured at the electrodes. In this exercise the output current was measured at the chart recorder to include the error up to the recording point.

Table (D.2) summarizes the results. The current ranges from 4 to 20 mA corresponding to percent flow of the full flow meter range. Relative error ranges from 0.07% at the lower range to 0.025% at the upper flow range.

D.3. Rotary Cup Viscometer:

D.3.1. Description:

Figure (D.8) illustrates the operating principle of the viscosity-sensing unit. As the inner rotary cup rotates at a preset speed, the fluid between the inner and outer cups is subjected to shear stress at the inner and outer surfaces of the rotary cup. The sheared layer is kept thin enough so that turbulence is not allowed to distort the shear stress. The fluid viscosity resists motion by exerting torque on the electrical motor. Temperature is kept constant through a cooling/ heating jacket that circulates the cooling fluid in a cascade of temperature control baths. The shear stress is proportional to rotary speed in radians per second where the constant of proportionality is the Newtonian viscosity.

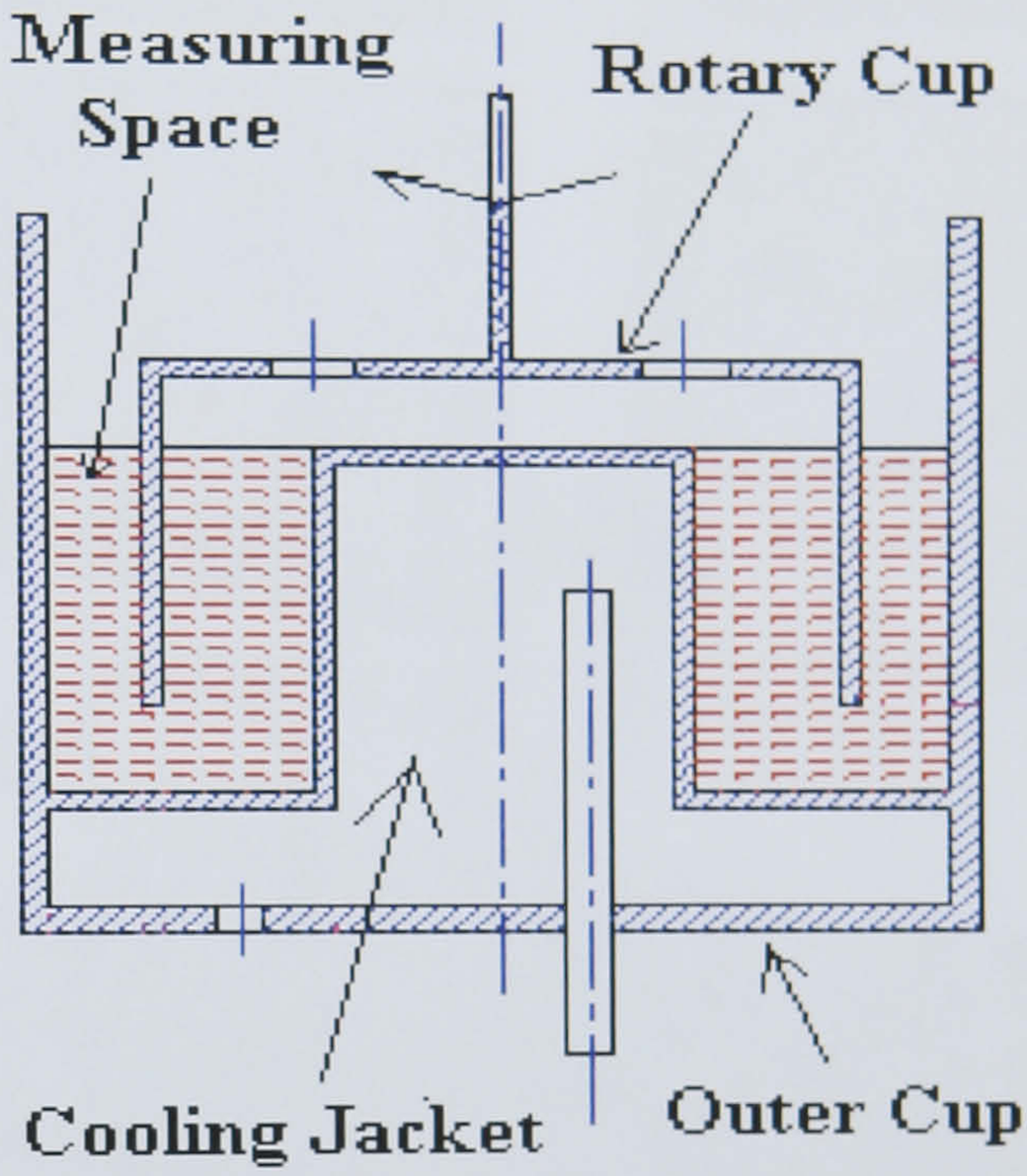

Fig. (D.8), Rotary Cup Viscometer Sensing Unit

Viscosity measurement set-up is pictorially shown in fig. (D.9), which comprises rotary cup viscometer (Rotovisco® RV 20, Measuring System M)[58] and temperature control cooling/ heating circulators. The viscometer comprises a motor, a sensing unit and a control unit. The motor rotary speed is controlled and can be set at different values. Torque and shear stress ranges can be selected. Digital readout shows measured shear stress and shear rate through a selector switch.

Fig. (D.9), Pictorial View of the Rotary Cup Viscometer Set-up

D.3.2. Calibration:

Standard calibration fluid is used in the calibration process of predetermined viscosities at different temperatures. Table (D.3) summarizes the fluid properties.

Table (D.3), Specifications of the Calibration Fluid

Standard Trade Name: Canon ® Certified Viscosity Standard (Mineral Oil 100%) Conforming to ASTM Oil standard Standard Code: S60			
Temperature (°C)	Kinematic Viscosity ν (mm^2/S)	Dynamic Viscosity μ (m.Pa.S.)	Density (gm/ml)
20	161.1	139.7	0.8673
25	119.1	102.9	0.8642
37.78	60.13	51.49	0.8563
40	54.06	46.22	0.855
98.89	7.79	6.376	0.8185
100	7.598	6.214	0.8178

The calibration procedure is carried out through selecting the operating temperature, rotary speed setting and torque and shear stress ranges. Different settings of speed of rotation produces a table of values of shear stresses viz. shear rates. Table (D.4) summarizes the calibration measurements.

Table (D.4), Shear Stress - Shear Rate Viscometer Calibration Data

Shear rate in rad./sec	Shear Stress in Pa		
	T = 20 Deg.C	T = 25 Deg.C	T = 40 Deg.C
25.65	3.293	2.4475	1.49075
41.85	5.696	4.272	2.33625
75.6	9.612	7.209	3.7825
124.2	16.287	12.30425	6.0075
207.9	28.035	20.6925	9.90125
348.3	47.971	35.6	16.7765
579.15	80.634	61.143	28.90275
969.3	132.61	101.61575	48.6385
1615.95		163.24825	81.3015
2697.3			132.32075

Figure (D.10) is a plot of calibration results at different temperatures. The slopes of the straight lines represent the measured values of the dynamic viscosity of the calibration fluid at different temperatures. In a similar manner, dynamic viscosities can be measured for the fluids in the range of measurement of the apparatus.

Figure(D.10), Shear Stress - Shear Rate Calibration Curve for Viscometer at Different Temperatures

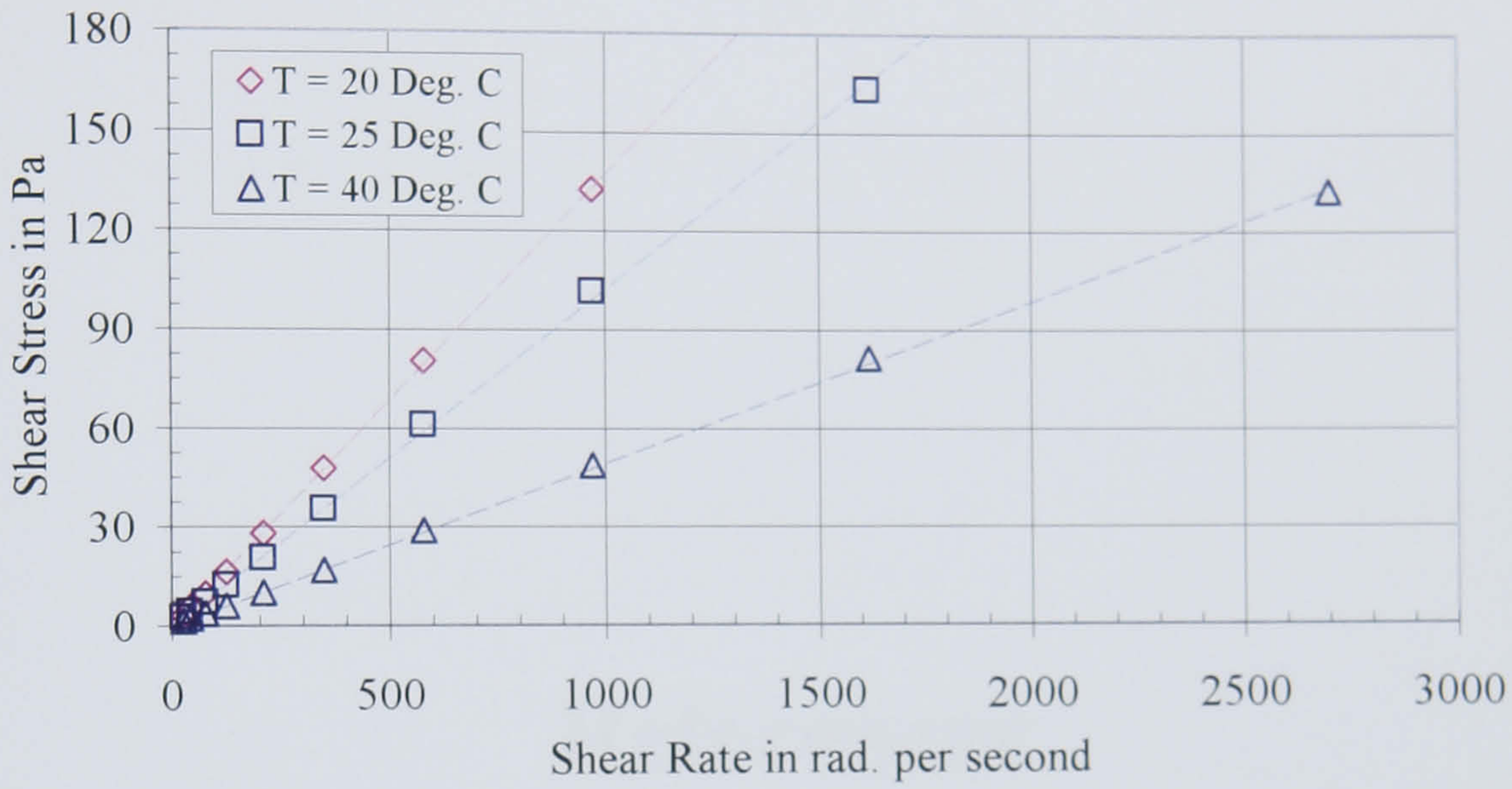

Table (D.5) compares the results of calibration with the reference results of the calibration fluid. An error range from –1.75% to 5.67% was observed.

Table (D.5), Reference viz. Measured Dynamic Viscosity in Pa.S. for Calibration Fluid

Temperature (Deg. C)	Reference	Measured	Relative Error
20	0.1397	0.1373	-1.75%
25	0.1029	0.1023	-0.59%
40	0.04622	0.049	5.67%

References

[1] Zandi, I. " Hydraulic Transport of Bulky Materials". Paper (1). Advances in Solid- Liquid Flow in Pipes and Its Applications, Edited by: Iraj Zandi, Pergamon Press (London) (1971).

[2] Durand, R. "Basic Relationships of the transportation of Solids in Pipes- Experimental Research". Proc. Int. Association for Hydraulic Research, Minneapolis, Minn. (1953)

[3] Fangary, Y.S., Abdel Ghani, A.S., Elhaggar and Williams, R.A. "The Effect of Fine Particles on Slurry Transport Processes". Minerals Engineering, Vol. 10. No. 4. pp. 427-439. (1997)

[4] Pirie, R.L.. "Transport of Coarse Particles in Water and Shear-Thinning Suspensions in Horizontal Pipes". PhD Thesis submitted to the University of Wales, UK. (1990)

[5] Turian, R. M., Hsu, F.L. and Ma, T. W. "estimation of the Critical Velocity in Pipeline Flow of Slurries". Powder Technology, Vol. 51, pp. 35-47. (1987)

[6] Swamee, K.P "Design of Sediment Transporting Pipeline", Journal of Hydraulic Engineering (ASCE), Vol. 121, No. 1, pp. 72-76. (1995)

[7] Peters, M.S. and Timmerhaus, K.D. "Plant Design and Economics for Chemical Engineers". Third edition, McGraw- Hill Book Co., New York, pp 512. (1980)

[8] Brown, N. and Heywood, N., "Classification and Characterisation of Slurries". Ed. Brown, N. P. and Heywood, N. I., "Slurry Handling, Design of Solid Liquid Systems". Elsevier Applied Science (London), pp. 1- 16. (1991)

[9] Doron, P. and Barnea, D. "Flow Pattern Maps in Solid Liquid Flow in Pipes". Int. J. of Multiphase Flow, Vol.22, No. 2, pp.273- 283. (1996)

[10] Doron, P. and Barnea, D. "A Three Layer Model for Solid Liquid Flow in Horizontal Pipes". Int. J. of Multiphase Flow. Vol.19, No. 6, pp. 1029- 1043. (1993)

[11] Yan, Y. "Guide to the Flow Measurement of Particulate Solids in Pipelines. Part 1: Fundamentals and Principles". Powder Handling and Processing. Vol.13, No. 4, pp. 343- 352. (2001)

[12] Patanakar, N.A., Ko, T., Choi, H.G., and Joseph, D.D. "A Correlation of the Lift- Off of many Particles in Plane Poiseuille Flows of Newtonian Fluids". Journal of Fluid Mechanics, Vol. 445, pp 55-76. (2001)

[13] Govier, G.W. and Aziz, K. "The Flow of Complex Mixtures in Pipes". Van Nostrand Reinhold Co. (New York), pp. 628. (1972)

[14] Rastiero, M. G., Figueiredo, M. M., Maia, M. C. and Scarlett, B."Modeling of Solid/ Liquid flow in Pipes". Powder Handling and Processing, vol.5, No. 3, pp. 253-259. (1993)

[15] Carleton, A. J. and Cheng, D, C-H "Pipeline Design for Industrial Slurries". Chemical Engineering, April 25, pp. 95- 100. (1977)

[16] Darby, R., Mun, R. and Borger, D. "Predicting Friction Loss in Slurry Pipes". Chemical Engineering, September, pp. pp. 116-119. (1992)

[17] Lin, S.H. "Pressure Drop for Slurry Transport". Chemical Engineering, pp. 115-117. May 17, (1982)

[18] Babcock, H. "Heterogeneous Flow of Heterogeneous Solids". Paper 8, Advances in Solid Liquid Flow in Pipes and its Applications, Edited by: Iraj Zandi. Pergamon Press (London). (1971)

[19] Khan, A.R., Pirie, R.L. and Richardson, J.F. "Hydraulic Transport of Solids in Horizontal Pipelines- Predictive Methods for Pressure Gradients". Chemical Engineering Science, Vol. 42, pp. 767- 778. Pergamon Journals Ltd. (1987)

[20] Wasp, E.J., Aude, T.C., Seiter, R.H., and Thompson, T.L. "Hetero-Homogeneous Solids/Liquid Flow in The Turbulent Regime". Paper 13, Advances in Solid Liquid Flow in Pipes and its Applications, Edited by: Iraj Zandi. Pergamon Press (London). (1971).

[21] Sobota, J. "A Procedure for the Prediction of the Pressure drops for Poly-Fractional Mixtures". 13th Int. Conf. On Slurry Handling and Pipeline Transport, (HT 13), pp. 283- 296. (1996)

[22] Charles, M.E. and Charles, R.A. "The Use of Heavy Media in Pipeline Transport of Particulate Solids". Advances in Solid Liquid Flow in Pipes and Its Applications, Ed. Zandi, I. Pergamon Press, Oxford, UK. PP. 187-197. (1971)

[23] Kenchnington, J.M.. "Prediction of Critical Conditions for Pipeline Flow of settling Particles in a Heavy Medium". 4th. Int. Conf. On Slurry Handling and Pipeline Transport (HT 4), pp. 31-48. (1976)

[24] Wilson, K.C. "A Unified Physically Based Analysis of Solid Liquid Pipeline Flow". 4th. Int. Conf. On Slurry Handling and Pipeline Transport (HT 4), Paper A1, pp. A1-1-A1-16. (1976)

[25] Gillies, R.G., Husband, W.H.W. and Small, M.H. "A Study of Flow Conditions arising in Horizontal Coarse Slurry Short Distance Pipelining Practice, Phase 1: Sand Slurry Tests in A 250 mm Pipeline". Saskatchewan Research Council. Publication R-833-2-C-85, pp. 1-94. (1985)

[26] Wilson, K.C. "Pipeline Design for Settling Slurries". Slurry Handling Design of Solid Liquid Systems Ed.: Brown, N.P. and Heywood, N.I. Elsevier Applied Science (London). pp. 103-124. (1991)

[27] Mishra, R. Singh, S.N. and Seshadri, V. "Improved Model for the Prediction of Pressure Drop and Velocity Field in Multi-Sized Particulate Slurry Flow Through Horizontal Pipes". Powder Handling and Processing, Vol. 10, No. 3. pp. 279-289 (1998)

[28] Televantos, Y. "The Flow Mechanism of Hydraulic Conveying at High Solids Concentration". PhD Thesis submitted to the Faculty of Engineering. University of London. (1977)

[29] Gillies, R.G., Shook, C.A. "A Deposition Velocity Correlation for Water Slurries". The Canadian Journal for Chemical Engineering, Vol. 69, pp. 1225- 1227. (1991)

[30] Gillies, R.G., Shook, C.a. and Wilson, K.C. "An Improved Two Layer Model for Horizontal Slurry Pipeline Flow". The Canadian Journal of Chemical Engineering, Vol. 69, pp. 173-178. (1991)

[31] Wilson, K.C. "Stationary Deposits and Sliding Beds in Pipes Transporting solids". 1st Int. Conf. On Slurry Handling and Pipeline Transport (HT1). Paper C3, pp. 28-40. (1970)

[32] Matousek, V. "On a Solid Particle Suspension in a Slurry Pipeline". Advances in Fluid Mechanics, Vol. 9, pp. 317-326. (1996)

[33] Khan, A.R. and Richardson, J.f. "Comparison of Coarse Slurry Pipeline Models". 13th Int. Conf. On slurry Handling and Pipeline Transport, (HT13), pp. 259-282. (1996)

[34] Riet, E.J. van, Matousek, V. and Miedema, S.A. "A Theoretical Description and Numerical Sensitivity Analysis on Wilson's Model for Hydraulic Transport in Pipelines". Journal of Hydrology and Hydromechanics, Slovak Academy of Science. (1996)

[35] Miedema, S.A., Riet van, E.J., and Matousek, V "Theoretical Description and Numerical Sensitivity Analysis on Wilson Model for Hydraulic Transport of Solids in Pipelines". WEDA Journal of Dredging Engineering. March. (2002)

[36] Matousek, V. "Distribution and Friction of Particles in Pipeline Flow of sand Water Mixtures". Handbook of Conveying and Handling of Particulate solids. Elsevier Science, edited by: Levy, A. and Kalman, H., pp 465- 541. (2001)

[37] Doron, P. Granica, D. and Barnea, D. "Slurry Flow in horizontal Pipes- Experimental and Modeling". Int. J. of Multiphase flow, Vol. 13. No. 4. pp535-547. (1987)

[38] Matousek, V. "Flow Friction of Mixture Composed of Fine Sand and Coarse Sand". Proc. the 4th Int. Conf. on Multiphase Flow, New Orleans (Proceedings on CD). (2001)

[39] Kazanskij, I., Bruhl, H. and Hinsch, J. "Influence of Added fine Particles on the Flow Structure and the Pressure Losses in Sand Water Mixtures". 3rd Int. Conf. On Slurry Handling and Pipeline Transport (HT 3), pp. D2-11-D2-21. (1974)

[40] Matousek, V. and Ni, F. "On the economy of Transportation of Highly Concentrated, Broadly Graded sand- Water Slurries: Results of Laboratory Tests". Proc. XXth WEDA Technical Conf. and XXXIst Texas A&M Dredging Seminar. (2000)

[41] Maghsoodi, I.S. and Streat, M. "Hydraulic Conveying of Coarse Coal: Prediction of Headloss". 11th Int. Conf. On Slurry Handling and Pipeline Transport, (HT 11). pp. 19- 32. (1988)

[42] Roco M.C, and Balakrishnam N. "Multi- Dimensional Flow Analysis of Solid Liquid Mixtures". Journal of Rheology, vol. 29, No. 4, pp 431- 456. (1985)

[43] Wang G.Q., and Ni J.R. "The Kinetic Theory for Dilute Solid- Liquid Two-Phase Flow". Int. J. Multiphase Flow, Vol. 17, No. 2. pp 273- 281. (1991)

[44] McTigue, D.F. "Mixture Theory for Suspended Sediment Transport". J. of the Hydraulics Division (ASCE), Vol. 107, No. HY6, pp 659- 673. (1981)

[45] Aziz, N.M., Bhattacharya, S.K. and Prasad, S.N. "Suspended Sediment Concentration Profiles Using Conservation Laws". J. of Hydraulic Research, Vol. 30, No. 4, pp 539- 554. (1992)

[46] Wang, G. and Ni, J.R. "Kinetic Theory for Particle Concentration Distribution in Two Phase Flow". J. of Engineering Mechanics (ASCE), Vol. 116, No. 12, pp 2738- 2748. (1990)

[47] Brown, N. P. "The Settling Behavior of Particles in Fluids". Ed. Brown, N. P. and Heywood, N. I., "Slurry Handling: Design of Solid Liquid Systems", Elsevier Science Publishing Ltd. (U.K), pp 17-40. (1991)

[48] Swamee, P.K. and Ojha, C.S.P. "Drag Coefficient and Fall Velocity of Non Spherical Particles" J. Hydraulic Engineering (ASCE), 117 (5), 660-667(1991)

[49] Wilson K.C., G.R.Addie and R. Clift "Review of Fluid and Particle Mechanics", "Slurry Transport Using Centrifugal Pumps", Chap. (2), pp44-45. (1992),

[50] Abdulrahman, A.M. "Introduction in Econometrics". First Edition. King Saud University Press. Pp. 31. (1996)

[51] Kennedy, J.B. and Neville, A.M. "Basic Statistical Methods for Engineers and Scientists". Third Edition. Harper and Row Publishers (New York). Pp. 256. (1986)

[52] SPSS for Windows, Release 11.0.0, Copyright of SPSS INC.- USA.

[53] Jensen, A.N. "Durbin Watson Statistic for First-Order Autocorrelation Testing" College of Business Administration, California State University. (2001)

[54] Montgomery, D., Runger, G.C., and Huble, N.F. "Engineering Statistics". John Wiley and Sons, Inc. PP.318. (1998)

[55] Alphaline ® Draft range differential Pressure transmitter, Product Data Sheet: PDS 4294, Rosemount Inc., Measurement Division, USA. (February 1993)

[56] Pressure Calibrator PC 106, Publication No. 8816440/SEPC106/902264, OY Beamex AB- Finland.

[57] Flow measurement Operating and Installation Manual, Endress and Hauser Flowtec- Germany.

[58] Instruction Manual, Rotovisco® RV20, Measuring System M, Haake Mess-Technik GmbH, Germany, Publication No. 2.1.044.2- 10.91